Design of a Motion Compensation System for Offshore Wind Turbine Installation

J. Hogerheijde

Master of Science Thesis

TU Delft

Boskalis

Design of a Motion Compensation System for Offshore Wind Turbine Installation

by

J. Hogerheijde

In partial fulfillment of the requirements for the degree of

Master of Science
in Offshore and Dredging Engineering

at the Delft University of Technology,
to be defended publicly on Friday 8 May, 2020 at 13:00 AM.

Project duration:	June 3, 2019 – May 8, 2020	
Chairman:	Prof.Dr. A. Metrikine,	Delft University of Technology
Supervisor:	Ir. P. G. F. Sliggers,	Delft University of Technology
Supervisor:	Ir. A. Cabboi,	Delft University of Technology
Company Supervisor:	Ir. I. K. van Giffen,	Royal Boskalis Westminster

This thesis is confidential and cannot be made public until May 8, 2025.

TU Delft Delft University of Technology

Boskalis

ABSTRACT

To reach the Paris Agreement goals, switching from fossil fuels to renewable energy is inevitable. Wind power has proved to play a critical role in this transition. To speed up this transition, the wind industry must keep innovating. The major part of Wind Turbine Generators (WTGs) is installed by a jack-up which not only has its limitations from an engineering point of view, such as water depth, soil characteristics and lifting capacity but also from a financial point of view. To overcome these limitations, this research aims at developing an innovative concept design for the installation of offshore WTGs. A 12 MW WTG comprises a tower, nacelle and three blades is considered. A problem analysis is conducted in which the existing installation problems and proposed solutions are analysed. Based on this problem analysis, a list of inputs for which the design is developed is given.

A vessel dynamic analysis is performed in Seaway Octopus, a hydrodynamics program which computes the vessel motions in the frequency-domain by using strip theory. The analysis showed that the Mighty Servant 1 is the most suitable Boskalis vessel to install WTGs from. The same dynamic analysis also highlighted that a motion compensation system is required to mitigate wave-induced dynamics, enabling WTG installation in floating conditions.

After developing multiple concepts of motion compensation systems, a multi-criteria analysis in the form of an analytic hierarchy process is performed. The two most feasible concepts are assessed on their technical challenges. It is found that the most promising concept should rely on a Stewart platform which motion compensates the WTG at the bottom of the tower with six hydraulic cylinders. The Stewart platform is connected to the Transition Piece (TP) after which the WTG is skidded towards it, reducing the motions the further it is skidded. This connection is required to limit the overturning moment on the Stewart platform. The connection between the Stewart platform and the WTG is made with a clamp below a flange on the tower.

A kinematic optimization is carried out by means of a genetic algorithm to find the optimal values of the five parameters describing the Stewart platform's geometry. Three indices are used to indicate the kinematic performance of a parameter set: the global conditioning index, global gradient index and, self-made, global force index. The indices describe respectively the dexterity, the gradient of the dexterity and the sum of the cylinder forces. Optimizing for each index individually highlighted that the optimization should include all three indices, since improving the performance of one index has a negative impact on the other indices. The optimal set of design parameters is selected by taking advantage of the Pareto front, which is computed with a multi-objective optimization including all indices. A design sensitivity analysis is performed to obtain the sensitivity of the kinematic indices with respect to changes in the design parameters. The results of the sensitivity analysis showed that the optimal design of a Stewart platform is a design choice based on a trade-off between performance and required power.

A model is developed in MATLAB and Simulink to simulate the dynamics of the motion compensation system. Only the installation phase where the Stewart platform is not yet connected to the TP and where the WTG is in the centre of the platform is considered. The simulated results showed that a controller with velocity feed-forward and position feedback is the preferred way to go. It is found that the maximum required flow in all cylinders combined is 84000 l/min with a required net power of 10.4 MW. This required amount of hydraulic power has a great impact on the economic feasibility of the system. By adding a passive system in the form of a hydraulic accumulator, the system's performance is drastically improved. Based on the results of this research, it can be concluded that the next generation offshore wind turbine generator can be motion-compensated with a Stewart platform including hydraulic accumulators. This, with a compensation efficiency up to 94.8 %, a maximum net power of 4.2 MW and a maximum flow in all cylinders combined of 28000 l/min. Further research should be carried out by assessing more installation phases in combination with a wider range of load cases.

CONTENTS

List of Figures

List of Tables

List of Acronyms

AHP	Analytic Hierarchy Process
AMC	Active Motion Compensation
CAPEX	Capital Expenses
CI	Consistency Index
CoG	Centre of Gravity
DNV	Det Norske Veritas
DoF	Degree of Freedom
DP	Dynamic Positioning
GA	Genetic Algorithm
GCI	Global Conditioning Index
GFI	Global Force Index
GGI	Global Gradient Index
GPI	Global Payload Index
HLV	Heavy Lift Vessel
HSE	Health, Safety & Environment
IMC	Ideal Motion Compensation
JONSWAP	Joint North Sea Wave Observation Project
LCI	Local Conditioning Index
MCA	Multi-Criteria Analyses
MRU	Motion Reference Unit
MSL	Mean Sea Level
OPEX	Operational Expenses
PAMC	Passive Active Motion Compensation
PID	Proportional Integral Derivative
PMC	Passive Motion Compensation
QTF	Quadratic Transfer Function
RAO	Response Amplitude Operator
TIV	Turbine Installation Vessel
TP	Transition Piece
WTG	Wind Turbine Generator

List of Symbols

a	Added mass	kg
a_i	Acceleration in i direction	$\frac{m}{s^2}$
A	Surface Area	m^2
b	Damping Coefficient	$\frac{kg}{s}$
b_i	O_b to leg i vector	m
c	Wave speed	$\frac{m}{s^2}$
C	Chord length	m
d	Displacement from CoG	m
D	Diameter	m
e_i	Unit vector of leg i	-
E	E-Modulus	$\frac{kg}{m \cdot s^2}$
E_k	Kinetic energy	$\frac{kg}{m^2 \cdot s^2}$
E_p	Potential energy	$\frac{kg}{m^2 \cdot s^2}$
f	Frequency	$1/s$
F_{acc}	Force by acceleration	$\frac{kg \cdot m}{s^2}$
F_{cyl}	Axial force in cylinders Stewart platform	$\frac{kg \cdot m}{s^2}$
$F_{external}$	External force and moment vector	$\frac{kg \cdot m}{s^2}$
F_{wind}	Force by wind	$\frac{kg \cdot m}{s^2}$
g	Gravitational Acceleration	$\frac{m}{s^2}$
GM	Metacentric height	m
h	Vertical distance between O_o and O_p	m
H_{max}	Maximum wave height	m
H_s	Significant wave height	m
I	Moment of inertia	$kg \cdot m^2$
J_F	Force part of Jacobian matrix	-
J_n	Normalized Jacobian matrix	-
J_{nn}	Non-normalized Jacobian matrix	- & m
J_T	Torque part of Jacobian matrix	m
k	Spring constant	$\frac{kg}{s^2}$
KG	Keel to CoG	m
$k_i(J_n)$	Condition number normalized Jacobian	-
K_{ii}	Radii of gyration around i axis	m
K_d	Damping gain constant	$\frac{kg}{s}$
K_p	Spring gain constant	$\frac{kg}{s^2}$

L_{tower}	Tower length	m
$l_{ext,i}$	Required leg extension of leg i	m
L_j	Jacobian normalization factor	m
l_i	Length of leg i	m
$l_{n,i}$	Nominal length of leg i	m
L_i	Unit vector of leg in i direction	-
L_u	Integral length scale	m
$L1$	Length of cylinder tube	m
$L2$	Length of piston rod	m
m	Mass	kg
m_0	Zero moment of spectrum	m^2
M_{wind}	Moment by wind	$\frac{kg \cdot m^2}{s^2}$
n	Adiabatic constant	-
N	Number of points in workspace	-
O_o	Origin base coordinate system	-
O_p	Origin platform coordinate system	-
p	Pressure	$\frac{kg}{m \cdot s^2}$
p_i	O_p to leg i vector	m
Pa	Pascal	$\frac{kg}{m \cdot s^2}$
P_E	Actual maximum load	$\frac{kg \cdot m}{s^2}$
P_E	Buckling load	$\frac{kg \cdot m}{s^2}$
q	Vector from O_o to O_p	m
Q	Flow	m^3/s
R_{matrix}	Rotation matrix	–
R	Radius circle	m
R_b	Radius base circle	m
R_t	Radius platform circle	m
S	Stroke length	m
S_f	Safety factor	-
$S_\zeta(\omega)$	Wave energy spectrum	-
$S_u(f)$	Wind energy spectrum	-
t	Tonne	$1000 \cdot kg$
$T_{n,roll}$	Natural roll period	s
T_p	Peak period	s
T_w	Quadratic transfer function	-
T_z	Zero-crossing period	s
U	wind speed	m/s
V	Volume	m^3
v_{max}	Maximum impact velocity	$\frac{m}{s}$
W	Watt	$\frac{kg \cdot m^2}{s^3}$
W_{GCI}	Weight factor GCI	-
W_{GGI}	Weight factor GGI	-
W_{GFI}	Weight factor GFI	-
x_p	Piston displacement	m
x_v	Percentage valve is opened	%
z	Height above MSL	m
z_0	Terrain roughness	-

α	Wave safety factor	-
β_e	Effective bulk modulus	$\frac{kg}{m \cdot s^2}$
γ^{A_j}	Peak enhancement factor	-
δ_i	Displacement in i direction	m
θ	Pitch angle	rad
κ_1	Linear roll damping coefficient	-
κ_2	Quadratic roll damping coefficient	-
λ	Design parameters vector	m & rad
μ	Friction coefficient	-
ν	Poisson Ratio	-
ρ	Density	$\frac{kg}{m^3}$
$\sigma_{min}(J_{nn})$	Minimum singular value non-normalized Jacobian	-
$\sigma_{max}(J_{nn})$	Maximum singular value non-normalized Jacobian	-
σ_{max}	Maximum stress	$\frac{kg}{m \cdot s^2}$
σ_{out}	Standard deviation output motion	m & deg
σ_{in}	Standard deviation input motion	m & deg
σ_u	Standard deviation wind speed	$\frac{kg}{m \cdot s^2}$
σ_x^2	Position variance	m
σ_y	Yield strength	$\frac{kg}{m \cdot s^2}$
τ	Time lag dynamic positioning system	s
ϕ	Roll angle	rad
ϕ_b	Separation angle on base	rad
ϕ_p	Separation angle on platform	rad
ψ	Yaw angle	rad
ω	Wave frequency	$\frac{rad}{s}$
ω_p	Wave frequency at peak period T_p	$\frac{rad}{s}$

Please note, the variables used in Subsection 6.2.2 which belong to the DNVGL-RP-C202 standard are not explained here but in that subsection.

COORDINATE SYSTEM

Except if stated otherwise, during this thesis the vessel's geometry, displacements, velocities, accelerations and loads are defined regarding the following right-hand coordinate system, see Figure 1 [DNV-GL-RU-SHIP]. Surge, sway and heave are indicated by X, Y and Z respectively. Roll, pitch and yaw are indicated by ϕ, θ and ψ respectively.

origin	=	at the intersection among the longitudinal plane of symmetry of ship, the aft end of L and the baseline.
X axis	=	longitudinal axis, positive forwards
Y axis	=	transverse axis, positive towards port side
Z axis	=	vertical axis, positive upwards.

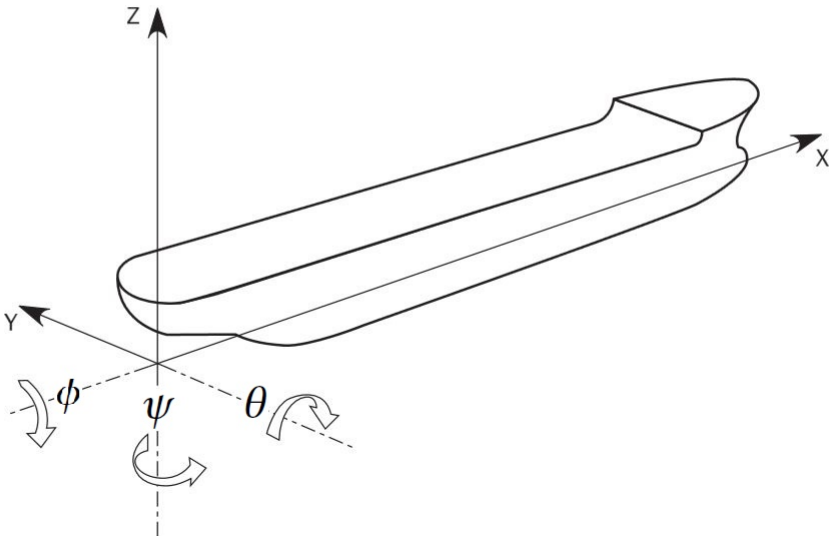

Figure 1: Reference coordinate system

PREFACE & ACKNOWLEDGEMENTS

This report is part of the graduation of the study Offshore and Dredging Engineering with a specialization in Bottom Founded, Artic & Wind.

First of all, I would like to thank my Boskalis supervisor, Ike van Giffen, for his initiation of this interesting research topic, for his helpful advice and for challenging me throughout the research. Besides, I would like to thank my colleagues at the R&D department. Oscar Sainz Avila, for showing me how to make complex engineering problems simple and understandable and for his help during the weekly progress meetings. Hans Duba, for sharing his knowledge about the hydrodynamics software Octopus Seaway and for providing useful vessel data. Thanks to Sandor den Braven for his help with the Simulink model and for sharing his knowledge about hydraulic systems. I would like to show my gratitude to all the Boskalis colleagues who took part in the concept survey which let to the final design. In conclusion, without the opportunity Boskalis gave me and without the spirit and enthusiasm of all colleagues, this would not have been possible.

I would like to thank the committee members from the TU Delft, my supervisor Alessandro Cabboi and chairman Frank Sliggers. Thank you for the useful and critical insights during the regular progress meetings. Both of you were available for questions throughout my thesis and gave me academical insights on how to improve my work.

Last but not least, I am especially thankful to my family and girlfriend for unconditionally supporting me throughout my study. Without you, this would not have been possible.

J. Hogerheijde
Delft, University of Technology, May 2020

1

INTRODUCTION

1.1. RESEARCH MOTIVATION

Up till now, 197 countries signed the Paris Agreement to combat climate change. The common goal to limit the temperature rise this century well below 2 degrees was set. To reach this goal it is inevitable to switch from fossil fuels to renewable energy sources. More and more energy is produced with renewable energy sources such as wind and solar power. However, this transition toward renewable energy sources is going too slow causing the targets set in the Paris Agreement to slip out of reach. To reach the targets, the cost and time required to transition towards green energy sources must drastically be reduced. The answer to this problem is innovation.

Wind energy has proved to be a critical source in the transition. With offshore wind having advantages in comparison with onshore wind such as higher and more consistent revenues because of offshore wind being more reliable. Besides, less sight and sound pollution exists. Meanwhile, offshore wind has some disadvantages such as a challenging part of the installation: installing the Wind Turbine Generator (WTG) on top of a foundation. The WTG consists of the tower, nacelle and three blades and not the transition piece (TP) and the foundation. It becomes more difficult because ever since the first offshore WTG was installed the size and depth in which turbines are installed has increased. This trend is shown in Figure 1.1.

This trend has been kept controllable by also increasing the size of the installation equipment. The major part of WTGs are installed by a jack-up vessel which not only has limitations from an engineering point of view but also from a financial point of view. To overcome these limitations, this research aims at developing an innovative concept design for the installation of offshore WTGs. Designing a new installation method could make installation cheaper, less time consuming and future generation WTG proof.

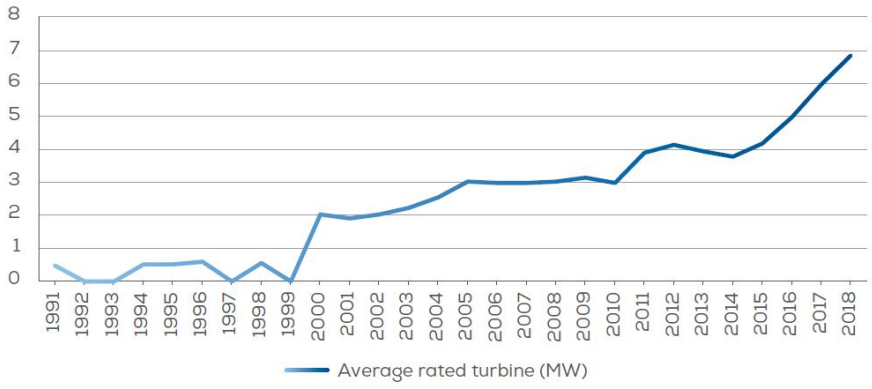

Figure 1.1: Yearly average of rated capacity of newly installed offshore wind turbines [1]

1.2. CURRENT INSTALLATION METHODS

In this section, the most used installation methods for installing offshore WTGs, thus not the foundation, is briefly elaborated. The advantages, disadvantages and limitations of each installation method are discussed.

Jack-up - The major part of offshore WTGs is installed by a jack-up vessel also known as Turbine Installation Vessel (TIV). The main advantage of a jack-up is the stability and relative motion-free platform compared to a floating vessel resulting in relative simple installation. The TIV acquires its stability by lowering jacks or legs into the seabed. Only the jacks, which a trend is to use lattice structures, are loaded by waves and current which drastically reduces the environmental impact on the total structure. At last, a jack-up is a proven installation method and used in multiple successful projects. A new jack-up under construction is the Voltaire, ordered by Jan De Nul. With its 3000 t crane it can install WTGs with a nacelle height of up to 165 m in water depths until 80 m. Thus, also capable of installing the largest turbines, up to 15 MW [2]. The Voltaire, which will be the largest turbine installation vessel ever constructed, is shown in Figure 1.2a.

Major drawbacks in using a jack-up structure for the installation of offshore WTGs are the dependence on a suitable weather window for the jacking operation and the dependence on water depth and soil characteristics. Typical sea states for jacking range from significant wave heights of about 1 to 1.5 m depending on wave period and heading. This with extremes of 2 to 2.5 m wave height together with a wave period ranging from 6 to 8 s [3]. Higher than 2.5 m induces too high impact loads on the lifting system which results in non-availability of the jack-up. Since the North Sea is dominated with sea states with high waves, the non-availability of a jack-up is significant. Another drawback is the time-consuming installation procedure. This, since the jack-up has to be jacked after which the wind turbine is installed in several steps: tower, nacelle and three blades. Above all, the time-costly jacking operation requires most of the time. Taking a financial point of view, the Turbine Installation Vessels (TIVs) are cost expensive with daily rates going up from 150,000 to 250,000 USD. In the current market, there is more demand than supply resulting in vessels being booked more than a year in advance. [4].

Heavy Lift Vessel - Apart from jack-up vessels being used for almost all offshore WTG installations, there is one exception. This exception is made in constructing the first floating wind farm, Hywind Scotland. A Semi-Submersible Crane Vessel (SSCV) has been used, the SAIPEM 7000, see Figure 1.2b. Installation with a SSCV in comparison with a jack-up makes time expensive jacking and modular installation time vanish. The trend for increasing depth is not a problem anymore, for the simple reason the installation vessel floats. The problem the jacks has in coping with environmental influences and lifting heavier vessels has been avoided. Installation during the Hywind project with a SSCV was feasible since the wind farm is located nearshore in Scotland where environmental conditions were close to ideal. Installing offshore wind turbines from floating vessels with more severe sea states than the Hywind Scotland case will reduce the feasibility because of high vessel motions.

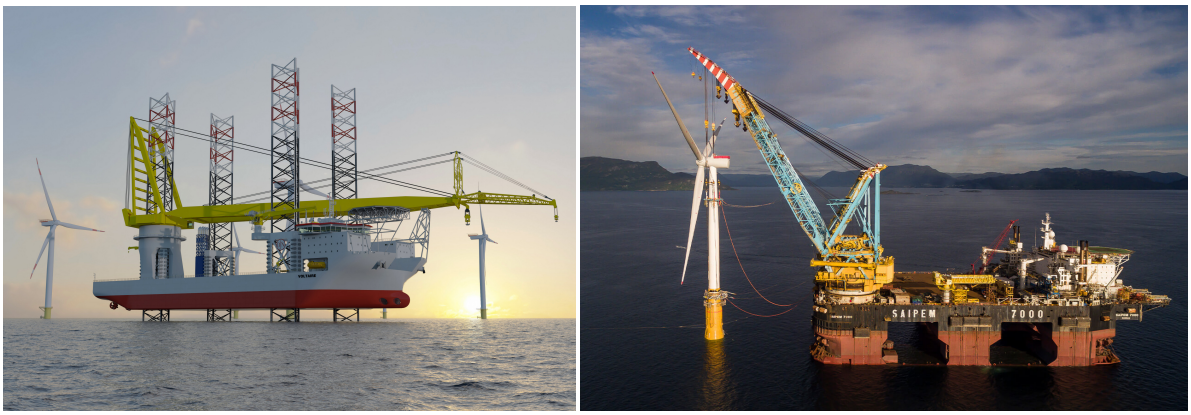

(a) Voltaire, Jack-up [2] (b) Heavy Lift Vessel [5]

Figure 1.2: Most used installation methods for offshore WTGs

1.3. RESEARCH OBJECTIVE

The objective of this thesis is to design an innovative concept for the installation of next-generation offshore Wind Turbine Generators with a floating vessel. The design must be feasible, competitive and above all safe. The design should be able to compete against and overcome the limitations of the most used type of installation, a jack-up vessel. The research question to achieve the research objective is defined as:

How can the next-generation offshore wind turbine generator be installed, enabling competitive installation by using an existing floating vessel without a crane?

The objective can be obtained by answering the following sub-questions:

1. What are the wave-induced motions of a vessel with a wind turbine generator on deck?
2. How can these wave-induced motions be mitigated, enabling installation from a floating vessel?
3. How can the motion compensation system be optimized kinematically?
4. What is the performance of the motion installation system?
5. How can the performance of the motion compensation system be improved?

1.4. SCOPE

This thesis will focus on the installation and not on the construction phase of an offshore WTG. The installation of a complete WTG, consisting of the tower, nacelle and three blades is divided into two phases. Phase one comprises the installation of the monopile and transition piece. Phase two consists of the installation of the WTG including the tower, nacelle and blades. Only the second phase is considered. First, the WTG is assembled onshore and loaded onto a floating asset. The components of a WTG can be partly or fully assembled onshore in different configurations. Different assembly configurations require different transportation and installation configurations. After sailing to site the components are transported and connected onto a foundation. The permanent connection of all components will be assured and the vessel will sail back to shore after which the cycle starts again. All installation steps for a jack-up are schematically shown in Figure 1.3. Assumed is the tower, nacelle and blades are not pre-assembled. The steps which are within the scope of this research are shown within the red box of Figure 1.3. The goal is to replace the red box. A new configuration developed by Boskalis for installing the tower, nacelle and blades will be used in this thesis. The tower and nacelle are pre-assembled and the three blades are vertically positioned against the tower in a blade rack, see Appendix A. From now on, this configuration is referred to as the carousel configuration. This configuration can be installed onto the foundation after which the blades are detached from the blade rack and lifted into the hub with an internal lifting tool. This system will not be developed in more detail. The scope starts with the carousel WTG positioned on deck attached to sea-fastening. The sea-fastening is not part of the scope and will not be designed for. Decommissioning will also be no part of the scope.

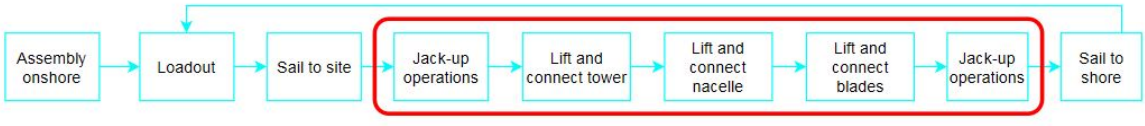

Figure 1.3: Overview of WTG installation steps with a jack up. Thesis scope within the red box

Only the installation from floating vessels without the use of a crane will be within the scope of this research. A floating vessel, since this is new and innovative compared to a jack-up. And floating can overcome limitations such as water depth and soil characteristics. Much research has been performed on installing a WTG with a crane from a floating vessel. For now, this has only been achieved in calm weather conditions. In North Sea conditions this has not been achieved yet. A crane on a floating vessel will induce high motions between the WTG and foundation resulting in a challenging installation. Therefore, a floating vessel in combination with a crane will not be researched here.

Only the installation of WTGs on bottom founded structures and in particular monopiles and jackets will be within this research. This, since installing a WTG from a vessel onto a foundation is assumed to be simpler than installing it onto a bottom founded foundation. This, since relative motions between the vessel and foundation can be minimized. The different bottom founded foundations used in offshore wind are monopiles, Gravity Based Structures (GBS), tripods, suction buckets and jackets. Only monopiles and jackets are considered since the major part of the wind turbine foundations consists of these foundations. There is special a interest in monopile foundations since it holds the largest share, see Figure 1.4.

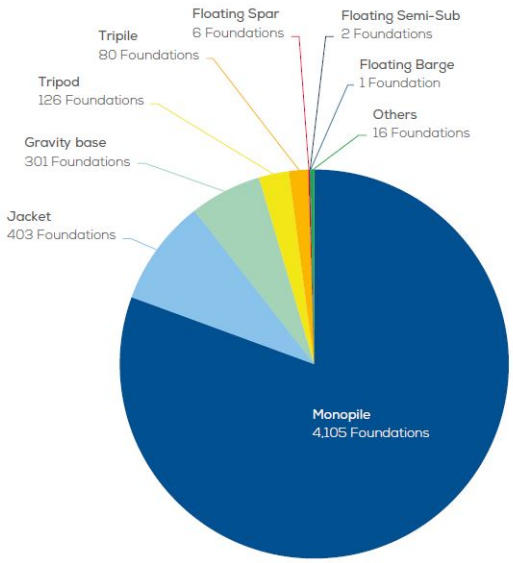

Figure 1.4: Share of substructures types for grid-connected offshore wind turbines at the end of 2018 [1]

1.5. REPORT STRUCTURE

To reach the objective set, the following steps are adopted in this report.

- First, a problem analysis is conducted in which existing installation problems and the proposed solutions are discussed, see Chapter 2.
- Design inputs consisting of design criteria, a reference WTG, standards and guidelines are discussed in Chapter 3. Also, a site with environmental conditions which is designed for is given.
- In Chapter 4, a vessel dynamics analysis is performed in which the dynamic behaviour of two vessels with the partly assembled WTG on deck is assessed. Octopus SEAWAY is used for this analysis. From this assessment, the most suitable Boskalis vessel including the offloading location is given.
- In Chapter 5, different concepts are developed and discussed in detail. To determine the most feasible concept, a Multi-Criteria Analysis is conducted. The MCA is backed up by a survey among Boskalis employees and by listing the technical challenges, advantages and disadvantages of each concept.
- The most feasible concepts are analysed on their technical challenges, see Chapter 6. One concept is chosen based on this concept development.
- In Chapter 7, the most feasible concept is described by five parameters. Three indices are used to indicate the kinematic performance a parameter set. By conducting a kinematic optimization, the most optimal design can be found. At last, a sensitivity analysis is conducted to assess the optimal design's sensitivity to changing design parameters.
- At last, the optimal design is modelled in MATLAB and Simulink, see Chapter 8. A hydraulic system and a passive system are modelled. Insights into the motion compensation efficiency, remaining motions and required power are gained. Besides, the added benefit of including a passive system besides the active system is assessed.

2

PROBLEM ANALYSIS

Ever since the first offshore WTG has been installed the slogan *"Bigger is better"* has been adopted by the industry, as shown in Figure 2.1. This slogan is true since bigger turbines with a larger rotor diameter extract more energy from the wind. With the same amount of turbines installed, higher total power capacity can be reached. Also, the trend of larger wind farms installed in deeper waters can be observed. These trends bring cost reduction because foundation cost do not rise in proportion to the size of a WTG. Besides, maintenance, grid connection and electrical control systems are almost independent of the size [6]. The trends in offshore WTGs are discussed more elaborate in Subsection 3.2.

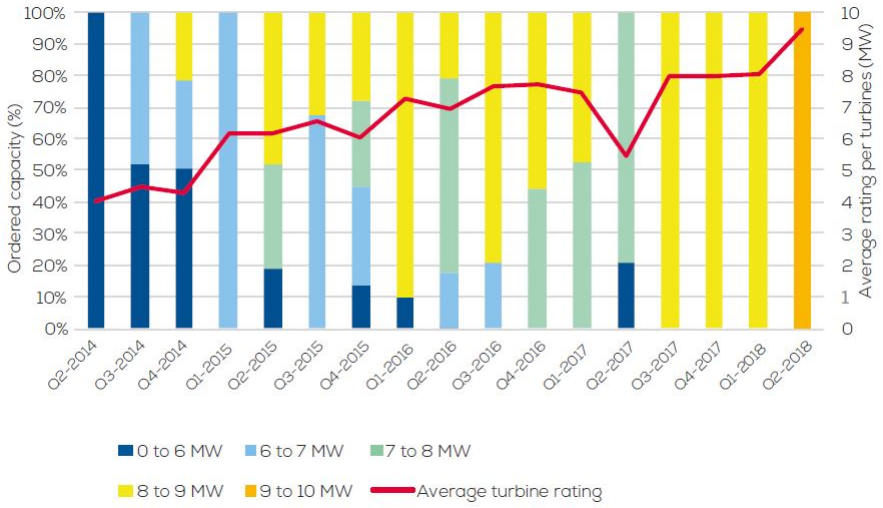

Figure 2.1: Ordered offshore wind turbine power rating in Europe [7]

2.1. PROBLEM

Turbine manufacturers such as Siemens, Vestas and General Electric have expanded the size of turbines ever since the first turbine was installed. Much faster as expected by jack-up owners. To keep up with the ever-increasing size of turbines, companies have been building larger vessels and upgrading exiting vessels. It seems the industry has underestimated the pace of this trend in the past and the challenges it generates. Building an asset which costs about 300 million USD requires a long asset lifetime. With the current pace of the offshore wind trends it is a gamble to construct such an asset with the possibility of it being too small and not being able to lift future wind turbines or being too big and the asset economics will not add up. Some vessels have been upgraded to install larger turbines but upgrading the assets does not fix the job for future generation turbines. Much research has been done to develop more efficient and less costly methods to install future turbines. From improving the jack-up method which uses crane operations to installation from a floating asset.

Focusing on the installation phase, the most used method of installation is a jack-up. Different companies and institutions acknowledge that jack-up vessels might no longer fix the job as WTG size, mass and installed depth increases. Transitioning from jack-ups to a floating installation vessels might be the solution to cope with the ongoing size expansion of turbines and to set forward the trend of increasing the total installed offshore wind capacity.

2.2. PROPOSED SOLUTIONS

Several innovative floating concepts have been proposed to compete against a jack-up. The most promising concepts which use floating vessels will briefly be discussed below.

Ulstein has developed the Ulstein Windlifter concept [8] as shown in Figure 2.2a. A dynamically positioned vessel which can store up to four fully assembled wind turbines. With the use of a mechanical, modular skidding system a WTG is skid onto a foundation. This concept seems technically challenging because of several factors. The support structure which holds the wind turbines is located only at the lower part of the tower, resulting in huge overturning moments on the support structure. Besides, without any motion compensation, the motions at the nacelle will be high. The motions of the vessel relative to the foundation need to be minimal and the skidding system will have to resist huge loads from the WTGs. Nevertheless, the idea to install WTGs without using a crane and installing fully assembled wind turbines will drastically reduce investment cost and reduce installation time. Also, since this concept might be feasible on an existing floating asset overcoming the limitations of a jack-up.

Huisman developed the Wind Turbine Shuttle concept, a SWATH (Small Water Plane Area Twin Hull) type vessel [9]. A SWATH has the characteristic of having low vessel motions. This concept uses a DP3 system in combination with a heave compensation system to keep the WTGs stationary. With this concept, the motions and accelerations at the top of the towers are significantly reduced compared to the Ulstein concept. As seen in Figure 2.2b, it can carry up to two fully assembled WTGs. The concept has its limits at a 1000 t turbine which is approximately 8 MW. Huisman opted to build a multipurpose vessel which can also install different type of foundations, achieving a better tender position. With high workability to decrease downtime, the concept is claimed to increase the efficiency of turbine installation resulting in a reduction of installation time [9]. A major drawback for this concept is that a new vessel must be constructed which comes with a huge capital investment. This compared to the solution of Ulstein which might be constructed by adjusting an existing vessel, reducing the capital expenses significantly.

(a) Ulstein Wind Lifter [8] (b) Huisman Shuttle [9]

Figure 2.2: Innovative concepts for WTG installation

3

Design Input

In this chapter, the inputs for the design will be discussed. First, the design criteria which are the boundary conditions for this design process will be given. After that, based on the ongoing trends in WTG dimensions, the reference turbine which will be designed for is given. All standards and guidelines used during this design will be given. At last, the location and corresponding environmental conditions, which the design has to be employable in, are discussed.

3.1. Design Criteria

The following design criteria are set. These criteria are boundary conditions to which the concept must be designed.

- Attachable onto an existing floating vessel
- Competitive to jack-up
- Install next generation WTG
- Install WTG in a pre-assembled carousel configuration
- Install WTG onto monopiles and jackets
- Employable during installation season in North Sea conditions
- Carry at least 2 WTGs
- No crane is used

As stated in Chapter 2, the concept must be attachable onto an existing floating asset. This to install the next generation wind turbine, to avoid the dependence on depth and soil and to reduce installation time and capital cost. This all will make the design competitive to a jack-up. The competitiveness of the concept can be increased by reducing investment and operating cost and having better tender perspectives than a jack-up vessel. A possibility to reduce investment costs is to adjust an existing vessel and attach the new concept on it. A possibility to reduce operational cost can be a combination of installing the next generation WTG in the pre-assembled carousel configuration and being employable during the installation season in North Sea conditions, April to August. The next generation offshore WTG is the reference turbine as described in Section 3.2.

Operational expenses depend heavily on the number of turbines per sail out. Carrying 2 instead of 1 WTG lowers the cost per turbine by a factor 1.5. Starting from 2 WTGs, installing WTGs is assumed to be cost-effective. This will be elaborated more in Section 4.1. Having less CAPEX and OPEX together with being able to install larger WTGs than the competition, the concept will be highly competitive. As stated in Chapter 2, the usage of a crane is without the scope. Holding on to all the design criteria will make the design a competitive and innovative installation method.

3.2. REFERENCE WIND TURBINE GENERATOR

The concept design will be performed for a reference WTG. The dimensions of this WTG will be set by investigating the trends of WTG dimensions in the offshore wind industry. The trends are also used to get an insight into the future proofness of the jack-up installation method and to get an insight into the required specifications of the innovative concept. The trends will be used to introduce the predicted future WTG which will be used as a reference WTG to design for.

TRENDS

The following trends will be researched in which the last three are coherently involved in each other:

- Increase in water depth
- Increase in hub height
- Increase in rotor diameter
- Increase in MW per turbine

Water depth - With the most ideal sites already being occupied the trend of wind farms being constructed further offshore with increasing water depths can be found. This results in a more challenging construction and installation of turbines. Especially with the bottom founded installation method of a jack-up.

MW per turbine - Starting from the half-megawatt turbines used in 1991 for the first offshore wind farm to the currently largest turbine of 8.8 MW installed the generator size has increased ever since. Since the start of 2018, all WTGs ordered have a capacity of 8 to 9.5 MW [7], see Figure 1.1 and Figure 2.1. Also, one can see the trend of increasing average turbine rating over the past years. Starting with 4 MW in 2014 going to 9.5 MW in 2018. The ones ordered in 2018 are expected to be commissioned until 2022. GE Renewable Electrics plans to commercialize a 12 MW turbine in 2021, the Haliade-X. This turbine has a rotor diameter and hub height of respectively 220 and 150 m [10]. Based on the specific power output the rated capacity is likely to increase.

Hub height - In the past, the increase in hub height enabled WTG manufacturers to increase other parameters such as rotor diameter which resulted in more energy production per turbine. However, an increase in hub height means an increase in loads on installation equipment. Cranes on jack-ups cannot lift turbine with higher hub heights. For this reason, it is expected that the hub height will not undergo major developments in the coming years.

Rotor diameter - The increase in hub height implies an increase in rotor diameter which equals a larger swept area. More swept area results in higher energy extraction potential. The rotor diameters have been increased from several meters with the first turbine to nowadays the 220 m of the Haliade-X. The rotor area increases with the square of the rotor diameter. This means a turbine with twice the rotor diameter has four times higher rated capacity. Since the rated capacity is likely to increase, expected is the trend of increasing rotor diameter also continues. This however at much smaller pace than the rated capacity.

As stated before, the "bigger is better" trend in the development of WTGs has so far proved true. More energy is extracted with the same amount of turbines. Nevertheless, there is an optimum in increasing the size of turbines. More energy extraction per turbine means less construction and installation of foundations, towers and array cables. Together with higher annual energy production, this will reduce the cost significantly. Meanwhile, the investment costs of a new and larger turbine are huge. GE spends about 400 million on the development and deployment of the Haliade-X [10]. Also, the blade cost appears to be a limiting factor. Thus, the optimum is a trade-off between cost reduction and cost increase of larger turbines. Expected is this optimum lies within the range of 10 to 13 MW for offshore wind farms of 500 MW [11].

The innovative concept will be designed to install the reference WTG of which its specifications can be found in Appendix A. This WTG is inspired by the Haliade-X, since this is the largest WTG designed so far. To increase its future proofness the Haliade-X design has been adjusted to be more conservative, meaning having larger dimensions. The largest jack-up under construction, the Voltaire, will be the only one capable of lifting this WTG. Thus, designing a new installation system has high economic potential. Table 3.1 shows the acceleration limits of the nacelle in a transport frame. Since a transport frame might not be part of the design, these limits are up to changes depending on the design. Only the nacelle's CoG acceleration limits are given since the acceleration in the nacelle will be the highest and will be the first to be exceeded. This because of the large height or arm the nacelle is located at.

In Table 3.1 the foundation specifications are also given. The foundation diameter is the same as the diameter of the lower part of the tower. The height above Mean Sea Level (MSL) of the foundation is taken as 20 m. This is approximately required for a jacket which is more than required for a monopile. Hence, to comply for both foundation types, the height required for a jacket is chosen. At last, Table 3.1 shows the used steel. The tower is made of S355 steel with a yield strength of 335 MPa. This is the strength of S355 for thicknesses between 40 and 63 mm [12]. This matches with the bottom and top tower thickness of respectively 50 and 40 mm

Table 3.1: Acceleration limits and foundation specifications, 1 $g = 9.81\ m/s$

Component	Criteria	Value
Nacelle	Longitudinal acceleration	[redacted] g
	Transversal acceleration	[redacted] g
	Vertical acceleration	[redacted] g
Foundation	Height above MSL	20 m
	Diameter	8 m
S355 Steel	Yield limit σ_y	335 MPa
	E-modulus E	210 GPa
	Poisson ratio ν	0.3
	Density ρ	7850 kg/m^3

3.3. IMPACT VELOCITY

During installation, the WTG needs to be set down on the TP. To make sure no permanent damage or plastic deformation occurs, a maximum allowable impact velocity must be set. Two methods are used to calculate this velocity which both assume the impact is transferred into purely axial elastic deformation. First, the *Joukowsky equation* for solids is used, see Equation 3.1. This equation calculates the stress by impact. The equation depends on the density ρ, Elastic modulus E and the wave speed c in the solid. σ_{max} is the maximum allowable stress with a safety factor of 0.6 for axial force [AISC] being 201 MPa. With the inputs as given in Table 3.1 the maximum allowable impact velocity calculated is 5 m/s

$$\sigma_{max} = -\rho \cdot c \cdot v_{max} \qquad c = \sqrt{\frac{E}{\rho}} \quad [13] \tag{3.1}$$

The second method makes use of an energy equilibrium. Assuming ideal conditions, the setting down of the WTG on the TP can be seen as an elastic response. Assumed is the energy before impact, kinetic energy E_k, is fully converted into elastic deformation energy which is the spring deformation energy E_p. Setting them equal to each other gives Equation 3.2.

$$E_k = E_p \tag{3.2}$$

Combining the following Equations gives the final expression of maximal allowable impact velocity, see Equation 3.3. L is the total length of the tower, A is the surface area, m the mass of the WTG The maximum allowable impact velocity calculated is 3.9 m/s

$$\begin{aligned} \frac{1}{2} m v_{max}^2 &= \frac{1}{2} k x_{max}^2 \\ x_{max} &= \frac{F_{max}}{k} \\ F_{max} &= \sigma_{max} \cdot A \\ k &= \frac{EA}{L} \end{aligned}$$

$$v_{max} = \frac{\sigma_{max} \cdot A}{\sqrt{m \cdot k}} \tag{3.3}$$

Method 1 and 2 result in velocities of respectively 5 and 3.9 m/s. These velocities are rather high and do not seem reasonable. However, these high results can be explained by the following. Method 1 only account for purely elastic strain in the material, overestimating the allowable impact velocity. For method 2, the assumption of the elastic strain taken by the total tower, thus k being rather small, gives high maximum velocities. Also, these methods assume full contact between the two cylinders, while in real-life only part of the areas may have contact. Since these two methods do not take into account limiting factors such as local buckling and local plastic deformation, the maximum allowable set-down velocity will be based on experience. By applying the experience of Boskalis with installing jackets on this installing case, the limit of set-down velocity is set at 0.05 m/s.

3.4. STANDARDS & GUIDELINES

For this research, different standards and guidelines are used. The complete list of standards and guidelines is shown below and will be cited throughout this thesis. The clearance between a vessel and a foundation is a critical parameter because of its significant influence on the concept design and selection. Setting the clearance at a minimum of 10 m and adding 4 m for monopile radius adds up to 14 m between the centre of the monopile and the vessel's side. Using a float over will then result in a required 18 m of the gap in the vessel. These clearances will increase when the foundation is a jacket. This because the underwater part of a jacket is under an angle. Thus, the horizontal distance between the bottom of the vessel and the jacket is leading. An increase in clearance will also increase the overturning moments exerted on the installation system and will reduce the stability of the vessel. Hence, the clearance must be as low as possible. The standards state that the required clearance depends on multiple factors such as capabilities of the DP system, environmental conditions and fendering [OS-H205]. For this design, the clearance between vessel and TP is set at 5 m.

- DNV-OS-H204 Offshore Installation Operations
- DNV-OS-H205 Lifting Operations
- DNVGL-CG-0194 Hydraulic Cylinders
- DNVGL-RP-H102 Marine Operations During Removal of Offshore Installations
- DNVGL-RP-H103 Modelling and Analyses of Marine Operations
- DNVGL-RP-C202 Buckling Strength of Shells
- DNVGL-RP-C205 Environmental Conditions and Environmental Loads
- DNVGL-RU-SHIP Pt.3 Ch.1
- AISC Specification for Structural Steel Buildings

3.5. SELECTED SITE

The Dogger Bank is chosen as the installation location, see Figure 3.1. This location is chosen because it has harsh North Sea conditions. Thus, if a concept is employable in these conditions, other sites in the North Sea can be serviced too. This site has promising prospects because the site is in the UK, Netherlands, Germany and Denmark with large planned capacity [14]. A scatter diagram is computed from a time-series ranging from 1997 to 2006 with 3-hourly wave data. This diagram is shown in Appendix B. At this site, the bathymetry ranges from 15 to 36 m. For this entire research, a water depth of 30 m is chosen.

Figure 3.1: Dogger bank

3.6. LIMITING DESIGN CONDITIONS

To be highly competitive to a jack-up, the design must at least be able to install at the same limiting design conditions as a jack-up. As stated in Section 1.2, the limiting design conditions of the largest jack-up ever under construction is at a significant wave height of 2 m with a wave period ranging from 6 to 8 s [3]. Besides, a mean wind speed at 10 m elevation of 15 m/s with maximum wind gusts of 25 m/s is set as limiting. These limits are also set for the innovative concept design, see Table 3.2. As stated before, the design must be employable in North sea conditions during installation season. Approximately ranging from April to August. To also take into account uncertainties in both monitoring and forecasting of environmental conditions an α-factor is taken into account. For waves and wind respectively 0.84 and 0.80 [DNV-OS-H101].

Table 3.2: Limiting environmental conditions

Parameter	H_s	T_p	Wind speed	Wind gusts	Current speed
Value	2 m	8 s	15 m/s	25 m/s	1 m/s

The theoretical energy spectra to represent these ocean waves is the JONSWAP spectrum which is a never fully developed spectrum. The spectrum has variables H_s and T_p. Equation 3.4 with inputs of Equations 3.5 represents this spectrum [DNV-RP-H103]. Another option is the Pierson-Moskowitz spectrum. This spectrum is similar to the JONSWAP spectrum. However, the JONSWAP spectrum continues to grow over distance and time because of the A_j term and the peak is more pronounced because of the γ term. JONSWAP is chosen over Pierson-Moskowitz because JONSWAP's characteristics better suit the Dogger bank. For this entire research, all the waves are assumed to be unidirectional. Also known as a long-crested sea, all waves are coming from the same direction.

$$S_\zeta(\omega) = \frac{320 \cdot H_s^2}{T_p^4} \cdot \omega^{-5} \cdot e^{\frac{-1950}{T_p^4} \cdot \omega^{-4}} \cdot \gamma^{A_j} \tag{3.4}$$

$$\gamma = 3.3 \quad A_j = e^{-\left(\frac{\frac{\omega}{\omega_p} - 2}{0.08\sqrt{2}}\right)^2} \quad \omega_p = \frac{2\pi}{T_p} \tag{3.5}$$

H_s = Significant wave height — ω = Wave frequency — γ^{A_j} = Peak enhancement factor

T_p = Wave peak period — ω_p = Peak wave frequency — $S_\zeta(\omega)$ = Spectrum

4

Dynamic Analysis of Installation Vessels

In this chapter, the wave-induced motions and dynamic behaviour of a vessel on which a WTG is loaded will be researched. The assessed motions include displacements, velocities and acceleration. The assessment gives insight into the extent to which motion compensation is required. Besides, it gives an insight into the behaviour of a vessel with a WTG on deck. The assessment will be conducted for two different Boskalis vessels with a turbine at two different locations. The vessels are the Mighty Servant 1 and the White Marlin, see Appendix D. A WTG is positioned at two locations where the WTG can be offloaded onto a foundation, see Figure 4.1. The first location, starboard, is at midship. The second location, the stern, is located at the origin of the axis system.

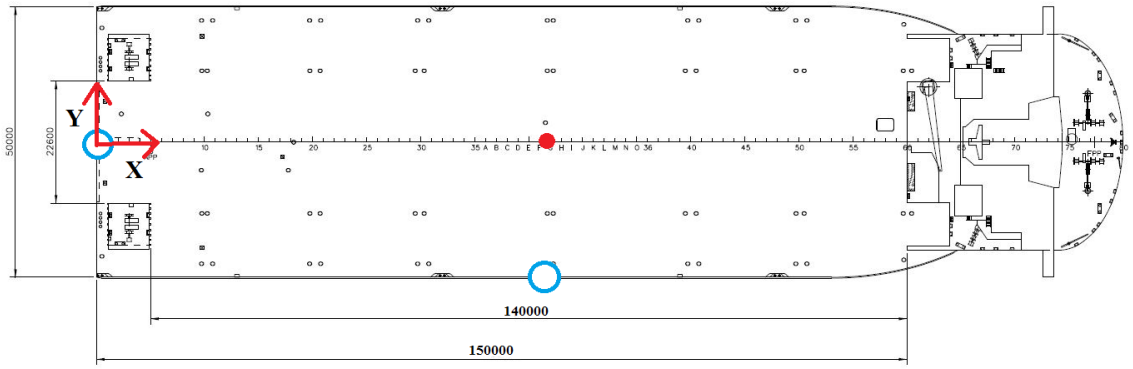

Figure 4.1: Mighty Servant 1 top view with blue indicating the offloading locations starboard and stern. Red point indicates CoG of combined vessel and WTG. Larger figure in Appendix D

For each location, two measurement points will be set at which the motions will be computed. The first point is at the bottom of the tower, this to get insight into the required capabilities of a possible motion compensation system attached to the bottom of the tower. The second point is at the nacelle's CoG, this to get insight into the nacelle's accelerations and whether they are below the limits as set in Section 3.2. Since the WTG needs to be installed on a 20 m high TP, the bottom of the WTG is positioned at this height above MSL. Table 4.1 shows all options of vessel, WTG offloading location and motion measurement point on the turbine with given coordinates. All combinations of options are assessed.

Table 4.1: All options of vessels, WTG offloading locations and motion measurement points on the WTG with given coordinates. All combinations of options are assessed.

Vessel	Offloading location	Measurement point	Coordinates x,y,z
Mighty Servant	Starboard	Tower bottom	80,-25,28
		Nacelle CoG	80,-25,153
	Stern	Tower bottom	0,0,28
		Nacelle CoG	0,0,153
White Marlin	Starboard	Tower bottom	103,-31.5,29
		Nacelle CoG	103,-31,5,154
	Stern	Tower bottom	0,0,29
		Nacelle CoG	0,0,154

One WTG will be stationed on deck instead of multiple. With one WTG the GM is higher than with multiple turbines which results in greater initial stability against overturning. The higher GM also results in a lower natural roll period. The natural roll period of the vessel with one WTG loaded on deck is located more in the vicinity of the peak period of the wave spectrum than the natural roll period of the vessel with more WTGs. This results in higher motions for the case of one WTG on deck. Hence, one turbine on deck will be the extreme load case for the displacements, velocities and accelerations. Another reason to analyze the vessel with one turbine is that during installation there will always be a moment where only one last turbine is left on the deck to be installed.

The considered vessels are semi-submersible heavy transport vessels. This vessel type is chosen because of its suitable characteristic for installing WTGs. These characteristics are large deck space, ballast capacity and high breadth/draft ratio with a large waterplane area thus increasing stability. The Mighty Servant 1 and White Marlin are chosen because of their diversity in dimensions and capacity and their feasibility to carry a WTG. Larger vessels such as the Vanguard are not considered because of its overcapacity and high day-rates.

4.1. COST

Before going into depth with vessel dynamics, an economic assessment is conducted. This, to support the decision process in which the most feasible vessel for installing WTGs is made. Figure 4.2 shows costs per WTG as a function of the number of WTGs per sail out. These cost comprise multiple factors which can be found in Appendix C. One can see a steep decline in cost when installing two instead of one turbine per sail out. The Mighty Servant 1 is more cost-effective with two WTGs than the White Marlin is with six. This is due to the significant higher day-rate of the White Marlin. The cost build up is shown in Appendix C.

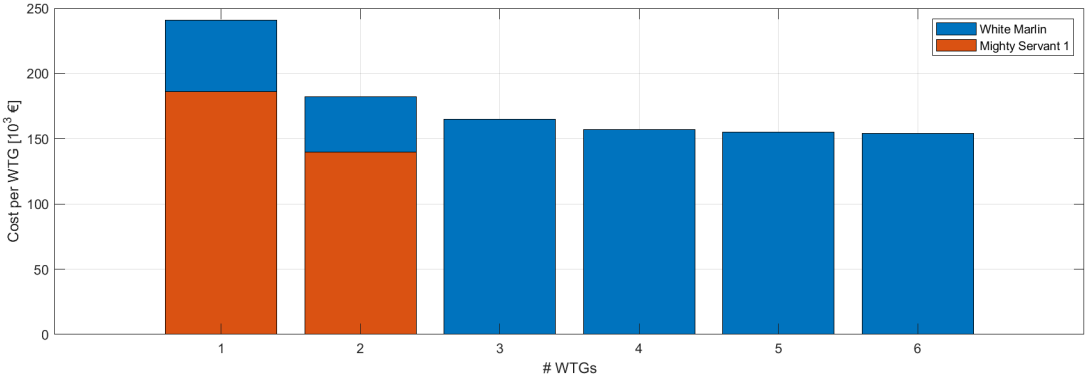

Figure 4.2: Cost comparison between Mighty Servant 1 and White Marlin. Number of WTGs per sail out.

4.2. STABILITY

Previously conducted research by Boskalis [15], in which stability checks are done, showed that the Mighty Servant 1 and White Marlin can carry respectively 2 and 6 turbines in the carousel configuration. Carrying more WTGs results in non compliance of the stability criteria. The stability can be improved by adjusting vessel characteristics by for example adding sponsons to the vessel. As stated in Section 3.1, a design which can install a minimum of 2 WTGs is required to enable economically feasible installation. Hence, a design which can install 2 WTGs will be designed for. However, this dynamic analyses will be conducted for one WTG as that is the most severe case regarding the wave-induced motions.

4.3. SOFTWARE AND MODEL

The software used for the dynamic analysis is OCTOPUS Seaway 5.2.16. This is a hydrodynamic analysis program which computes vessel motions in the frequency-domain. It uses linear strip theory to calculate hydrodynamic loads, wave-induced loads, motions, added resistance and internal loads for six degrees of freedom. This for regular and irregular waves in deep and shallow water depths [16]. With linear strip theory, the vessel is divided into multiple cross-sections. The program solves the 3D problem of hydro-mechanical and exciting wave forces and moments on a vessel by integrating the 2D potential solutions over the vessels length. Finally, the differential equations will be solved to obtain the motions. In this model, the fluid is considered homogeneous, incompressible, free of surface tension and irrotational. Only the external loads on the underwater part are considered, thus wind loads are not considered. When neglecting other environmental conditions, constant wind will give a constant offset in for example roll. Since only gusts have a significant influence on the dynamics, neglecting wind is assumed acceptable. To support this decision, hand calculations are performed which showed that the overturning moment by wind is small compared to the underwater forces and moments. Neglecting viscous effects can deliver significant problems when computing roll motions around the resonance frequencies. Therefore, by adding viscous roll damping components to the roll damping coefficient the viscous effects in roll direction are taken into account. This will be explained in more detail in Section 4.4. The vessel motions are supposed to be small, relative to the cross-sectional dimensions of the vessel since strip theory is based on linearity. Strip theory and its limitations have been researched in the past. It is found that despite the limitations, strip theories are the most successful and practical tools for computing the wave-induced motions of a vessel at an early design stage [17].

4.4. INPUT SEAWAY

The input parameters and settings used in OCTOPUS Seaway are discussed below.

Vessel characteristics - A hull model of the vessel is used as input. This hull model is an existing Boskalis Seaway hull. In Seaway the hull is considered rigid. The Mighty Servant 1 and the White Marlin are drafted to respectively 8 and 9 m with no initial heel or trim which correspond to the operating conditions. The ballast tanks filled as in operational conditions and assumed is that the ballast tanks are completely full or empty resulting in zero free surface correction. The KG values are calculated by multiplying the vessel, tower, nacelle and blades masses by their keel to CoG (KG) distance and dividing it by the sum of the masses.

Radii of gyrations - are input parameters which have a significant influence on the computed dynamic behaviour of the vessels. The radii of gyration are divided into a vessel part and a WTG part. Adding both results in the complete radius of gyration. All moments of inertia of all separate WTG parts are calculated. The radii of gyration of the vessels are retrieved from available Boskalis data and converted to moment of inertia. These radii of gyration are computed with the ballast tanks filled as in operational conditions. Steiner's theorem, see Equation 4.1, is used to convert the moment of inertia of the vessel and WTG parts from their COG to the overall CoG of vessel and WTG. Afterwards, the moments of inertia are converted with Equation 4.2 to radii of gyration. Both equations apply to the x direction are also applicable to the y direction. An overview of all radii of gyration can be found in Table 4.2.

$$I_x = I_0 + m \cdot d_x^2 \tag{4.1}$$

$$k_{xx} = \sqrt{\frac{I_x}{m}} \tag{4.2}$$

m = Mass

I_0 = Moment of inertia

d_x = X displacement from own to overall CoG

I_x = Displaced moment of inertia

k_{xx} = Radius of gyration

Table 4.2: Radii of gyration of vessels with one WTG at starboard or stern

Vessel	**Radii of gyration**	**Starboard** $[m]$	**Stern** $[m]$
Mighty Servant 1	k_{xx}	26.00	25.59
	k_{yy}	47.30	49.50
	k_{zz}	42.99	45.17
White Marlin	k_{xx}	24.97	24.54
	k_{yy}	53.19	55.28
	k_{zz}	51.54	53.12

Regular waves - Regular waves are used to compute the RAOs in all six degrees of freedom of the vessel. To get these RAOs, which are frequency dependent, the waves spectrum is discretized with frequencies between 0.05 and 2.5 rad/s. This, with a step size of 0.05 rad/s. Following from the displacement RAOs, the acceleration RAOs are derived by using Equation 4.3.

$$RAO_{\ddot{x}}(\omega) = \omega^2 \cdot RAO_x(\omega) \tag{4.3}$$

Irregular waves - The RAOs following from the regular waves are used to find the displacements and accelerations. The RAOs are used together with irregular waves, which give a more realistic outcome. The irregular waves come from a JONSWAP spectrum with a T_p between 3 s and 18 s. This covers 99.9 % of the total waves, see Appendix B. By using Equation 4.4, the peak period is converted to zero-crossing period, which can be used as input for Seaway. A significant wave height of 1 m is chosen, resulting in easy computing of displacements and accelerations with higher wave heights. This, since the motions are assumed to be linearly proportional to the wave height. Hence, an acceleration coming from a wave height of 3.5 m can be calculated by simply multiplying the acceleration of a 1 m wave height with 3.5. For the roll, this assumption only holds for small roll angles in comparison with the vessel dimensions. The viscous or non-linear part of roll, which is discussed more elaborate further on, does not follow this linear behaviour. This results in an underestimating of motions for larger waves. The proportionality of this non-linear part is checked in Seaway by computing the viscous part of the roll coefficient and the motions for higher waves. There it is found that the influence of the wave height on this viscous part is not significant for small roll angles. Thus, a linear approach is adopted to calculate motions for higher waves.

$$T_z = 0.777 \cdot T_p \tag{4.4}$$

Vessel speed - is set at zero. This, since during the installation of a WTG the vessel is maintained at one position.

Water depth - influences the wave characteristics and the vessel motions. A water depth of 30 m is chosen, see Section 3.5. The hydrodynamic coefficients can be calculated by the potential theory of Keil or the potential theory of Frank [16]. Keil's theory is used for shallower water depths. Frank's theory is used for deeper waters. For this water depth, both theories can be applied. Frank's theory will be applied because this theory gives slightly higher motions. Thus, by choosing Frank's theory a more conservative approach is adopted.

Roll damping - Roll motions which are only weakly dampened are influenced by viscous effects resulting in a nonlinear roll damping coefficient. An accurate estimation of the roll damping must be made because the natural roll frequency lies within the range of frequencies of the chosen JONSWAP spectrum. Overestimating of the roll damping coefficient results in lower predictions of the roll motions. Underestimating of the roll damping coefficient results in a higher prediction of the roll motions. Hence, a highly accurate estimation of roll damping is required.

A method to determine the roll damping coefficient is the Ikeda-method [16]. Ikeda's method combines several independent effects. This empirical method estimates the viscous roll damping contributions to forward vessel speed, skin friction, eddy making, lift and bilge keels. The method is not sufficiently accurate for vessels with high breadth to draft ratio [18]. Hence, this method will not be used. Along with Ikeda, the roll damping method of Miller can be used to estimate the roll damping coefficient [19]. This method will also not be used since it is designed for slender hull forms. The chosen method computes the total roll damping coefficient at the natural frequency and adds the non-linear part for other frequencies. The total roll damping coefficient is calculated by using Equation 4.5. The inputs for this equation are the linear and quadratic roll damping coefficient respectively κ_1 and κ_2. κ_1 is 0 and κ_2 is 0.35. These values are estimates from existing Boskalis experience. The non-linear part, $\kappa_2 \cdot \phi_a$, is frequency-dependent and depends on the roll amplitude, see Equation 4.5. In the software, an iterative process is used to get the correct total roll damping coefficient for a roll amplitude and frequency of oscillation. For this iteration, a known average wave amplitude is required to get the roll amplitude. The mean amplitude is $1.25\sqrt{m_0}$ and the significant wave height is $4\sqrt{m_0}$. Thus, the mean wave amplitude is 0.3125 times the significant wave height [16].

$$\kappa = \kappa_1 + \kappa_2 \cdot \phi_a \tag{4.5}$$

Wave Directions - The angles of incidence of the waves are between 0 and 180°. This with a 30° step size, giving 7 directions. Because of the vessel symmetry in the X-axis, only one half of a total circle of 360° is considered. For offloading at starboard the difference between 150 and 210° matters. But with 150° being more severe, a conservative approach is taken. Zero degrees is defined as a wave going from stern to bow. Waves going from starboard to portside are defined as 90°.

An overview of the input parameters used in SEAWAY for the motion analysis are given in Table 4.3

Table 4.3: Input parameters Seaway

Parameter	Value	Unit
Peak period band T_p	3 - 18	s
Zero-crossing period band T_z	2.3 - 14	s
Wave frequency band ω	0.05 - 2.5	rad/s
Number of wave components	50	-
Wave directions	0 - 180	deg
Number of wave directions	7	-
Significant wave height H_s	1	m
Water depth	30	m
Vessel speed	0	m/s
κ_1 coefficient	0	-
κ_2 coefficient	0.35	-
KG Mighty Servant 1	11.48	m
Draft Mighty Servant 1	8	m
KG White Marlin	12.99	m
Draft White Marlin	9	m

4.5. RESULTS

Following the motions analysis of the two vessels with a WTG at starboard or the stern, the significant motions and significant accelerations in the X, Y and Z direction are computed. This at the bottom of the tower and the nacelle's CoG. The RAOs, significant displacements and significant accelerations of all combinations of vessels, WTG location and measurement point are given in Appendix E. One should note these motions are without any interference of dynamic position or motion compensation system. These motions originate from the first-order wave forces. The given significant displacements are amplitudes thus if one wants to know the total displacement the amplitude displacements should be multiplied by two. Also, the computed natural periods of heave, roll and pitch for the WTG at the CoG are shown in Table 4.4.

Table 4.4: Natural periods of Mighty Servant 1 and White Marlin with a WTG on deck

Vessel	**Mighty Servant 1**		**White Marlin**	
Offloading location	**Starboard**	**Stern**	**Starboard**	**Stern**
Natural heave period [s]	9.34	9.34	10.29	10.29
Natural roll period [s]	13.05	12.89	10.99	10.85
Natural pitch period [s]	8.93	9.08	9.94	10.06

The results are validated in multiple ways. The RAOs have been checked by comparing them to regular RAOs. An example is the roll RAO which should start at zero and have a peak at the roll natural frequency. And the heave RAO for frequencies going to minus infinity, equivalent to very long waves, should approximately be one. In the results, the value is approximately 0.8 instead of 1. This is probably due to the relative shallow water depth, resulting in elliptical orbits of the water particles instead of circular orbits. These elliptical orbits give less vertical displacement of the water particles than the circular orbits do.

The natural roll periods, see Table 4.4, of the vessels are analytically checked by comparing them to the outcome of Equation 4.6. The unmodified equation to estimate the natural roll period used in literature [20] is adjusted to take added mass into account. The added mass is taken into account into the calculation of the radii of gyration. Hence, adding a part of added mass to the radii of gyration k_{xx}. This equation is used during existing Boskalis projects, so it must be said that this equation is partly based on experience and estimation. The results of the comparison are given in Table 4.5. For both starboard and the stern no significant differences can be found when comparing it to the Seaway results.

$$T_{n,roll} = \frac{2.5 \cdot k_{xx}}{\sqrt{GM}} \tag{4.6}$$

Table 4.5: Comparison of natural periods calculated with analytical or computational method. This for the Mighty Servant 1 and White Marlin with a WTG at starboard or the stern

Vessel	**Mighty Servant 1**		**White Marlin**	
Offloading location	**Starboard**	**Stern**	**Starboard**	**Stern**
Computational [s]	13.05	12.89	10.99	10.85
Analytical [s]	13.40	13.19	11.59	11.39

To compare the vessels, all Figures in Appendix E are assessed. The Y-direction is the direction in which the motions are the highest and the accelerations are the closest to the nacelle limits. To have a clear overview of all data and to compare the two vessels, the significant displacements and accelerations in Y-direction in the nacelle are given in Figure 4.3. The difference in height and location of the peaks can be explained by the different natural roll periods of the vessels, see Table 4.4. The White Marlin's natural roll period is lower than the one of the Mighty Servant 1. The natural roll period of the White Marlin is located more in the high spectral density part of the wave spectra resulting in higher displacements and accelerations closer to resonance.

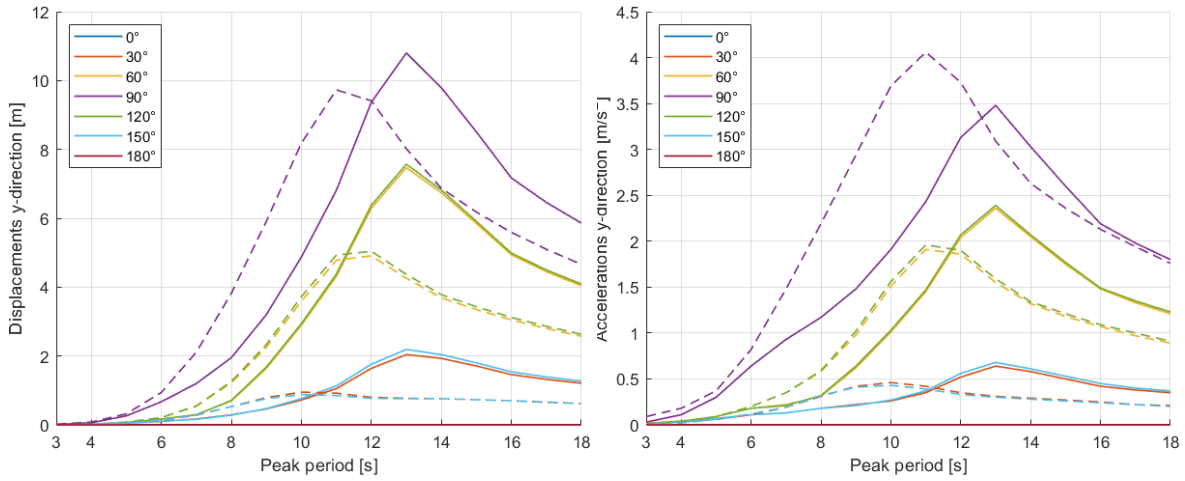

(a) Amplitude significant displacements

(b) Significant accelerations

Figure 4.3: Significant Y-direction motions in nacelle, Mighty Servant 1 (Continuous line) and White Marlin (Dotted line) with a turbine at starboard. H_s 1 m.

4.6. NACELLE LIMITS

The results of Seaway are given as significant motions coming from the significant wave height of 1 meter. To check the nacelle acceleration limits, the maximum acceleration instead of the significant accelerations must be used. The maximum wave height is calculated with Equation 4.7 for a 3-hour storm. This equation uses a Rayleigh distribution in which the number of waves, which is 3 hour or 3*60*60 seconds divided by the zero-crossing period of the waves, determine the factor to go from significant wave height H_s to maximum wave height H_{max}. With a T_p of 8 s, the factor to go from H_s to H_{max} is 1.93. As discussed before, to compute the maximum accelerations at a maximum wave height the significant acceleration at 1 m can be multiplied by the maximum wave height.

$$H_{max} = \sqrt{\frac{1}{2}\ln\left(\frac{3\cdot 60\cdot 60}{0.777 T_p}\right)} \cdot H_s \text{ [18]} \tag{4.7}$$

As set in Section 3.6, the operational limits of jack-ups are a H_s of 2 m and peak period of 8 s. The maximum accelerations with these conditions are shown in Table 4.6. The 150° angle is the second most ideal angle of incidence and should be checked according to the DNV-standards. This, since 150° unidirectional waves will be more representative to a real-life multi-directional wave spectrum. Waves will not be exactly unidirectional with one incident wave angle. Furthermore, 180° gives zero motions in Y-direction which, due to the multi-directional waves, will not be the case in real-life. The 90° angle is also shown to give insight into the most severe angle of incidence. The 120° angle is given as an intermediate step. One has to note that these maximum accelerations are for a maximum wave height of 1.93 × 2 m and a peak period of 8 s. Obviously, increasing the wave height will result in all accelerations going over the set limits.

Table 4.6: Comparing vessels on maximum accelerations of nacelle in X, Y and Z direction. Limit exceeding indicated in red. H_{max} 3.86 m. T_p 8 s. Wave directions 90°, 120°, 150° and 180°

	90°			120°			150°			180°		
Vessel and WTG location	**X**	**Y**	**Z**	**X**	**Y**	**Z**	**X**	**Y**	**Z**	**X**	**Y**	**Z**
Mighty Servant 1 starboard [m/s^2]	0.23	4.52	1.20	1.31	1.24	0.27	0.62	0.69	0.23	0.81	0	0.15
Mighty Servant 1 stern [m/s^2]	0.23	4.59	0.58	1.47	1.51	0.73	0.62	0.77	0.39	0.77	0	0.54
White Marlin 1 starboard [m/s^2]	0.42	8.45	1.89	0.73	2.28	0.50	0.42	1.24	0.31	0.62	0	0.08
White Marlin 1 stern [m/s^2]	0.19	8.65	0.35	0.77	2.39	0.42	0.42	1.31	0.23	0.62	0	0.46

4.7. CONCLUSION

For both vessels, the displacements and accelerations are the highest at the natural frequencies. This results in technical challenges when encountering waves with frequencies near the natural frequencies. The natural periods of both vessels are relatively high. However, at the North Sea during the summer period, the probability of occurrence of high peak periods together with high waves is low.

The highest displacements and accelerations can be found in the nacelle because of the long arm with respect to the CoG. Thus, reducing the distance between the nacelle and the CoG results in lower displacement and acceleration. As expected, waves coming in perpendicular to the length of the vessels, 90°, result in the highest and most severe roll motions resulting in high displacements and accelerations. These accelerations also exceed or are close to the nacelle limits as set by the manufacturer. Thus, the vessel's heading must avoid the 90° incident wave direction. As shown in Table 4.6, all accelerations in the nacelle for 120°, 150° and 180° incident wave direction do not exceed the nacelle limits as set in Table 3.1. The preferred heading of the vessel will be with an incident wave angle of 180° because on average this gives the lowest motions. However, an incident wave angle of 150° is chosen for further calculations. This, since 150° unidirectional waves will be more representative to a real-life multi-directional wave spectrum. Waves will not be exactly unidirectional with one incident wave angle. Furthermore, 180° gives zero motions in Y-direction which, due to the multi-directional waves, will not be the case in real-life. Concluding, when avoiding the 90° angles no motion compensation is required to keep the nacelle accelerations below the limits. However, to keep the vertical velocity of the WTG below the impact velocity, compensating the wave-induced motions thus reducing the motions of the WTG is inevitable.

Mighty Servant 1 vs White Marlin - To compare the two vessels, all Figures in Appendix E are assessed. The vessels are compared on peak periods below 8 *s* because higher periods change the dynamic behaviour significantly, those peak periods do not occur often in the North Sea installation period and jack-ups can also not install beyond 8 *s*. As shown in Figure 4.3, the differences in displacements and accelerations depend on the vessel, the peak period and incident wave direction. One can see that the differences between the vessels reduce for lower peak periods, below the natural frequencies of the vessels. At frequencies closer to the natural frequencies, the differences become more significant. This especially for the 90° angle. The motions beyond 10 *s* are less important since these high peak periods rarely occur at the North Sea and are not within the environmental design criteria.

To have a clear overview Table 4.7 is presented. Here the maximum motions, thus not the significant motions, for the preferred incident wave angle of 150° with operational limits of 2 m H_s and 8 s T_p are given. This for the displacement and accelerations at deck and nacelle height with a WTG at starboard or the stern. For comparison, the difference between the significant and maximum motions is irrelevant because the same proportionals remain.

Table 4.7: Overview of maximum displacements (amplitude) and accelerations in X, Y and Z-direction for operating conditions. H_s 2 m. T_p 8 s. Wave direction 150°

	Displacement $[m]$						**Acceleration** $[m/s^2]$					
	Deck height			**Nacelle CoG**			**Deck height**			**Nacelle CoG**		
Vessel and WTG location	**X**	**Y**	**Z**	**X**	**Y**	**Z**	**X**	**Y**	**Z**	**X**	**Y**	**Z**
Mighty Servant 1 starboard	0.23	0.12	0.43	1.00	1.08	0.42	0.15	0.12	0.23	0.62	0.69	0.23
White Marlin starboard	0.15	0.12	0.62	0.59	4.11	1.41	0.12	0.15	0.31	0.42	1.24	0.31
Mighty Servant 1 stern	0.23	0.35	0.70	0.66	2.05	0.62	0.15	0.19	0.39	0.62	0.77	0.39
White Marlin stern	0.19	0.26	0.48	0.63	4.48	0.48	0.11	0.33	0.26	0.42	1.31	0.23

The following results can be found when assessing Table 4.7.

X-direction - The White Marlin has lower displacements and accelerations than the Mighty Servant 1. However, this difference is less significant than the differences in motions for the Y and Z-direction.

Y-direction - The highest displacements and accelerations in the nacelle occur in the Y-direction. In this direction, the Mighty Servant 1 perform significantly better than the White Marlin. This is because the White Marlin's lower natural period is more located in the high-density part of the spectrum than the natural period of the Mighty Servant 1.

Z-direction - The Mighty Servant 1 performs significantly better than the White Marlin when offloading at starboard. The White Marlin significantly performs better than the Mighty Servant 1 when offloading at the stern.

Besides the dynamic behaviour, economics should be taken into account. As has been discussed in Section 4.1, the Mighty Servant 1 is more cost effective with lower installation cost per WTG than the White Marlin. This as expected since the White Marlin is a much larger vessel with a higher day-rate.

In conclusion, the Mighty Servant 1 is chosen as the preferred vessel over the White Marlin for the installation of a WTG because of the results shown above. This vessel has better sea-keeping characteristics with a WTG loaded on board especially for the most important DoF, roll. Besides, the Mighty Servant 1 is more cost effective.

Starboard vs Stern - After choosing the Mighty Servant 1 and when considering peak periods below 10 *s* with 150° angle, starboard is the preferred location for offloading. Under these conditions, starboard has significant lower displacements and accelerations in X, Y and Z-direction, see Table 4.7.

5

BASIC DESIGN

5.1. METHODOLOGY

First, a divergent approach is adopted to construct multiple concepts. Afterwards, a convergent approach is adopted to select the most feasible concept. To design the most feasible concept, different steps are taken. First, the functional requirements for the most essential functions of a new installation method will be set. Options to fulfil these requirements will be discussed. With the use of a morphological overview, multiple concepts will be conceived. The technical challenges of each concept will be discussed. To reduce the number of concepts a combination of a Multi-Criteria Analysis (MCA), a survey among Boskalis employees and the technical challenges of each concept will be used, see Figure 5.1. For the MCA, the Analytic Hierarchy Process (AHP) is used, see Section 5.4. One should note, a concept will not directly be chosen only based on having the highest score in the MCA. The selection must also be backed up by the survey among Boskalis employees and the technical challenges with the advantages and disadvantages of each concept. After the selection, the selected concepts will be developed into more detail and their technical challenges will be addressed.

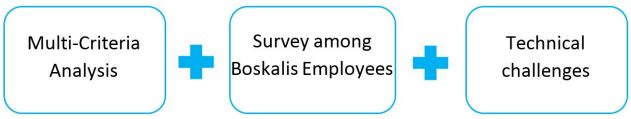

Figure 5.1: Building blocks used for the selection of the most feasible concepts

5.2. FUNCTIONAL REQUIREMENTS

The following functional requirements are set for the design.

- Reduce motions WTG
- Orientate WTG
- Vertical transport WTG
- Horizontal transport WTG
- Vessel station-keeping

A functional requirement can have an option, a way to fulfil the requirement, which can also partly or completely fulfil another requirement. For example, A motion compensation system can be used for reducing the motions of the WTG and for vertical transportation. Thus, one should take into account the relation between the functional requirements. One option to fulfil a requirement might need an option from another requirement. For example, a support structure will only reduce deflection motions of the WTG but not the motions induced by the vessel. Thus, this option requires an extra option to compensate the WTG motion for example, two X-Y tables. The options to fulfil these functional requirements are given below. An overview of the functional requirements with the options can be found in Table 5.1.

REDUCE MOTIONS WTG

The motions of the WTG should be reduced because of the following three reasons:

1. Acceleration limits of the tower, nacelle and blades
2. Relative motion to the foundation
3. Fatigue

The acceleration of several components of the WTG must be limited because exceeding these limits could cause damage to the components. These limits are set by turbine manufactures for the tower, nacelle and blades. Expected is that the nacelle will undergo the highest accelerations due to its high position at the top of the pre-assembled turbine. The relative motions of the WTG to the foundation should also be reduced. This since impact with high velocities results in huge impact forces, potentially damaging the components. Also, the cycled loading must be minimized to reduce fatigue damage and increase the residual lifetime. The options defined below are options for the installation system. Thus, adjustments to the vessel like a bilge keel or an anti-roll tank are not considered.

- WTG support structure
- WTG moored to vessel
- Active motion compensation (AMC)
- Passive motion compensation (PMC)
- Tuned Mass Damper (TMD)

Both active and passive motion compensation are techniques used in offshore operations to reduce environmental influences. The difference lies in the active motion compensation system having a control system that actively controls the system with external energy. This, while passive motion compensation reacts to an external force without additional external energy to control the motion. A Tuned Mass Damper (TMD) is a device which reduces the amplitude of the vibrations of the WTG.

ORIENTATE WTG

The orientation of the WTG during transportation, installation and final configuration on the foundation might differ. Therefore, orientating of the WTG is required. The required orientation is determined by the orientation of the TP because some components of the WTG have a designed orientation with respect to the transition piece. The options to rotate the WTG to its final orientation are:

- Rotate tower
- Active motion compensation with yaw
- Change heading vessel

The WTG can be orientated by rotating the tower without rotating the installation system. The WTG can also be orientated with an AMC system, given that this system can control yaw motions. Changing the heading of the vessel is the last option proposed. This could be achieved by using thrusters. For all options, the WTG can be orientated during loadout. When knowing the environmental conditions one can estimate the optimal heading of the vessel at the installation site. Thus, knowing the orientation of the WTG on the vessel with respect to the foundation. Anticipating on this, the WTG can be orientated during loadout to have a near correct orientation when installing.

VERTICAL TRANSPORT WTG

The foundation height and the height at which the bottom of the tower is located differ. To complete the installation, the bottom of the tower must equal the foundation height.

- Ballast vessel
- Active Motion Compensation
- Inclined skidding
- Mechanical lift

Ballasting the vessel can change the draft of the vessel, thus changing the WTG height. However, ballasting the vessel is a time-consuming activity. The AMC, which is also an option for other functional requirements, can also be used to transport the WTG vertically. When using a skidding system to transport horizontally an inclination can be added to enable vertical transport. This option will require a highly robust skidding system. At last, a mechanical lift can be used.

HORIZONTAL TRANSPORT WTG

To install the WTG it has to be transported from the vessel onto the foundation. As stated in 3.1, no crane will be used for this process. The following options are defined:

- Skidding system
- Float-over
- Extending arm
- Rotate mechanism
- X-Y table

The first option is a skidding system which enables precise horizontal transportation of heavy loads. Another option is to float the vessel over the foundation, a float-over. This will require an opening or additional support structures at the vessel's edge. Using an arm which can be extended to move the turbine atop of a foundation is another option. With the use of a tower or rotating mechanism, the turbine can be lifted and transported above the foundation by turning. At last, X-Y tables will allow horizontal motions along an X and Y-axis by using linear slides. X-Y tables are also used in the proposed solution of IHC, see Section 2.2.

VESSEL STATION-KEEPING

The installation vessel requires station-keeping to maintain a certain distance between the vessel and the foundation. Drifting off will exceed the limits of the horizontal transportation option chosen. Approaching the foundation and hitting it will cause damage to the foundation, WTG and vessel. Mooring the vessel to the foundation is not considered a feasible option because this is highly time consuming.

- Dynamic Positioning
- Connect vessel to foundation
- Ballast vessel
- Spud pole

DP can control the surge, sway and yaw motions. Connecting the vessel to the foundation can reduce motions in the same DoF as the DP. Besides, it will enable a more secure and stable connection between the vessel and the foundation. Such as connection requires spring and damping systems to reduce the forces exerted on the vessel or TP and preventing damage between either of them. A gripper frame can also connect the vessel to the foundation. Nowadays a gripper frame is mostly used for the installation of monopiles. Mooring is another option to construct a connection. Mooring will also require additional spring and damper systems. Another option is ballasting the vessel. This can minimize vessel motions thus reducing the extent to which further station keeping is required. However, this effect will be insignificant and ballasting the vessel too much will decrease the stability of the vessel. At last, a spud pole can be used for vessel station-keeping. A spud pole enables a connection between the vessel and the seabed.

5.2.1. MORPHOLOGICAL OVERVIEW

The functional requirements and options are presented in a morphological overview, see Table 5.1. Different concepts will be defined by combining options for functional requirements.

Table 5.1: Morphological overview with different options to fulfil the functional requirements

Requirement	**Options**				
Reduce motions WTG	Support structure	WTG moored to vessel	AMC	PMC	TMD
Orientate WTG	Rotate tower	AMC	Vessel heading		
Vertical transport WTG	Ballast vessel	AMC	Inclined skidding	Mechanical lift	
Horizontal transport WTG	Skidding system	Float-over	Extending arm	Rotate mechanism	X-Y table
Vessel station-keeping	Dynamic Positioning	Connect to foundation	Ballast vessel	Spud pole	

5.3. CONCEPTS

In this section, all concepts following from the morphological overview are given. The concepts are discussed and the technical drawbacks are listed. All concepts are sketched in Autodesk Inventor 2020 to give a clear view and thorough understanding of the concepts. As discussed in Section 4.7, the offloading location is starboard. However, some concepts are drawn at the stern to give a clearer view. The concepts conceived from the Morphological overview can be found in 5.2. Below each concept, the main technical drawbacks are listed.

Table 5.2: Concepts conceived from morphological overview

Concept | Requirement	Reduce WTG motions	Orientate WTG	Vertical transport	Horizontal transport	Vessel station-keeping
1 Hexapod	AMC	Rotate tower	AMC	Skidding system	DP
2 Double tower	Support structure	Vessel heading	Mechanical lift	X-Y table	DP
3 Skidding tower	Support structure	Vessel heading	Mechanical lift	X-Y table	DP
4 Wind spirit one side	AMC	Vessel heading	Mechanical lift	Extending arm	DP
5 Wind spirit float over	AMC	Vessel heading	Mechanical lift	Extending arms	DP
6 Rotating and lifting tower	Support structure	Rotate tower	Mechanical lift	X-Y table	DP
7 Hexapod float-over	AMC	AMC	AMC	Float-over	Connect vessel to foundation
8 Hexapod on extending arm	AMC	AMC	AMC	Skidding system	DP

5.3.1. CONCEPT 1, HEXAPOD SKIDDING

The first concept uses an Active Motion Compensation (AMC) system to reduce the motions of the WTG, see Figure 5.2. This AMC system will also be used for vertical transportation. A flange between the end of the skidding beam and TP will reduce the overturning moment on the hexapod. Besides, the more the WTG is skidded towards the TP the more the motions remain. This, since the TP can be seen as a rigid body. The turbine will be orientated by rotating the tower around its base. A DP system will keep the vessel in position.

- High vertical forces on AMC system
- High overturning moments on AMC system when transporting the WTG horizontally
- Connection to the TP

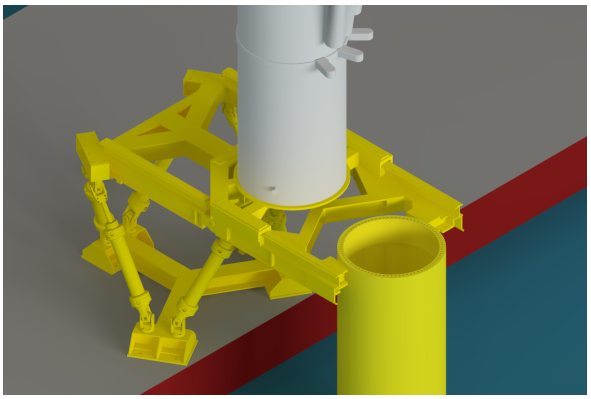

Figure 5.2: Concept 1, Hexapod skidding

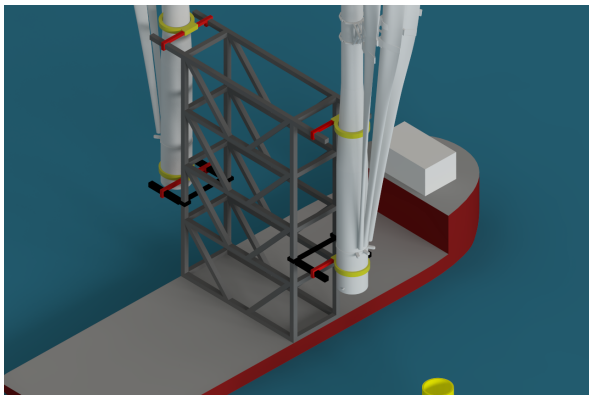

Figure 5.3: Concept 2, Double tower

5.3.2. CONCEPT 2, DOUBLE TOWER

In concept 2 the WTGs are supported by a high structure, see Figure 5.3. This structure can hold 2 turbines and does not have to be reloaded to install more WTGs. The tower has four grippers which include an X-Y table thus ensuring horizontal transport and motion compensation. A mechanical lift in these tables provide vertical transport. A DP system will keep the vessel in position. The correct orientation of the WTG will be ensured by changing the vessel's heading. This concept is inspired by the Huisman shuttle, see Figure 2.2b.

- Large support structure on deck
- High deck loads
- Instability after installing one of the two turbines

5.3.3. CONCEPT 3, SKIDDING TOWER

Concept 3, Figure 5.4, is similar to concept 2. However, the tower carries one turbine and can be skidded on deck. The tower is skidded toward a WTG which is sea-fastened after which is grabs and transports it to the foundation. Hence, reloading of the system is possible. As in concept 2, this concept uses two X-Y tables, a DP system and by changing the vessel's heading the correct orientation of the WTG will be ensured.

- Large support structure on deck
- Skidding with a large tower

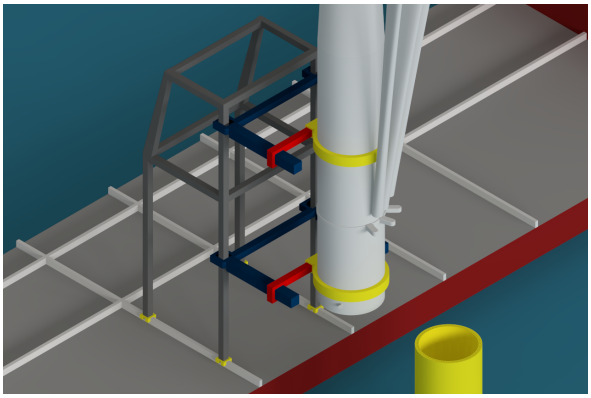

Figure 5.4: Concept 3, Skidding tower

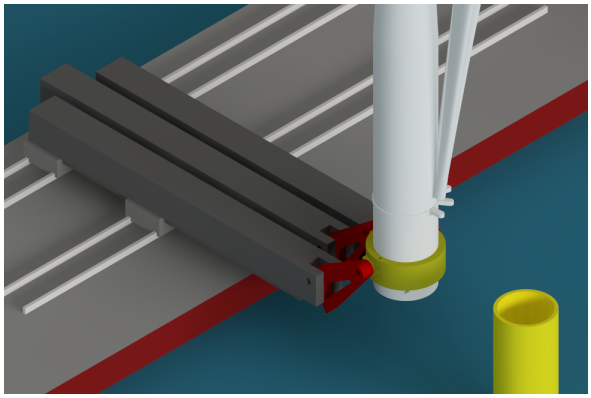

Figure 5.5: Concept 4, Wind spirit one side

5.3.4. CONCEPT 4, WIND SPIRIT ONE SIDE

This concept, Figure 5.5, will use an extending arm with a mechanical lift at the end. This to ensure respectively horizontal and vertical transportation. The mechanical lift proposed is a swivel-arm system at the beams end. By extending the arm outside the vessel the WTG can be stationed over the foundation after which it is lowered with the mechanical lift. This process will be controlled by an AMC within the arm to reduce the motions. The connection of the swivel-arm and the tower will be done with a clamping system. This connection requires ball joints to enable roll, pitch and yaw motion. A DP system will keep the vessel in position. This concept is inspired by the Pioneering Spirit, a vessel operated by Allseas.

- High overturning moments on connection between arm and vessel
- High overturning moments on clamping system
- Three heavy arms also require motion compensation

5.3.5. CONCEPT 5, WIND SPIRIT FLOAT OVER

This concept, Figure 5.6, almost equals the previous concept in Subsection 5.3.4. They differ since this concept uses two extending arms 180 degrees opposite to each other. This with extending arms placed perpendicular to the length of the vessel over an opening at the stern. A float-over is considered but using this concept with a structure extending beyond the stern is also possible. The WTG can be lowered with a mechanical lift at the end of the arms. A DP system will keep the vessel in position.

- Adjustments to vessel to create an opening and enable a float-over or extend beyond the vessel's edge
- High overturning moments on clamping system
- Two heavy arms also require motion compensation

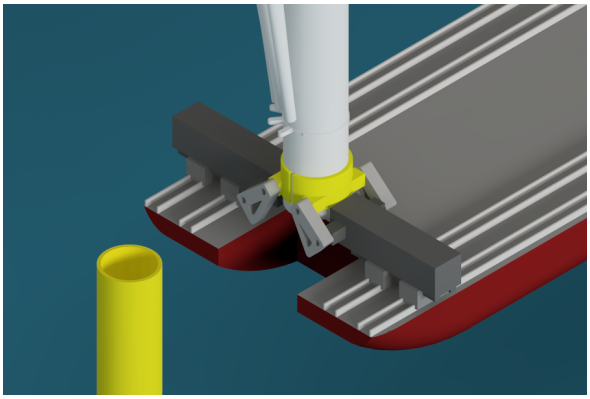

Figure 5.6: Concept 5, Wind spirit float over

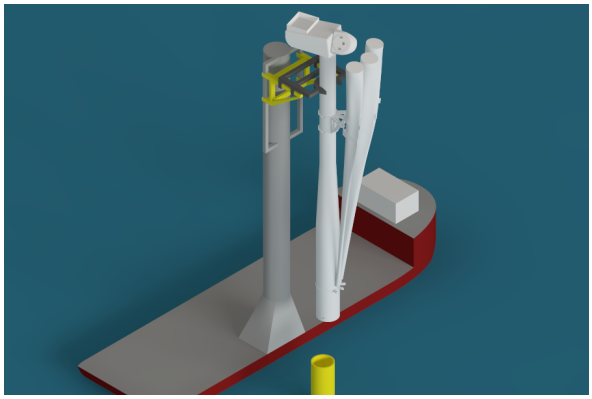

Figure 5.7: Concept 6, Rotating and lifting tower

5.3.6. CONCEPT 6, ROTATING AND LIFTING TOWER

This concept, Figure 5.7, consists of a tower with a clamping mechanism which can mechanically lift the WTG. The tower can rotate which results in horizontal transportation of the WTG. By using the tower and the X-Y table the tower can be correctly orientated. A DP system is required for vessel station-keeping.

- X-Y table and vertical transportation equipment at high height
- Large tower on deck

5.3.7. CONCEPT 7, HEXAPOD FLOAT-OVER

This concept, Figure 5.8, will mainly rely on its AMC system. This to reduce the motions, orientate and vertically transport the WTG. This requires the AMC system to yaw. The vessel will connect to the foundation with a gripper to have station-keeping characteristics. The horizontal transport will be done by a float-over in combination with a skidding system. This requires an opening in the vessel's edge or a structure which extends beyond the vessel's edge.

- High dependence on AMC system
- Hard to achieve correct orientation and location of hydraulic cylinders

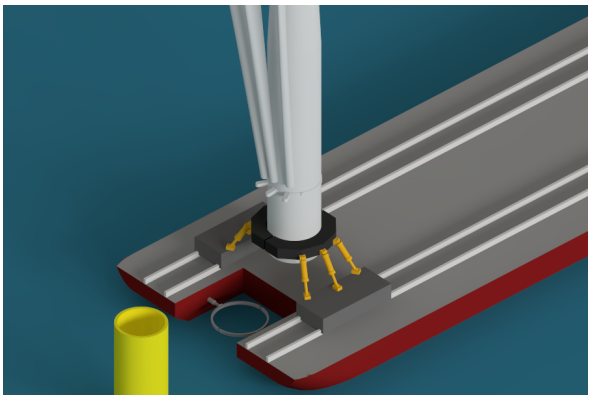

Figure 5.8: Concept 7, Hexapod float-over

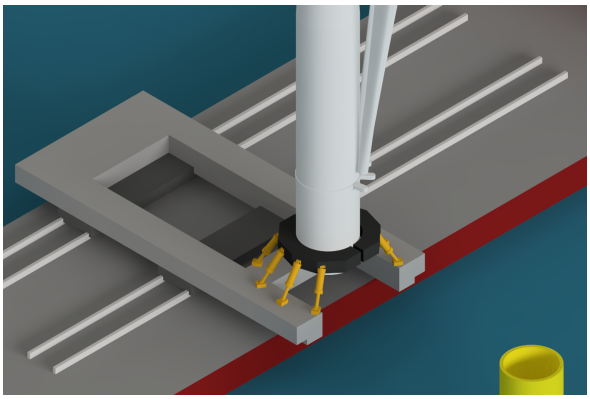

Figure 5.9: Concept 8, Hexapod on extending arm

5.3.8. CONCEPT 8, HEXAPOD ON EXTENDING ARM

This concept, Figure 5.9, will mainly rely on its AMC system. This to reduce the motions, orientate and vertically transport the WTG. This requires the AMC to yaw. A DP system will keep the vessel in position. This concept differs from Concept 7 in the way the horizontal transport is done. The horizontal transport will be done by extending the arm which is on an X-Y table. No float-over is required in this concept.

- High dependence on AMC system
- Hard to achieve correct orientation and location of hydraulic cylinders

5.4. MULTI CRITERIA ANALYSES

Hereafter, a convergent approach will be adopted to reduce the number of concepts. The criteria which are used during the Multi-Criteria Analyses (MCA) are defined and discussed below. An overview is given in Table 5.3. Economics will not directly be taken into account in this MCA. Nevertheless, a concept which can quickly install future WTGs from an existing vessel will probably have low investment and operational costs thus being economically feasible. The criteria will be assessed based on sub-criteria. One should note, this assessment is qualitative since on forehand no exact data is available about the different concepts.

Table 5.3: Criteria for MCA with sub-criteria

Criteria	**Sub-criteria**			
Technical feasibility	Compensate dynamics WTG	Structural integrity	Station-keeping capabilities	
Applicable for future WTGs	Install reference turbine	Adaptability	Scalability	
Installation time per WTG	Workability	Preparation time	Operation time	Deck logistics
Attachable to existing vessel	Structural integrity vessel	Deployment time	Vessel Modifications	System size
HSE	Operations	Decommissioning	Risks at failure	Redundancy

Technical feasibility - is the first criteria of the MCA. The criteria is added since installing a WTG from a floating vessel and without the use of a crane has not been performed yet. Technical feasibility accounts for several sub-criteria. The extent to which a concept can compensate for the dynamics of the WTG and keep it station with respect to the foundation will be assessed. Besides dynamics, the feasibility of achieving structural integrity will be taken into account.

Applicable for future WTGs - is key for a concept to be future proof and to operate during its full-service life. This will make the concept more competitive to a jack-up. As a minimum requirement, the concept needs to install the reference turbine as defined in Section 3.2. This criterion will also be assessed on the adaptability to install other sized WTGs and the scalability to install more WTGs in one sail out.

Installation time per WTG - will affect operational expenses and thus the competitiveness of a concept. This criterion will be assessed on the time required for preparations and skidding or lifting operations. Also, the expected amount of down-time because of weather conditions, also known as workability, will be assessed. Deck logistics will ensure easy and fast reloading of the turbine installation system.

Attachable to existing vessel - takes into account the quality and ease of being attachable on an existing vessel. This enables the vessel to be multi purpose with fast deployment. Attachable to existing vessel is evaluated on the required modifications and the structural integrity of the vessel. Also, the deployment time and system size are assessed.

HSE - (Health, Safety and Environment) enables sustainability, low environmental impact and a safe working environment. This criterion is evaluated by assessing the skidding or lifting operations on risk at failure, required time and redundancy. Also, decommissioning possibilities for WTGs and for the system itself will be taken into account.

5.4.1. ANALYTIC HIERARCHY PROCESS

For selecting the most feasible concept the Analytic Hierarchy Process (AHP) method is used [21]. This method is chosen because it uses pair-wise comparisons, simplifying the selection. Furthermore, with the AHP method, a quantitative analysis can be conducted. This method will be used as a decision support tool and not just for selecting the most feasible concept. Thus, the final scores will only indicate which concepts are the most feasible [22]. The decision will also be made by the assessment of the other blocks shown in Figure 5.1.

To increase the value and quality of the AHP a survey is conducted among Boskalis employees. The diverse group employees consisted of senior structural, hydraulic, installation, R&D and project engineers. With the experience and expertise of the employees, a primary indication of the concept ranking is made. This indication will back-up the decision process with the AHP.

The input, MATLAB processing script and results of the AHP are shown in Appendix F. The process of conducting the AHP with the input values is regulated with a MATLAB script. This script conducts not only the AHP and gives the output but also calculates the Consistency Index [21]. If the Consistency Index is below 10 % a correct analysis is conducted [21].

The results, shown in Table 5.4, are obtained after evaluating the MCA criteria by using the AHP. Technical feasibility has the highest score. This because of the importance of the combination of the *Compensate dynamics WTG* and *Station-keeping capabilities* sub-criteria. Without these criteria, the motions cannot be reduced so the WTG can not be safely offloaded. Also, *Installation time* and *Attachable on existing vessel* have high weights. This because the economical feasibility is of significant importance. *HSE* is the criteria with the lowest weight. This because, during the concept design, criteria which will make the concept technical and economical feasible are more important. Obviously, *HSE* must always be of the highest importance, but during the design phase more weight is put on the factors which ensure the most feasible concept is chosen.

Table 5.4: Weighing factors for MCA criteria obtained with the AHP

Criteria	**Weight [-]**
Technical feasibility	0.38
Applicable for future WTGs	0.10
Installation time	0.27
Attachable to existing vessel	0.17
HSE	0.08

All concepts are evaluated against each other on the criteria with weighing factors as set in Table 5.4. The results are shown in Table 5.5. One can see, hexapod skidding is the most feasible concept followed by skidding tower and double tower. All three scored well on technical feasibility which has the highest weight. Hexapod skidding scored better on the technical feasibility and the attachable to existing vessel criteria. Especially on reducing the motions of the WTG. The 2 other concepts scored well on the installation time criteria.

Table 5.5: Results of the Analytic Hierarchy Process

#	**Concept**	**Result**	**Rank**
1	Hexapod skidding	0.24	1
2	Double tower	0.17	3
3	Skidding tower	0.19	2
4	Wind spirit	0.08	6
5	Wind spirit float-over	0.11	4
6	Rotating and lifting tower	0.05	8
7	Hexapod float-over	0.10	5
8	Hexapod on extending arm	0.06	7

5.5. CONCLUSION

Concept 1, Hexapod skidding, and concept 3, Skidding tower, have the highest score following the MCA with AHP. Both concepts also scored well in the Boskalis survey. Both have technical challenges which can be dealt with. Therefore concepts 1 and 3 are chosen to be developed further. Despite the high score of concept 2, this concept is not chosen. This because sizing this system up to carry more WTGs per sail out is difficult. Twice the amount of turbines requires twice the amount of systems because of the inability to reload a WTG in the system. This will significantly increase the cost and technical feasibility. Besides the high MCA results, concept 1 and 3 are chosen because of the following advantages. Concept 1 has the benefits of carrying the WTG at the bottom, making it easier to transfer vertical loads and reducing the required amount of motion compensation. Also, this system is proven to work at smaller scale, is relatively small and easy to install on the vessel. The disadvantage of it being the high overturning moment at the bottom. Concept 3 has two clamping system. The higher one reducing the overturning moment on the lower one. But, the high clamping system requires more motion compensation because of the longer arm. An advantage of concept 3 is its adaptability and scalability. Its ease to reload enables installation of multiple WTGs in one sail out. The chosen concepts which will be developed further and assessed on technical challenges are listed below:

- Concept 1, Hexapod skidding
- Concept 3, Skidding tower

6

Concept Development

As discussed in Section 5.5, two are selected, see Figure 6.1. In this chapter, both concepts will be assessed on their critical parts and technical challenges. The concepts will not be assessed on challenges they both encounter such as impact velocity on the foundation, ballasting or fast connection since this will not make one concept more favourable over another. However, an option considered for a fast connection is the flange clamp tool, developed by IHC. This tool temporarily secures the axial connection between the flanges of tower and foundation prior to and during the installation of permanent bolting. Before going into the individual concepts, the motion envelope and the dynamic positioning system of the vessel will be discussed. This, to have a clear overview of the total motion envelope which must be compensated. The concept development is only performed for the Mighty Servant 1 with offloading at starboard. The assessment will be done for the limiting conditions as set in Section 3.6 together with an incident wave angle of 150 degrees.

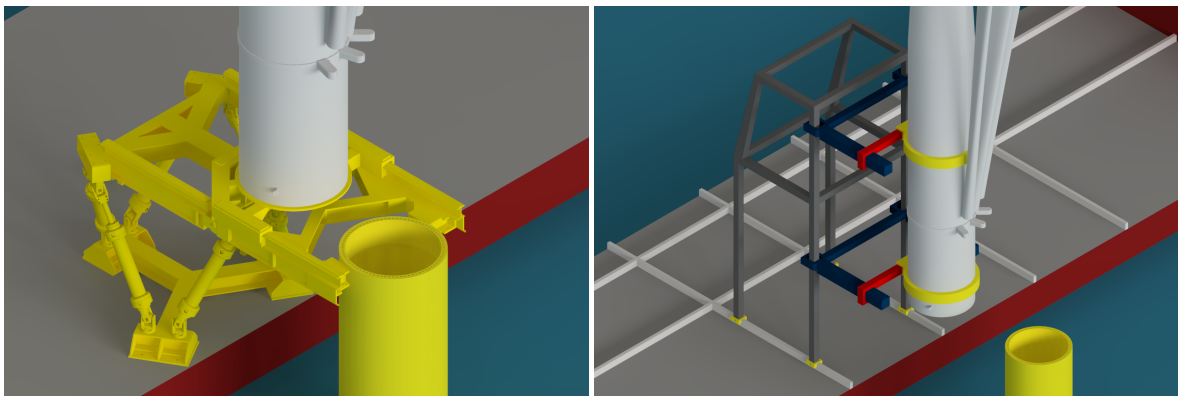

(a) Hexapod skidding (b) Skidding tower

Figure 6.1: Selected concepts for concept development

6.1. Motion Envelope

The motion envelope consists of the maximum motions the concepts will have to compensate. The radii of inertia to compute the motion envelope in Chapter 4 are calculated by adding the inertia of one WTG to the one of the vessel and ballast. When assuming the motion compensation systems in the concepts compensate all motions of the WTG, the WTG is static. When the WTG does not move, its inertia has no significant influence on the vessel motions. Besides, the weight of the WTG can be assumed small compared to the vessels weight and also has no significant influence. In real-life this will not be the case since there will be a dynamic coupling between the WTG and the vessel. However, for preliminary calculations this approach suffices. If after compensation, the motions of the WTG remain significant, the mass and inertia of the WTG can not be neglected. This will be the case for more severe sea-states or a system with low motion compensation capabilities.

To compute the motion envelope for both concepts, the radii of gyration and KG value of the vessel without a WTG, which is the same as a vessel with one motion compensated WTG, are used. The same explanation as stated in Chapter 4 applies to the decision to choose zero WTGs as the most severe condition. See Table 6.1 for the values used in the SEAWAY runs. Besides those values, the same inputs and assumptions as stated in Chapter 4 are used.

Vessel	k_{xx} [m]	k_{yy} [m]	k_{zz} [m]	KG [m]
Mighty Servant 1	15.93	43.50	43.50	8

Table 6.1: Radii of gyration and KG of Mighty Servant 1 with one motion compensated WTG loaded on deck.

Following from the vessel motion analysis in Seaway, the motion envelope is computed. This envelope consists of maximum motions which are the significant motions multiplied by 1.93. This 1.93 factor is calculated and explained in 4.7. To take into account the uncertainty of monitoring and forecasting of environmental conditions, an α-factor of 0.84 has been taken into account to make sure the systems do not operate at limiting environmental conditions [DNV-OS-H101]. The motions are divided by the α-factor to get the final motions. These motions consist solely of first-order wave motions. No second-order wave motions are taken into account. Table 6.2 shows the maximum motions at deck height and nacelle CoG. Besides the displacement envelope, the translational accelerations are required to give inside in the total motion envelope and to calculate forces and moments, see Table 6.2.

Location	δ_x [m]	δ_y [m]	δ_z [m]	v_x [$\frac{m}{s}$]	v_y [$\frac{m}{s}$]	v_z [$\frac{m}{s}$]	a_x [$\frac{m}{s^2}$]	a_y [$\frac{m}{s^2}$]	a_z [$\frac{m}{s^2}$]
Tower bottom	0.46	0.39	2.47	0.19	0.15	0.97	0.15	0.50	0.73
Nacelle CoG	2.01	12.44	2.47	0.73	4.75	0.97	0.62	4.09	0.73

Table 6.2: Maximum first-order displacements, velocities and accelerations of Mighty Servant 1 with one motion compensated WTG loaded on deck under limiting environmental conditions

To get the complete motion envelope, the error of the dynamic positioning system should be added to the first-order motions. Currently, the Mighty Servant 1 has no DP system. Since designing a DP system is out of the scope of this thesis, the exact system and corresponding DP footprint cannot be computed. Therefore an estimate for the position variances in surge and sway are calculated by using the method of J.M.J. Journée and W.W. Massie [18]. An idealized simplification of the DP system with a PD-controller is made, see Figure 6.2. The DP system is ideal and can be modelled as a spring-damper system with the spring and damper respectively being the P (K_p) and D (K_d) controller. Assumed is the ideal DP system can completely compensate for the mean second-order drift motions originating from the second-order wave drift forces. However, assumed is the position variance of the drift motion cannot be compensated for. One should note this is an ideal primarily estimate of the error which does not take effects such as computational errors, wave effects, thruster-thruster interaction or saturation of the thrusters into account.

The DP system will maintain the change in the vessel's heading minimal around a set location which can be seen as a pivot point. By setting the WTG's CoG as this pivot point location instead of for example the vessel's CoG, the position variance due to yaw is minimized, see Figure 6.2. This, since the arm from the pivot point to the WTG is small. Therefore, the yaw position variance is assumed to be relatively small compared to the first-order motions.

Below, the calculation is explained for the surge direction, indexed by 1 but can also be applied for sway, indexed by 2. First, the spectral density S_F is calculated with Equation 6.1. $S_\zeta(\omega)$ is the wave spectrum for which, as stated before, a JONSWAP spectrum is used. $T(\omega)$ is the Quadratic Transfer Function (QTF) and a is the added mass. Both are retrieved from the Boskalis R&D department which used AQWA to compute the values. The K_1^P can be calculated by Equation 6.2. Knowing the mass m and added mass a, the K_1^P term will be chosen so the natural period in surge direction is about 100 to 200 s, which is advised by literature [18]. The damper term, K_1^D, is calculated with Equation 6.3 and is 60% of the critical damping. To take viscous effects into account, the damping coefficient, $b11$, is assumed to be 5% of the critical damping, see Equation 6.4.

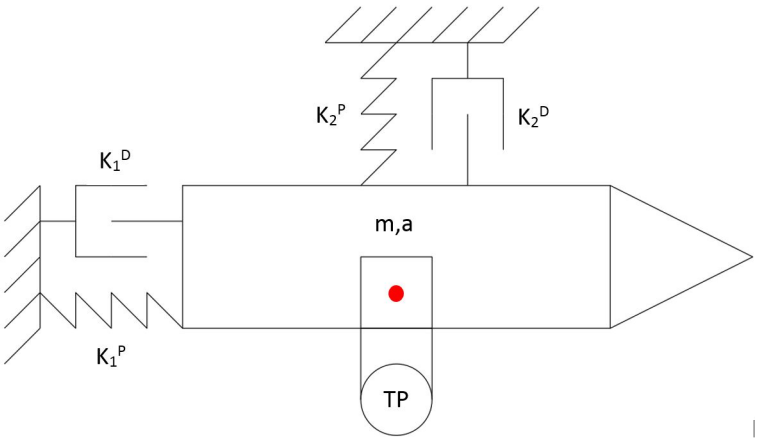

Figure 6.2: DP model of vessel with mass m and added mass a including PD controller for surge (1) and sway (2) with Proportional K_p Derivative term K_d. Red dot indicates the pivoting point set for yaw control.

At last, assumed is the PD-control which uses a Kalman-filter has a conservative time lag (τ) of 1 s. Knowing all input parameters, Equation 6.5 is used to calculate the position variance. This expression is only valid when assuming the DP system keeps the P and D term constant within time, which will not be the case for a more sophisticated DP system.

$$S_F = 8\int_0^\infty S_\zeta(\omega)^2 \cdot |T(\omega)|^2 \, d\omega \tag{6.1}$$

$$K_1^P = (m+a)\cdot(\frac{2\pi}{T_n})^2 \tag{6.2}$$

$$K_1^D = 0.6\cdot 2\sqrt{(m+a)\cdot K_1^P} \tag{6.3}$$

$$b11 = 0.05\cdot\sqrt{(m+a)\cdot K_1^P} \tag{6.4}$$

$$\sigma_x^2 = S_F\cdot\frac{\pi}{2}\cdot(\frac{1}{(b11+K_1^D-K_1^P\cdot\tau)K_1^P}) \tag{6.5}$$

S_F = Force spectrum
$S_\zeta(\omega)$ = Wave spectrum
$T(\omega)$ = Quadratic transfer function
K_1^P = Surge proportional term
K_1^D = Surge derivative term
m = Vessel mass
a = Vessel added mass
b_{11} = Surge damping coefficient
σ_x^2 = Position variance
τ = Time lag

To calculate the maximum position variance, equation 6.6 is used. N is the number of oscillation calculated for a 3-hour storm, by dividing 10800 s by the natural period of the system.

$$\sigma_{x,max}^2 = \sqrt{\sigma_x^2}\cdot\sqrt{2\ln(N)} \text{ [18]} \tag{6.6}$$

Figure 6.3 shows the footprint of position variance versus the natural period of the system. Table 6.3 shows the final displacement motion envelope with the position variance for the average advised natural period, 150 s [18]. These motions are solely translations and no rotational DoF. One should note the total footprint consists of the sum of first-order motions and the position variance of the DP system. At last, no variance for the velocity and accelerations are given since these are small compared to the first-order acceleration. The motion envelope is only given for deck height and nacelle CoG. Motions in other WTG components are found by interpolation.

The total motion envelope values are validated by comparing it to simulation and real-life measured data of the Bokalift 1 during operations. The Bokalift 1 is a similar-sized vessel. No significant or disturbing differences can be found between the data and calculations.

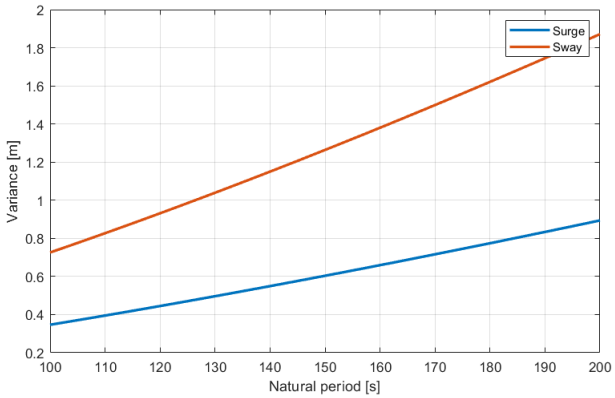

Figure 6.3: Maximum position variance versus natural period of the DP spring damper system

Location	$\delta_x\,[m]$	$\delta_y\,[m]$	$\delta_z\,[m]$	$v_x\,[\frac{m}{s}]$	$v_y\,[\frac{m}{s}]$	$v_z\,[\frac{m}{s}]$	$a_x\,[\frac{m}{s^2}]$	$a_y\,[\frac{m}{s^2}]$	$a_z\,[\frac{m}{s^2}]$
Deck height	1.08	1.68	2.47	0.19	0.15	0.97	0.15	0.50	0.73
Nacelle CoG	2.46	13.73	2.47	0.73	4.75	0.97	0.62	4.09	0.73

Table 6.3: Total maximum motion envelope consisting of the first-order motion and the variance of the DP system

6.2. CONCEPT 1, HEXAPOD

In this section, the technical challenges of concept 1 are discussed. The feasibility of tackling these challenges is assessed by calculations and bench-marking. Besides, the redundancy and fail-safe of the design is researched.

CONTROL 6 DOF

In concept 1 a hexapod also known as a Stewart platform is used to compensate all 6 DoF. It consists of six prismatic actuators. Hydraulic jacks or electrical linear actuators are commonly used. The 6 actuators need to be designed and programmed to work synergistically and all 6 DoF are controlled with this platform.

First, a basic design of the Stewart platform must be made to calculate the loads. This since the loads depend both on the pose of the platform and the design. The platform design is defined by the unit vectors of the cylinders and the location of the connection points between the cylinders and upper platform. All connection points are located on a 15 m diameter circle. See Table 6.4 for all parameters. The Stewart platform's origin is located at the centre of the system with positive y being the offloading direction and positive x being in the bow's direction, see Figure 6.4. The centre of the hexapod is 15 m from the centre of the TP.

Cylinder	**1**	**2**	**3**	**4**	**5**	**6**
X $[m]$	4.616	2.884	-7.5	-7.5	2.884	4.616
Y $[m]$	6	7	1	-1	7	6
L_x	-0.3	0.6	-0.3	-0.3	0.6	-0.3
L_y	0.5	0	-0.5	0.5	0	-0.5
L_z	0.812	0.80	0.812	0.812	0.80	0.812

Table 6.4: Hexapod design. X and Y are the locations of cylinder to upper platform connection. L are unit vectors of cylinders

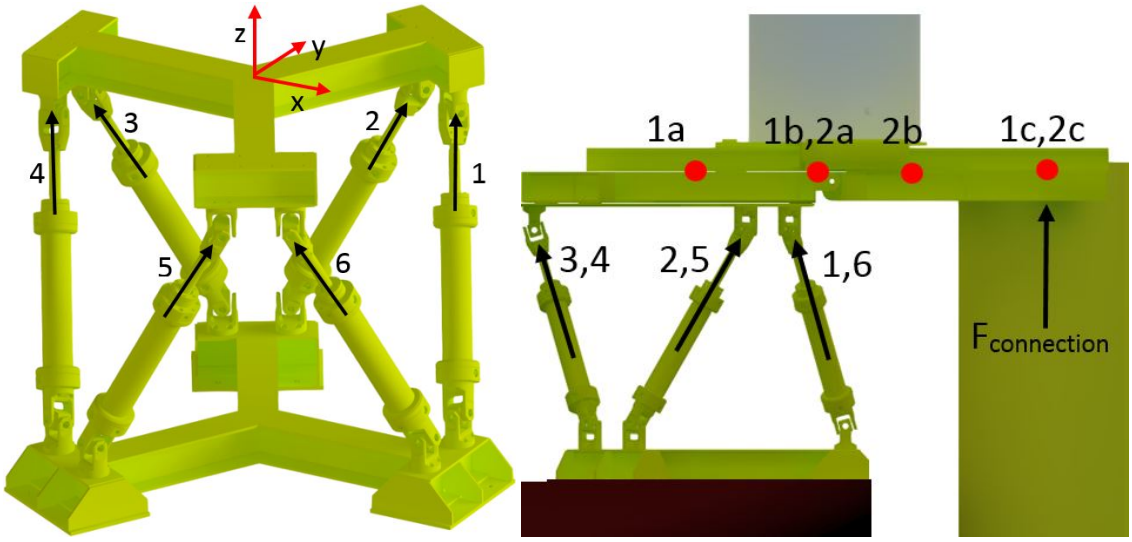

(a) Rotated view. Positive x-direction is the offloading direction (starboard)

(b) Load case 1 is without and load case 2 is with a vertical force connection to the TP. For both load cases, a,b,c indicate the position of the WTG's centre.

Figure 6.4: Schematic overview of axis system of hexapod with axial forces in cylinders and load cases

6.2.1. HYDRAULIC FORCES AND REQUIRED POWER

Since the WTG weighs approximately 2000 t, the six cylinders will be heavily loaded. To assure the system can withstand those high loads, two case studies, 1 and 2, are defined in which the cylinder loads are calculated. Case study 1 and 2 are respectively without and with a connection to the TP. Load case 1 without a connection results in high overturning moments on the hexapod when the WTG is skidded towards the TP. Load case 2 with a connection results in the TP taking more loads the further the WTG is skidded towards the TP. For both cases, 3 WTG locations are chosen to calculate the normal forces in the cylinders, see Figure 6.4. Besides the forces in the cylinders and connection, three external forces exist. Wind, accelerations and the self-weight of the WTG. All exerting forces and moments on the Stewart platform or the connection to the TP.

For the motion envelope calculations, the WTG motions are assumed to be compensated 100%. To take into account that the system will not compensate perfectly, the percentage the motions are compensated is assumed. With the remaining displacements and acceleration, the forces due to these motions are calculated. For both load cases, 95% motion compensation is assumed. Thus, 5% of the accelerations and displacements are used as input for the force calculations. One should note this 95% is an estimate of the motion compensation capabilities and is found by bench-marking with the Barge Master system [23]. This approach was not adopted in calculating the vessel motions because of the complexity of estimating the percentage of mass and inertia which influences the vessel motions after compensation.

EXTERNAL FORCES

The Free Body Diagram explaining the external forces can be found in Appendix A Figure A.2. From each WTG component, the tower, nacelle, blades and blade rack, there is an acceleration, wind and self-weight load. The accelerations are known from Table 6.3. The forces from these accelerations can be calculated with Newton's first law. The environmental force consists of wind load. The calculations of the wind load analysis are based on the DNV-guidelines [OS-H204]. This with a wind gust of 25 m/s constant over height and a drag coefficient for the tower and nacelle of respectively 0.7 and 1.05. The Wind Energy Handbook is used as reference to calculate the forces of the blades [24]. The wind direction is assumed to be in positive x-direction together with the blades orientated in maximal lift generating position. The most severe orientation of the blade rack is with 2 blades in the most severe angle of attack with solely lift forces and the third blade experiencing lift and drag forces. This gives the most severe loading condition.

The overturning moments coming from the wind forces are calculated by multiplying the force on each component by its own arm which is its vertical CoG. The displacements of each WTG component are calculated by multiplying the values from Table 6.3 by 0.05 which gives the remaining motions. The motions should be added to the arm to calculate the overturning moments. All forces and moments around the base of the tower are given in Table 6.5. The self-weight of the components also exerts moments on the Stewart platform. The arms for these forces are the horizontal distance between the Stewart platform centre and CoG of the components. For each load case, the arm which is used in calculating the overturning moments differs. Again, the displacement amplitudes of Table 6.3 must be added to these arms.

Load	$F_{wind,x}$	$F_{wind,y}$	$M_{wind,xx}$	$M_{wind,yy}$	$M_{wind,zz}$	$F_{acc,x}$	$F_{acc,y}$	$F_{acc,z}$	$F_{gravity}$
Value	0.71	0.26	-20.38	53.58	-3.35	0.92	5.75	-1.42	-18.99

Table 6.5: External forces [MN] by wind, acceleration and self-weight. Moments [MNm] of wind taken around the base of the tower

The pose of the platform is determined by the relative position between the upper and lower platform. With 95% assumed motion compensation and the upper platform is assumed to be level, the cylinder forces are caused by the translation and rotation of the bottom frame. This will be determined by the surge, sway, heave, roll, pitch and yaw of the vessel. For each pose and external loads, a unique solution exists for the axial forces in the cylinders. The worst pose is the pose in which the vertical component of the unit vector of the cylinders is minimal. The unit vectors in Table 6.4 give this pose.

LOAD CASE 1, WITHOUT FLANGE

Transferring all external loads to the centre of the hexapod gives 3 forces and 3 moments at the centre. The six axial forces in the cylinders can be found by solving a 6 by 6 matrix equation derived from the force and moment equations. See Table 6.6 for the axial forces for all 3 locations of the WTG. One can see the further the WTG is offloaded the higher the forces. This makes sense since the longer arm results in higher moments. With case 1a, no overturning moments apply to the hexapod except for the self-weight which is under an angle because of the rotational motions of the vessel. With case 1c the hexapod will experience the highest overturning moments thus the highest forces in the cylinders. The cylinders closest to the WTG will experience compression and the cylinders furthest away will experience tension. This WTG location will be the most severe one. With axial forces up to 24 MN, equivalent to approximately 2500 t, the cylinders will be heavily loaded.

Knowing the forces and maximum velocity of the base platform, the total required power can be calculated. The maximum velocity is calculated by taken the norm of the maximum X, Y and Z velocities which is 1.00 m/s. One should note this is a conservative approach since it does not take into account that the three velocities do not occur simultaneous and this resulting velocity is not exactly in the direction of the cylinder. For the most severe load case, 1c, the required power is 82.6 MW which is huge. Especially when comparing it to the pioneering spirit which requires approximately 60 MW for its lift. In conclusion, the forces in the cylinders and the required power are exceptionally high.

#	**Location**	**Y [m]**	**1**	**2**	**3**	**4**	**5**	**6**	**Total power [MW]**
1a	Centre hexapod	0	9.2	5.1	0.5	-1.1	1.7	8.2	25.7
1b	Above base last cylinder	5	14.0	5.1	-4.3	-5.9	1.7	13.0	44.0
1c	Above TP	15	23.7	5.1	-14.0	-15.6	1.7	22.7	82.6

Table 6.6: Axial forces [MN] in cylinders for 3 location of the WTG. Y is the distance between the hexapod's centre and the WTG's centre. Negative force is tension.

LOAD CASE 2, WITH FLANGE

Case study 2 where a connection is made between the TP and system is assessed. For now, this connection consists of two flanges at both sides of the TP. Both flanges only carrying vertical loading. The same calculation steps are taken as in case study 1. This except for cylinder 3 and 4 which are assumed to be idle after the WTG is skidded beyond the last cylinder. This gives zero force in these cylinders. Besides, the remaining motion percentage after compensation for load case 2b and 2c is set at respectively 2.5 and 0 % instead of 5 %. This since the closer the WTG is offloaded towards the TP, which is a static point, the less motions remain. See Table 6.7 for the axial forces for all 3 locations of the WTG. One can see the required power and axial forces in the cylinder are much lower when using a flange than when not using a flange. With case 2c the vertical forces will almost solely be taken by the flange. This only for the moment the WTG is above the TP. During the skidding phase, a load transfer will take place from the cylinders to the flange.

#	Location	Y [m]	1	2	5	6	Flange 1 (+x)	Flange 2 (-x)	Total power [MW]
2a	Above base last cylinder	5	10.0	4.8	4.1	10.6	0.3	-5.0	29.3
2b	Between hexapod and TP	8.5	2.5	0.9	0.2	3.1	9.8	3.8	6.8
2c	Above TP	15	-1.8	-1.0	-1.8	-1.3	14.2	9.6	5.9

Table 6.7: Axial forces [MN] in cylinders for 3 location of the WTG. Cylinder 3 and 4 are idle. Y is the distance between the hexapod's centre and the WTG's centre. Negative force is tension.

After assessing both case studies, the option to use a connection is chosen. This, to reduce the cylinder axial loads and the required power. Besides, offloading without a flange connection gives power requirements of 83 MW which is found beyond feasible for this system. For the system with a flange connection and with cylinder loads of 10 MN with 170 bar average working pressure give a required cylinder outer diameter of approximately 1 m. In other applications, cylinders with these characteristics and dimensions are proven to work.

ALTERNATIVE MOTION COMPENSATION

Instead of using a hexapod to control and compensate the motions, a combination of the Barge Master [23] and a XY-table can be used. The heave, roll and pitch will be compensated by 3 vertical cylinders. The XY-table compensates for the surge, sway and yaw. Also, an extending and retracting skidding platform can enable extra y-direction compensation. Hence, the 6 DoF are separated and compensated by more than one systems. The advantage is that the vertical force can solely be taken by the 3 vertical cylinders whereas the Stewart platform's cylinders are positioned under an angle thus requiring more axial loads to give the same vertical force. Another advantage is that less cylinder stroke is required at each cylinder. In this thesis, this alternative will not be researched further.

SKIDDING SYSTEM

The skidding system must ensure horizontal displacement of the WTG. During skidding, the WTG must be connected to the system. After skidding, the WTG must be disconnected from the system and the WTG must be positioned on the TP. For the skidding process, a continuous and quick process is required to reduce risks with the added benefit of minimizing installation time. Nowadays, most of the skidding methods make use of skidding track, friction-reducing materials and propulsion force to move the structure. For different applications, continuous skidding of loads up to 2000 tons has been achieved in the past.

6.2.2. ATTACH WTG TO SYSTEM

The connection between the system and WTG cannot be made at the underside of the tower since this will restrict connecting the WTG to the TP. An alternative is an external connection around the circumference of the tower. In the offshore branch, several external lifting tools exist which are used in for example monopile lifting. The tools consists of clamps with friction pads exerting a normal force on a monopile generating enough friction to overcome the gravity force. The disadvantage of these tools is that they plastic deform the monopile to increase the friction force. Plastic deforming the tower cannot be done since this will decrease the tower's structural integrity. Using a similar system to attach the WTG to the system without plastic deforming the tower is assessed.

The vertical forces of the WTG can be taken by either friction forces exerted by normal forces of a clamp on the tower or with a flange on the tower. Using friction instead of a flange is the preferred option because no adjustments to the tower design have to be made, which is a significant advantage. Therefore, this option is assessed on its feasibility.

FRICTION CONNECTION

The required normal force exerted on the tower by the clamp can be calculated by Equation 6.7. A safety factor S_f of 2 is used to cope with the imprecise WTG weight and friction coefficient. Especially the friction coefficient between the tower coating and the clamp material is variable because of material changes and having dry or wet material. Ethyl silicate zinc-rich paint is widely used as a primer for towers and has an experimentally determined friction coefficient S_f of 0.45 [25]. This is only used as an indication, since this friction coefficient is for primer-primer contact and for a dry connecting. Assumed is the clamping material consists of rubber, resulting in a steel to rubber friction coefficient for wet and dry conditions of 0.3 [DNV-RP-H102]. The pressure p exerted on the tower is calculated by dividing the normal force F_n by the area. Knowing the pressure, the stresses in the tower can be calculated with Equation 6.8 of which the parameters are shown in Figure 6.8. σ_t is the transferal stress which is governing. The tower is made of S355 steel with a yield strength of 335 MPa. This is the strength of S355 for thicknesses between 40 and 63 mm [12]. With a safety factor of $\frac{3}{5}$, following from the AISC standard, the maximum yield stress is 201 MPa [AISC]. Knowing all inputs, the required height of the flange is 2.08 m. This is the minimal clamp height for which the transferal stress does not exceed the yield strength of the steel. One has to note that this is a primarily calculation which shows the height and surface area of the clamp. This with perfectly distributed pressures and without taking buckling into account which is not representative for real-life.

$$F_n = \mu \cdot 9.81 \cdot m_{WTG} \cdot S_f \tag{6.7}$$

$$\sigma_t = \frac{p \cdot R_2^2}{R_1^2 - R_2^2} \cdot (1 + \frac{R_1^2}{r^2}) \tag{6.8}$$

F_n = Normal force	S_f = Safety factor	R_1 = Inner radius WTG
μ = Friction coefficient	σ_t = Transferal stress	R_2 = Outer radius WTG
m_{WTG} = WTG mass	p = External pressure	$r = \frac{R1+R2}{2}$

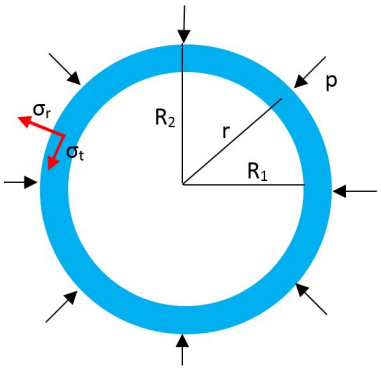

Figure 6.5: Intersection of the tower showing input parameters for Equation 6.8. Red indicates the radial σ_r and transferal stress σ_t.

The DNVGL-RP-C202 standard is used to asses whether the tower will buckle when exerting the normal force on the tower surface. Following from the standard, the tower is subjected to axial (a), bending (m), circumferential (h) and shear (τ) stresses. The external forces used for the cylinder force calculations in Subsection 6.2.1 combined with the circumferential clamp force are used as input. The total stress $\sigma_{j,Sd}$ is calculated with Equation 6.9. See the standard for more information about this equation. The characteristic buckling strength is calculated with Equation 6.10. The reduced yield strength of the material is f_{ks} and depends on λ_s which can be found in the standard. After calculating both the total stress $\sigma_{j,Sd}$ and the characteristic buckling strength f_{ks}, the stability requirement of the tower is given by Equation 6.11 in which f_{ksd} is f_{ks} divided by γ_m, which is the material factor.

$$\sigma_{j,Sd} = \sqrt{(\sigma_{a,Sd} + \sigma_{m,Sd})^2 - (\sigma_{a,Sd} + \sigma_{m,Sd})\sigma_{h,Sd} + \sigma_{h,Sd}^2 + 3\tau_{Sd}^2} \tag{6.9}$$

$$f_{ks} = \frac{f_y}{\sqrt{1 + \lambda_s^4}} \tag{6.10}$$

$$\sigma_{j,Sd} \leq f_{ksd} \leq \frac{f_{ksd}}{\gamma_M} \tag{6.11}$$

$\sigma_{j,Sd}$ = Design equivalent von Mises stress

$\sigma_{a,Sd}$ = Stress in longtidual direction due to uniform axial load

$\sigma_{m,Sd}$ = Stress in longtidual direction due to bending

$\sigma_{h,Sd}$ = Stress in in the circumferential direction

τ_{Sd} = Shear stress tangential to the surface

f_{ks} = Characteristic buckling strength

f_{ks} = Design buckling strength

f_y = Yield strength

λ_s = Reduced shell slenderness

γ_M = Material factor

From the buckling stability check, it can be found that the tower will buckle when subjected to all loading including the huge normal force induced by the clamp. Only when increasing the height of the clamp beyond reasonable dimensions, the tower will not buckle, see Table 6.8. The results of the buckling check with a clamp height of 2.1 m, enough to withstand the transferal stress, is shown in Table 6.8. However, since the buckling check is not achieved, the option to lift the tower by only using friction force exerted by a clamp is found not feasible.

Case	$\sigma_{j,Sd}$ $[MPa]$	f_{ksd} $[MPa]$	**Height one clamp** $[m]$
Friction connection 1	182.3	5.2	2.1
Friction connection 2	38.3	38.7	87.5

Table 6.8: Results of stability checks using DNV-RP-C202 standard. Clamp height 1 is sufficient for not exceeding the yield strength but not for the buckling check. Clamp height 2 is sufficient for not exceeding the buckling check.

FLANGE CONNECTION

An alternative to clamping is the use of a flange. A flange will be constructed around the tower's circumference below which the system will grab the tower with a clamp. Thus, no significant friction is applied since the vertical forces of the WTG are transferred from the flange to the clamp. The same structural checks are performed as done for the friction clamp. This is checking if the yielding stress is not exceeded and if the stability requirement is assured. For both concept 1 and concept 2 the checks are performed. The only difference being that concept 2, the skidding tower, has two clamps instead of one.

At each clamp, a force and moment are located coming from the external forces, see Figure 6.6. The external forces are the same as used in the friction connection calculations above. The force and moment at the clamp location are calculated by force and moment equilibriums including the force $F_{wind,acc}$ and moment $M_{wind,acc}$ exerted by the wind and compensated accelerations. To simplify the calculation it is assumed that this force and moment exert two normal forces at the upper right and lower left side of the clamp. Both resulting forces F_{clamp} resulting from the distributed loads are located at a height or arm of 1/3 the height of the clamp. This is at 2/3 of the distributed load. These resulting forces will resist the rotation of the clamp by the induced force and moment. Both forces exert a shear force on the tower, τ_{Sd}, which is used in the buckling check calculations, see equation 6.9. Besides the shear stress, the axial $\sigma_{a,Sd}$ and moment $\sigma_{m,Sd}$ stresses are calculated as done in the friction connection calculations. Since there is no circumferential pressure, the hoop stress $\sigma_{h,Sd}$ is zero. The only unknowns in this calculation are the height of one clamp and the distance in between the clamps. These can be changed until the structural checks are satisfied.

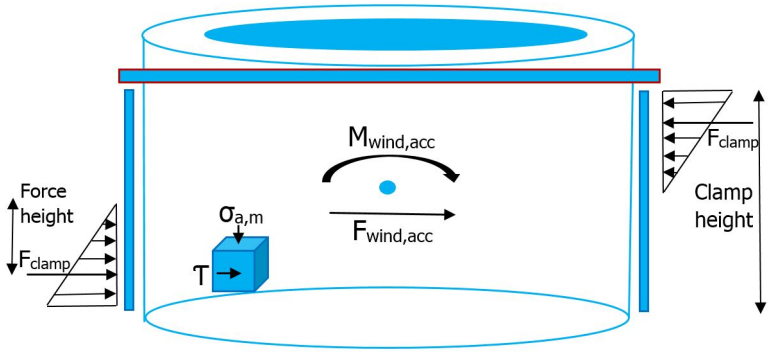

Figure 6.6: Intersection of the tower with clamp around circumference and flange indicated with red. External force and moment exerted by wind and accelerations indicated with respectively $F_{wind,acc}$ and $M_{wind,acc}$. Resulting clamp force F_{clamp} from distributed clamp force applies at force height from the clamps horizontal centre line. Cube shows the axial, bending and shear stress respectively σ_a, σ_m and τ.

For concept 2, solving the force and moment equations is an undetermined problem. This since there are more unknowns than equations. To solve this undetermined problem, the tower is assumed to have zero displacement and rotation at the clamp locations. Increasing the height of a clamp or height between the clamps reduces the stresses in the tower. For concept 2, a height between the clamps of 5 m is chosen because the lower the height the higher the loading. If the tower is stable for this height, it will also be stable to buckling for larger heights between the clamps.

An overview of both stability checks and the results are shown in Table 6.9. This shows the minimal required clamp size to assure stability to buckling. As stated before, a friction clamp is not feasible, see Table 6.8. Table 6.9 shows that for both concept 1 and 2 a flange connection is feasible.

Case	$\sigma_{j,Sd}$ $[MPa]$	f_{ksd} $[MPa]$	**Height one clamp** $[m]$	**Height between clamps** $[m]$
One flange concept 1	82.1	84.9	2.2	-
Two flanges concept 2	84.1	86.0	1.0	5.0

Table 6.9: Results of stability checks using DNV-RP-C202 standard, showing the minimal required clamp height. Height between clamps only applies for concept 2.

6.2.3. REDUNDANCY AND FAIL-SAFE

Designing this system with redundancy to make it fail-safe is a must. System components such as the Hydraulic Power Unit (HPU) or the control systems can be made redundant by for example having back-ups. However, adding hydraulic cylinders to make them redundant is not feasible. Adding a cylinder will change the 6 DoF compensation capabilities of the system negatively. Thus, in the case one of the 6 hydraulic cylinders fails the compensation capabilities will decrease and the there will be a risk of failure of the total system. This problem cannot be overcome, so measurements must be taken to reduce risk levels. This should be done by extensive test trials before starting the WTG offloading operations. Also, the system must never operate to its maximum capacity to reduce the risk of exceeding the limits.

6.3. CONCEPT 2, SKIDDING TOWER

In this section, the technical challenges of concept 2 are discussed. The feasibility of tackling these challenges is assessed by calculations and bench-marking. Besides, the redundancy and fail-safe of the design is researched.

XY-TABLES

Two XY-tables at distant vertical locations are used to compensate motions. The individual XY-tables provide horizontal motions in X and Y direction. Roll and pitch can be compensated by several configurations. By changing the X and Y motions of both tables relative to each other, roll and pitch motions can be compensated. Another option is to change the relative Z height of the connections between skidding tower and XY-table. With this configuration, a rotating clamping system is required since the tower will not be perpendicular to the XY-table when roll or pitch motions occur. Designing a rotating clamp which also transfers forces on the tower is technically challenging. Vertical motions can be provided by lifting the XY-tables. Yaw can be compensated by for example rotating the tower within the clamps or rotating the skidding tower around its base. In conclusion, several options to compensate 6 DoF can be selected. If this concept is chosen most feasible, all configurations must be assessed in more detail. A design consideration which must be researched is the height of the tables. The higher the XY-tables, the higher the motion envelope and the lower the overturning moments. Also, a XY-table is heavy and requires power and umbilical supply. The higher the XY-table is located the harder it will be to supply these requirements.

6.3.1. REQUIRED POWER

The total required power is calculated by multiplying the force by the velocity for the X, Y and Z direction. The total force is the sum of wind, weight, acceleration under 95% motion compensation for each direction separate. Comparing it to concept 1, all motions and forces are decoupled in X, Y or Z direction instead of being coupled. The advantage is that the forces do not have an angle under which they provide power. Hence, providing power more effectively in one direction. Approximately 24 to 46 MW is required for the configuration as shown in Figure 6.1. This is a range since the required power depends on the height between the lower and upper table, reducing with increasing height. See Figure 6.7 for the power curve. Since the vertical force is independent of the height between the clamps, the curve goes to a limit for high x-axis values.

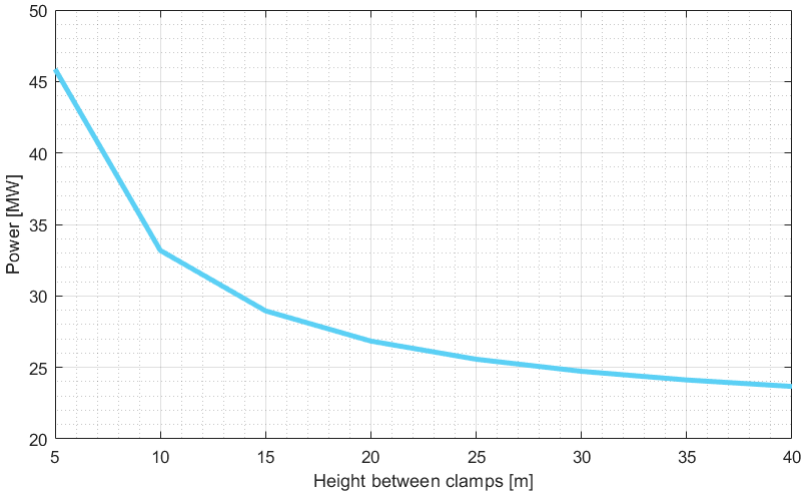

Figure 6.7: Required power for concept 2 dependent on relative height between the two clamps

6.3.2. TOWER CLAMP

The same tower clamp as in concept 1 can be applied. However, the upper clamp requires the ability to rotate around its X and Y axis to compensate for the misalignment of the lower and upper clamp when compensating for roll and pitch. Dividing the total required normal force among the two clamps will still not make it feasible to lift the WTG on friction. As discussed before, the most feasible option is to use a flange to provide vertical forces. Thus, a flange is chosen to exert a vertical force in which the best configuration is to solely transfer vertical forces in the lower clamp. This to reduce the amount of flanges on the tower. Thus, reducing the required tower adjustments.

6.3.3. REDUNDANCY AND FAIL-SAFE

Having a redundant system which is fail-safe is a must. Similar to concept 1, systems such as the power or control units can be made redundant by having back-up systems. However, the motion compensation systems cannot be made redundant since this will require a back-up cylinder for each operational cylinder. All cylinders having a back-up makes the system twice as expensive regarding the hydraulics. The difference between concept 1 and 2 lies within the consequences of failure. As discussed before if Concept 1 has a failure, this causes the platform to operate in a spherical motion around the failed cylinder. Hence, there will be a reduction in compensation capabilities of all DoF. For concept 2 if a motion compensation system fails, for example the Y motion of the X-Y table, this will completely restrict Y-motion compensation but will not restrict the X-motion compensation at all. In conclusion, failure in concept 1 and Concept 2 will cause respectively reduction of motion compensation capabilities in all DoF and a complete failure of one or multiple DoF without affecting the others.

Similar to concept 1, This problem cannot be overcome, so measurements must be taken to reduce risk levels. This should be done by extensive test trials before starting the WTG offloading operations. Also, the system must never operate to its maximum capacity to reduce the risk of exceeding the limits.

6.4. CONCLUSION

Based on the calculations, both concepts are technically feasible. One has to note these calculations are preliminary calculations and further designing each concept might prove otherwise. The power calculations show that the skidding tower requires less power than the hexapod. The hexapod requires up to 30 MW. This, while the skidding tower requires between 24 and 30 MW for heights between the clamps above 15 m. This difference is because the skidding tower provides power more effectively.

The hexapod provides the highest motion compensation capabilities. This, because the closer the WTG is skidded towards the TP the lower the Y and Z-motions become. Besides, the system is closer to deck reducing the wave-induced motions that have to be compensated.

The skidding tower has the advantage of having two clamps. Thereby dividing the external forces among both clamps, reducing the overturning moments. The disadvantage of the high clamp is that the higher it is located the higher the motion envelope. Also, the higher the XY-table is located the harder it will be to supply the power requirements.

For both concepts, lifting the WTG on friction is not feasible with buckling induced by circumferential stresses being the limiting factor. The feasible option is to lift the WTG with a flange on the tower.

In conclusion, concept 1 the hexapod is chosen as most feasible. This concept provides the highest motion compensation capabilities. And the higher required power compared to the skidding tower is relative small. Also, a failure in the hexapod's cylinders will reduce the motion compensation capabilities in all DoF instead of complete failure in one DoF. At last, smaller Stewart platforms are a proven technology and by combing it with existing large cylinders the concept can be made feasible.

7

STEWART PLATFORM OPTIMIZATION

In this chapter, the hexapod of Section 6.2 and Figure 6.4 will be optimized. From now on, the hexapod will be referred to as the Stewart platform. This optimization will be a kinematic optimization using inverse kinematics resulting in the kinematic optimal design which is used in further steps in this research. Besides, this optimization gives insight in the size of the Stewart platform. The part of the hexapod which is connected to the vessel will be referred to as the base. The part connected to the WTG will be referred to as the platform. In between the base and platform six actuators or cylinders are located which will be referred to as legs. MATLAB is used throughout this chapter for calculations and optimizations, see Appendix G for the scripts.

7.1. INVERSE KINEMATICS

The Stewart platform's kinematics can be solved with forward and inverse kinematics [26]. With forward kinematics, the position of the platform is a function of the leg length. Forward kinematics require an iterative process since multiple solutions exist for one problem. With inverse kinematics, the leg length is a function of the position of the platform. Inverse kinematics can be solved analytically in which only one solution exists. To conclude, inverse kinematics is used to optimize the Stewart platform design since it provides one solution solved analytically.

A clear difference must be made between the best approach for solving either a serial manipulator or a parallel manipulator with either forward or inverse kinematics. Serial manipulators use multiple actuators in serial order to provide motions while parallel manipulator, the Stewart platform, uses multiple actuator in parallel order to control a single platform also known as an end-effector. For serial and parallel manipulators the approach which give one solution to the kinematic problem are respectively forward and inverse kinematics.

7.2. DESIGN START

Apart from geometrical parameters, a Stewart platform can be described by the type and position of the joints and the type of prismatic actuators. For the type of joints, an UCU configuration is chosen. With the base and platform joints being universal joints (U) and the prismatic actuators being cylindrical joints (C). Thus, the hydraulic cylinders must be able to rotate freely around its axis relative to the casing. With this UCU configuration, a total of six DoF is achieved. The main advantage being that spherical joints are avoided which have lower robustness and higher cost. The position of the joints will be determined by the characteristics as discussed blow which follow from the configuration introduced by Faugère and Lazard [27].

Combinatorial is defined as the number of hydraulic cylinders sharing the same joint. This for the base and the platform. 6-3 means that there are 6 joints at the base and 3 at the top. Hence, at the base each cylinder has its own joint location and at the platform each cylinders shares its joint locations with another cylinder. For this design, a 6-6 configuration is chosen. This is the most widely used and simplest configuration. The 6-6 configuration together with 6 cylinders results in the system having 6 circular paths.

Planarity means the joints of both base and platform are in the same plane which simplifies the design. Besides, both the base and platform joints are located on a circle with 120 degrees in between the middle of two joints. This configuration is also known as rotational symmetric. The great advantage of this total configurations is that six identical cylinders can be used.

7.3. DESIGN PARAMETERS

First, the geometry of the Stewart platform must be described. As Xie et al. [28] proposed, the Stewart platform will be described by the 5 parameters listed below. An overview of the parameters is shown in Figure 7.1. The global axis system is located in the centre of the base circle of which the positive X-axis is the offloading location, starboard. O_o is the origin of the global axis system. The platform axis system is located in the centre of the platform circle, of which O_p is the origin. One should note the Stewart platform's axis system differs from the vessel's one. This axis system is chosen to be consistent with the existing literature.

- R_b Radius of base circle
- R_p Radius of platform circle
- ϕ_b Separation angle between adjacent actuator attachment points on base
- ϕ_p Separation angle between adjacent actuator attachment points on platform
- h Vertical distance between O_o and O_p

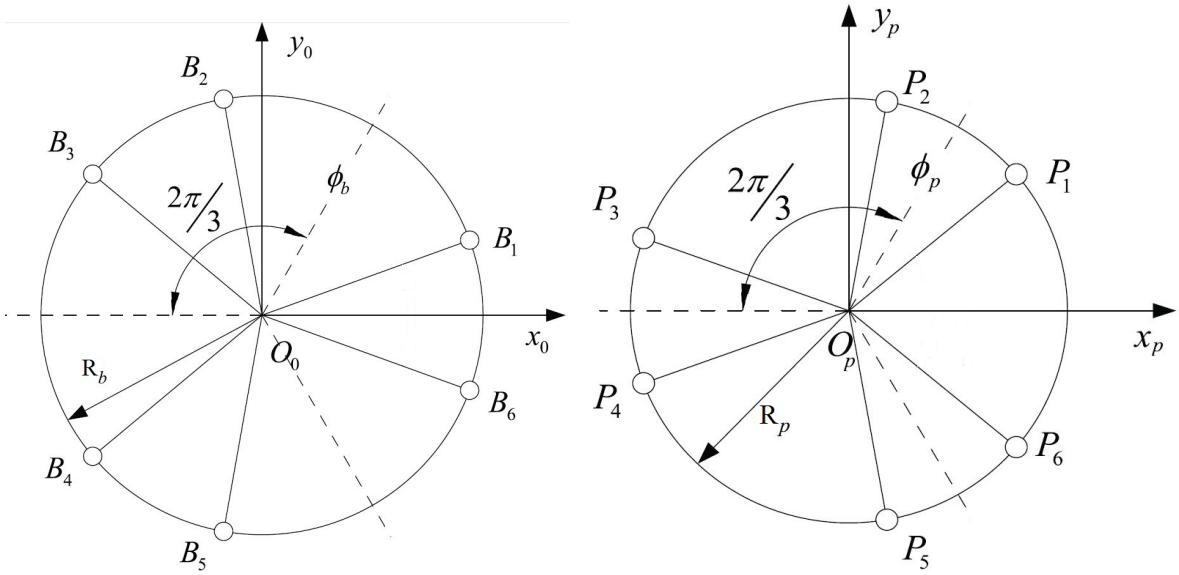

(a) Base with global axis system O_o

(b) Platform with local axis system O_p

Figure 7.1: Schematic overview of Stewart platform base and platform with design parameters [28]

Figure 7.2 schematically shows Stewart platform. The coordinates of O_p, relative to the global axis system are $q = [x, y, z, \psi, \theta, \phi]$. The Greek symbols describe the orientation of the platform with respect to the base responding respectively to yaw, pitch and roll. Knowing the locations of the base and platform joints, Equation 7.1 can find the actuator length for each cylinder. The rotation matrix R maps the local coordinates to global coordinates with the yaw ψ, pitch θ and roll ϕ convention, see Equation 7.2.

$$l_i = q + R_{matrix} \cdot p_i - b_i \tag{7.1}$$

l_i = Length of leg i

q = Base O_0 to platform CoG O_p

R_{matrix} = Rotation matrix

p_i = Joint coordinate i in platform plane

b_i = Joint coordinate i in base plane

ϕ = Roll

θ = Pitch

ψ = Yaw

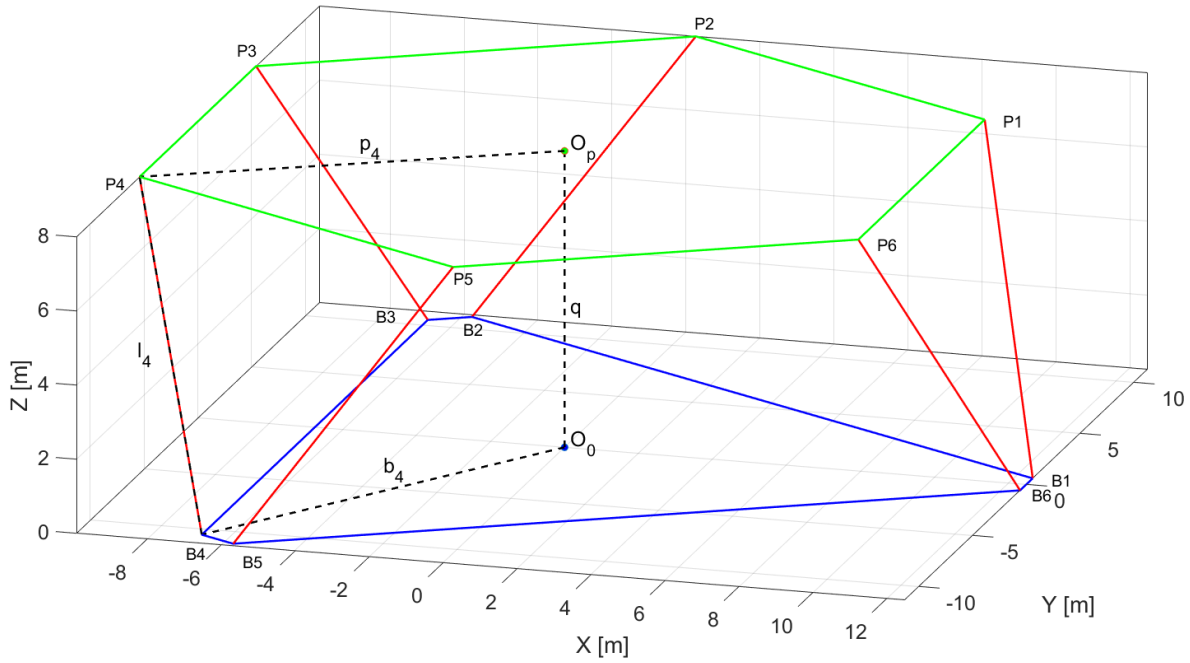

Figure 7.2: Schematic overview of Stewart platform. Green and blue respectively indicate the contours of the base and platform. Red indicates the cylinders.

$$R_{matrix} = \begin{bmatrix} cos\psi cos\theta & cos\psi sin\theta sin\phi - sin\psi cos\phi & sin\psi sin\phi + cos\psi sin\theta cos\phi \\ sin\psi cos\theta & cos\psi cos\phi + sin\psi sin\theta sin\phi & sin\psi sin\theta cos\phi - cos\psi sin\phi \\ -sin\theta & cos\theta sin\phi & cos\theta cos\phi \end{bmatrix} \tag{7.2}$$

Before starting the optimization, the upper and lower bounds of the design parameters have to be specified. The values are given in Table 7.1. The lower and upper bound of the radii R_b and R_p are limited by respectively the radius of the WTG which has to fit on the platform and the vessel width. To still have a design whose size is reasonable a maximum value of 12.5 m is chosen. The lower bounds of the angles are calculated with Equation 7.3 to prevent cylinder collisions. The chord length C or diameter of a cylinder is for simplicity taken as 1 m, see Section 6.2.1. The lower bounds of ϕ_b and ϕ_p dependent on the base and platform radii. The lower bounds of ϕ_b and ϕ_p are calculated with the upper bound of R_b and R_p. Since the angle between the joints is 120 degrees, the upper bound can be calculated. When only taking these bounds into account, cylinders will collide for designs with small ϕ_b or ϕ_p values. Therefore, two nonlinear constraints must be added, see Equation 7.4 and 7.5. These are a function of the base or platform radii together with the base or platform angle and make sure cylinder will not collide. The lower bound of h is chosen as 3 m which is the minimum required height to assure sufficient cylinder length to compensate the heave motions as set in Table 7.2. Again, the upper bound is chosen to be reasonable.

Table 7.1: Lower and upper bound for design parameters

Parameter	Lower bound	Upper bound
R_b $[m]$	5.0	12.5
R_p $[m]$	5.0	12.5
ϕ_b $[rad]$	0.08	2.01
ϕ_p $[rad]$	0.08	2.01
h $[m]$	3.0	15.0

$$\phi = 2\arcsin\left(\frac{C}{2R}\right) \tag{7.3}$$

C = Chord length R = Radius circle

$$2\arcsin\left(\frac{C}{2R_{b,p}}\right) - \phi_{b,p} \leq 0 \tag{7.4}$$

$$2\arcsin\left(\frac{C}{2R_{b,p}}\right) - (120 \cdot \frac{\pi}{180} - \phi_{b,p}) \leq 0 \tag{7.5}$$

R_b = Radius base R_p = Radius platform ϕ_b = Separation angle base ϕ_p = Separation angle base

7.4. WORKSPACE

The workspace of the Stewart platform is defined as all motions of the origin of the base O_o which originate from the vessel motions induced by the first and second-order waves. Again, the motions are computed in Seaway with the same inputs and assumptions as discussed in Section 6.1. The only difference being the location where the motions are computed. Assumed is the base radius R_b goes to the upper bound, resulting in the measurement location not being at the starboard edge but in between amidship and starboard edge. Besides, the height h of the Stewart platform is taken into account. For now, estimated to be the average of the lower and upper bound. The z location of the motion measurement point is taken as the TP height which is the neutral location of the base CoG O_o. Further in this chapter, these assumptions are verified. The measurement location is [80,-12.5,19]. Again, an α-factor of 0.84 has been taken into account to make sure the system does not operate at limiting environmental conditions [DNV-OS-H101]. The motions are divided by the α-factor to get the final motions in the workspace. The workspace or motions for this optimization can be found in Table 7.2 in which the rotational displacements are added, coming from the same Seaway computation as the translational displacements. These values represent the maximum translations and rotations of the base origin O_o. The workspace will be defined by n random points. Each random point will be defined by 3 translations and 3 rotations ranging in between the maximum workspace as defined in Table 7.2. Random generated points are chosen since they give an accurate representation of all possible poses of the platform. Also, by using random points the workspace will be discretized, extensively reducing the computational time for kinematic performance indices calculations. The required amount of random points will be discussed in Section **??**.

Table 7.2: Maximum vessel motions and required workspace of Stewart platform

DoF	**Value**
Surge X	$\pm$ 0.58 m
Sway Y	$\pm$ 1.24 m
Heave Z	$\pm$ 0.83 m
Roll ϕ	$\pm$ 2.83°
Pitch θ	$\pm$ 0.48°
Yaw ψ	$\pm$ 0.23°

7.5. KINEMATIC PERFORMANCE INDICES

The kinematic performance of the different designs will be assessed with three kinematic performance indices which are listed below. GCI and GGI are inspired by Lara-Molina et al. [29]. GFI is a self-made index which is explained below. According to several literature, these indices give most insight in the kinematic performance of a Stewart platform [28] [29] [30]. For each set of design parameters these indices can be compared. Before being able to compute the global indices, the local indices must be calculated. The local indices describe a single point in the workspace while global indices describe the total workspace. Therefore, only the global indices are used to find the optimal design.

- Global Conditioning Index (GCI)
- Global Gradient Index (GGI)
- Global Force Index (GFI)

The starting point for all indices is a series of algebraic computations resulting in the Jacobian Matrix. The Jacobian is computed with Equation 7.6 in which $\times$ is the cross product [31]. The first three columns are dimensionless while the last three have dimension meter. The left and right three columns belonging to the force F and torque T part of the external loading are indicated by J_F and J_T respectively. To give physical meaning to the indices, the approach to normalize the matrix as proposed by Fassi et al. has been applied [31]. Therefore the last three columns, J_T, are divided by L_j, see Equation 7.7 and 7.8. This normalized Jacobian J_n will only be used for the GCI and GGI and not for the GFI calculations. This since the GFI consists of forces and moments with units N and Nm which comply to the units of the non-normalized Jacobian J_{nn}.

$$J_{nn} = \begin{bmatrix} e_1^T & (R_{matrix} \cdot p_1 \times e_1)^T \\ e_2^T & (R_{matrix} \cdot p_2 \times e_2)^T \\ \vdots & \vdots \\ e_6^T & (R_{matrix} \cdot p_6 \times e_6)^T \end{bmatrix} = [J_F : J_T] \tag{7.6}$$

$$J_n = [J_F : \frac{J_T}{L}] \tag{7.7}$$

$$L_j = \sqrt{\frac{trace(J_T^T J_T)}{trace(J_F^T J_F)}} \tag{7.8}$$

e_i = Unit vector leg i

p_i = Joint coordinate i in platform plane

R_{matrix} = Rotation matrix

L_j Jacobian normalization factor

J_{nn} = Non-normalized Jacobian

J_n = Normalized Jacobian

J_F = Force part of Jacobian

J_T = Torque part of Jacobian

GLOBAL CONDITIONING INDEX

For each random generated point in the workspace, the Local Conditioning Index (LCI) is calculated with Equation 7.9 [29]. The LCI is calculated as the reciprocal of k_i in which k_i is the condition number of the normalized Jacobian matrix for point i in the workspace. To get insight into the global dexterity, the Global Conditioning Index (GCI) is calculated as the average of the LCI among all workspace points N, see Equation 7.10. The GCI ranges from 0 to 1, where 0 indicates the singular condition and 1 indicates isotropic condition thus high dexterity. The closer GCI is to zero the closer the Jacobian is near a singular point. Numerical difficulties in calculating the inverse Jacobian can occur which decrease the position accuracy. In such a singular point, the Stewart platform will gain an extra DoF, losing the ability to change the position and orientation of the platform arbitrarily. The higher the dexterity, the better the Stewart platform's ability to change the position and orientation of the platform arbitrarily during operation. Low dexterity is combined with small workspace and high cylinder forces. Dexterity can be seen as the ability to handle an object with accuracy [29].

$$LCI = \frac{1}{k_i(J_n)} \quad [29] \tag{7.9}$$

$$GCI = \frac{\sum_{i=1}^{N} LCI}{N} \tag{7.10}$$

$k_i(J_n)$ = Condition number of normalized Jacobian matrix for workspace point i

J_n = Normalized Jacobian matrix

N = Number of points in workspace

GLOBAL GRADIENT INDEX

The GCI only indicates the average dexterity among the workspace and does not take into account any poor local points. Thus, at one side of the workspace the dexterity can be significantly different from the other side of the workspace. The Global Gradient Index (GGI) is introduced to give insight into the gradient of the dexterity [29]. The GGI ranges from zero to infinity. For GGI is zero, the gradient of the dexterity or GCI is zero resulting in the dexterity being flat throughout the workspace. High dexterity gradients cause the dexterity to change significantly within a small change of the platform pose, resulting in a significant change in kinematic performance and a high sensitivity to position error. The GGI is calculated with Equation 7.11. The local gradient index is the norm of the six gradients in the six DoF of the dexterity. Then, the maximum value of all workspace points is taken to get the global gradient index. The gradients are calculated by adding a small value in a specific DoF and using the first-order difference equation [29].

$$GGI = max\|\nabla \frac{1}{k_i(J_n)}\| \tag{7.11}$$

GLOBAL FORCE INDEX

A self-made index, the GFI, is used instead of the GPI which is advised by literature [29] [32]. The GPI gives insight into the force transmission capability thus giving insight in the ability to support loads exerted on the platform. Equation 7.12 is used to calculate the GPI in which the non-normalized Jacobian matrix is used. This, since to calculate the force with Equation 7.13 the non-normalized Jacobian must also be used. As stated by literature, maximizing the GPI reduces the upper bound of Equation 7.14. However, this only gives insight into the capability which is a range and not the actual axial forces in the cylinders. Initial calculations showed that indeed the upper bound decreases but for certain designs and loads the actual force in the cylinders increases. This is caused by the type of external loading, which is having high overturning moments. Thus, maximizing GPI does not necessarily give lower cylinder forces for this design.

A new self-made index is introduced, the Global Force Index (GFI). GFI ranges from zero to infinity and is calculated with Equation 7.15 in which $F_{cyl,i}$ is computed for each workspace point i with Equation 7.13. The sum of the force vector in the 6 legs is computed. It is then divided by 100 to give it the same magnitude as the GCI and GGI. Again, to go from a local index to a global index the sum of all workspace points is divided by the number of points. Minimizing the GFI minimizes the sum of the forces in the six legs. Since the cylinder forces depend on the external loading, the optimal design for the GFI also depends on the external forces and moments. The load for which GFI is calculated will be the loads of load case 1b. This, since it is the most severe load case for the WTG offloading with a flange on the TP. Thereby, minimizing GFI results in lower cylinder forces for the most severe load case. In this most severe load case, the minimized cylinder forces will be the highest. Thus, lowering these forces results in lower required power and less heavy and expensive hydraulic cylinders. The same approach to calculate the loads as in Subsection 6.2.1 is used except now the measurement location, thus the displacements, velocities and accelerations differ.

$$GPI = \frac{\sum_{i=1}^{N} \sigma_{min,i}(J_{nn})}{N} \tag{7.12}$$

$$F_{external} = J_{nn}^{T} \cdot F_{cyl} \tag{7.13}$$

$$\frac{\|F_{external}\|}{\sigma_{max,i}(J_{nn})} \leq \|F_{cyl,i}\| \leq \frac{\|F_{external}\|}{\sigma_{min,i}(J_{nn})} \tag{7.14}$$

$$GFI = \frac{\sum_{i=1}^{N} \frac{\sum_{j=1}^{6} |F_{cyl,i}|}{100}}{N} \tag{7.15}$$

$\sigma_{min,i}(J_{nn})$ = Minimum singular value of non-normalized Jacobian matrix for workspace point i

N = Number of workspace points

$F_{external}$ = External force and moment vector

$F_{cyl,i}$ = Axial cylinder force vector for workspace point i

$\sigma_{max,i}(J_{nn})$ = Maximum singular value of non-normalized Jacobian matrix for workspace point i

CONCLUDING FOR ALL THREE INDICES

- GCI should be maximized to maximize the dexterity
- GGI should be minimized to minimize the gradient of the dexterity
- GFI should be minimized to minimize the cylinder forces and required power

7.5.1. RANDOM POINTS IN WORKSPACE

The workspace is discretized instead of integrated to reduce computational time. The higher the number of random points the closer the discretized approach will be to the integrated value. However, the number of points need to be as low as possible to reduce computational time. 50 different random distributions are used with a discrete number of points N, running from 1 to 2000. For each set and each number of random points, the kinematic performance indices are computed. For each amount of workspace points, the difference between the maximum and minimum value of the GCI and GFI for all 50 random distributions is calculated. This difference is shown in Figure 7.3. This difference must be minimized to make sure when running the algorithm twice, both with a different random distribution with N random points, the results are almost equal. One should note the GGI is not used to determine the number of points. This, since this index is calculated by Equation 7.11 which takes the maximum value of all points. Thus, if the first random point is the maximum value, the difference does not converge. The Figure shows that for $N \geq 500$ the difference is well below 1%. This difference is found acceptable and $N = 500$ is chosen.

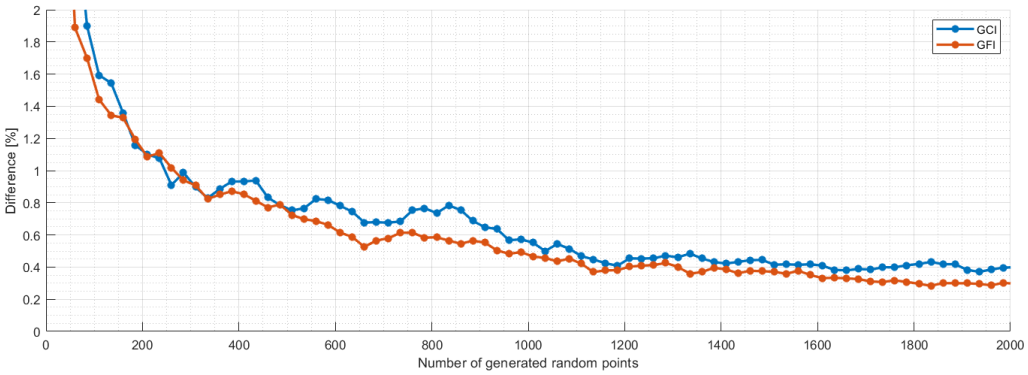

Figure 7.3: Difference between minimum and maximum index values for different random generated workspaces versus number of random points describing the workspace

7.6. GENETIC ALGORITHM

The final step to finding the kinematic optimized design is to implement all the above into an optimization algorithm. The MATLAB *Genetic Algorithm and Direct Search* Toolbox will be used to implement this problem [33]. In MATLAB a Genetic Algorithm (GA) will be used which finds the minimum of a problem. This algorithm is a proven technique to find a global minimum in engineering problems. [29] [34] [35]. *"GAs are high performance and robust optimization methods to solve engineering problems. They have been used in a variety of engineering fields such as in machine design"* [29]. Despite the higher computational time relative to for example the Pareto-search or Pattern-search algorithm, the GA searches for the global minimum while other faster methods might get stuck in local minimum. The algorithm options are chosen as the standard options to maximize the quality of the optimization.

In MATLAB, two different types of a genetic algorithm can be chosen. The Single-objective and the Multi-objective algorithm. With the Single-objective only one objective can be optimized while with the Multi-objective algorithm multiple objectives can be optimized. Both options are used as discussed below.

7.6.1. SINGLE-OBJECTIVE OPTIMIZATION

The problem has 3 indices, or objectives, for which the design must be optimized. The amount of objectives must be reduced to 1 to solve the problem with a single-objective algorithm. This can be done with a cost function containing all indices and belonging weight factors, see Equation 7.16. To minimize the GCI, which must be maximized, the reciprocal of the index is taken. The weights can be changed to divide the interest between the indices. This approach is known as the weighted-sum approach, first introduced by Zadeh [36]. The single-objective genetic algorithm will minimize a given cost function also known as the fitness function. In the single-objective optimization the cost function is used to optimize either GCI, GGI or GFI by giving a weight factor of 1 to the index that is optimized and giving a weight factor of 0 to the other two. The advantage of this approach is that it enables an easy and understandable computation because of the single cost function. This approach will result in three optimal designs for all three indices.

$$Costfunction = \frac{1}{GCI} \cdot W_{GCI} + GGI \cdot W_{GGI} + GFI \cdot (1 - W_{GCI} - W_{GGI}) \tag{7.16}$$

Besides optimizing a single index, the weights can be used to give preference to the indices. This will result in one design being partly optimal for one index and partly optimal for the others. However, these weighing factors are hard to determine. Different weight factors give different solutions thus different optimal designs. These weight factors must be chosen based on prior knowledge or preference of the designer. Another option is alternating the weight factors and analysing the results. However, this approach is not chosen to find the optimal design since it is too quantitative and will not be close to finding the actual optimum. Also, alternating the weight factors results in an unclear problem with significant size. This, because of the number of weight factors.

Based on the above, the approach which uses the single-objective with a cost function including only one index is chosen. This to get insight into the belonging design and the behaviour of the other two indices when optimizing a single index. The MATLAB script for this computation is shown in Appendix G. This script is for the Multi-objective case but also applies for the Single-objective case with the *gamultiobj* function changing to the *ga* function. Initial algorithm runs showed GCI is directly proportional to GFI and GGI. It also showed GGI is inversely proportional to GFI. These dependencies show that no optimal design can be found by just maximizing GCI and GFI and minimizing GGI. These runs also showed that the GCI and GFI perform very bad for a R_b/R_p ratio below 1. Besides getting insight into the dependence between the indices, one can find the optimal design for a single index. In total three optimizations are computed, one for each index. Figure 7.4 together with Table 7.3 show the optimal designs for a single index.

Table 7.3: Optimized designs for GCI, GGI or GFI

Optimized index	$R_b[m]$	$R_p[m]$	$\phi_b[rad]$	$\phi_p[rad]$	$h[m]$	GCI	GGI	GFI
GCI	12.39	8.95	1.99	0.39	8.56	0.66	0.21	0.63
GGI	10.98	8.10	1.15	1.15	14.41	2.6E-7	8.9E-7	1.7E4
GFI	12.37	11.50	1.40	1.83	14.85	0.13	0.07	0.31

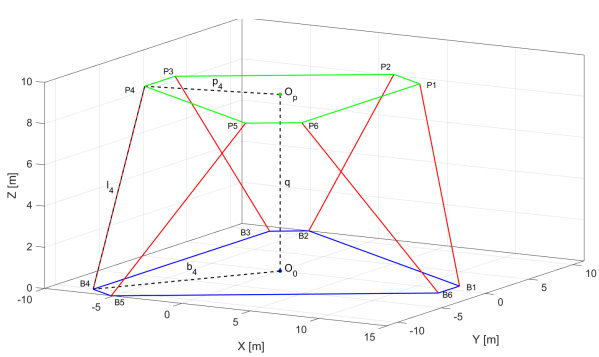

(a) GCI optimized

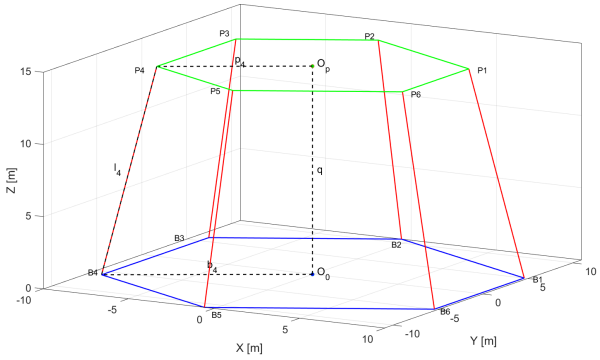

(b) GGI optimized

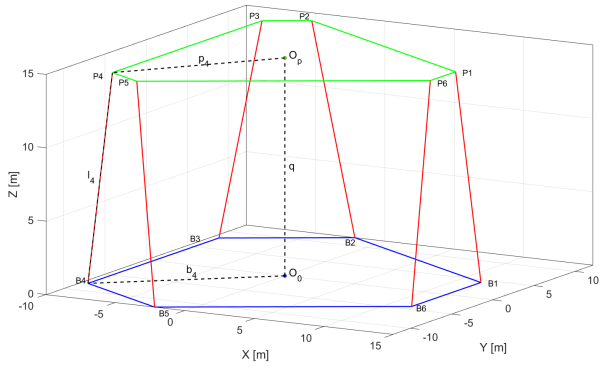

(c) GFI optimized

Figure 7.4: Optimal design for three different indices

Based on Figure 7.4 and Table 7.3, the following conclusions can be drawn. The GCI, GGI and GPI all have different optimal designs indicating inverse proportions. The R_b value for both GCI and GFI goes to the upper bound of 12.5 m as set in Table 7.1.

Optimizing for GCI, see Figure 7.4a, results in high R_b/R_p ratios. Hence, a large base radius and smaller platform radius. Besides, the joint pairs 1/2, 3/4 and 5/6 are located close to each other, so ϕ_b is large and ϕ_p is small. The height h is close to the R_p value. Designs which have GCI values close to the GCI optimum, thus can be found almost equally optimal, differ in the 5 parameters but do not differ significantly in the unit vectors of the legs. Keeping the unit vectors of the leg the same while changing the design parameters gives approximately the same GCI value.

Optimizing for GGI, see Figure 7.4b, results in ϕ_b/ϕ_p ratio being 1. This results in the joints of the lower and upper platform being above each other. Different designs which differ in the 5 design parameters can be found almost equally optimal if complying with the ϕ_b/ϕ_p ratio being approximately 1. For the GGI optimum design the changes in dexterity throughout the workspace are as low as possible but the GCI and GFI are far from optimal. One should note that minimizing the GGI comes with a risk. This, since the Jacobian matrix is near singular for low GCI values. Thus, taking the inverse of this matrix results in numerical difficulties. Generating a design by optimizing for GGI in which also GCI is minimized can cause incorrect analysis of the optimum.

Optimizing for GFI, see Figure 7.4c, results in ϕ_p and h going to the upper bound. Minimizing for GFI also gives low values of GGI. This behaviour will be researched in Section 7.6.2. This design gives 4 platform joints in the negative X-axis part and only 2 in front. This is the other way around for the GCI and GGI designs. One should note this gives the lowest sum of the forces in the cylinders but also results in huge forces in cylinders 1 and 6. To overcome this problem, 4 joints of the platform must be located in the positive X-axis. This will be taken into account in the multi-objective optimization by adding a linear constraint.

In conclusion, the optimization of a Stewart platform for offshore motion compensation must be a combination of the GCI, GFI and GGI. No single solution for the optimal design can be found by just maximizing GCI and minimizing GGI and GFI, since improving one index worsens the other.

7.6.2. MULTI-OBJECTIVE OPTIMIZATION

For the multi-objective algorithm multiple variables can be optimized. The multi-objective algorithm aims to optimize for all indices, resulting in multiple solutions because of conflicts in optimizing all indices. Thus, in contradiction with the single-objective optimization, there will not be a single cost function involving all three indices and weights. A set of Pareto fronts will exist in which one objective cannot be improved without worsening at least one other objective in the set. This is called a non-determinant or Pareto-optimal solution [37]. The standard inputs are used for the algorithm, see the MATLAB global optimization toolbox user's guide [33]. For the 3D Pareto front, the *PopulationSize* is increased from 50 to 500, increasing the computational time but also increasing the amount of Pareto front points thus increasing the visibility of the plot. An overview of the algorithm is shown below in which the bounds of Table 7.1 are used. The base platform radius must be larger than the platform radius, since initial optimization runs showed drastically low GCI values for designs in which this is not the case. ϕ_b must be larger than ϕ_p, else the optimization problem will have two identical optimal design which only differ in their orientation. One design orientated 180 degrees with respect to the other. A difference of 0.25 and 0.2 is chosen because initial optimization showed that design which do not comply with these constraints have low or high non-optimal index values. Without these constraints the extreme high and low values results in bad scaled Pareto front plots. These small values are shown in Table 7.3 when optimizing for GGI. The nonlinear constraints of Equation 7.4 and 7.5 are used as input to prevent cylinders from colliding.

$$\max_{\lambda}\{GCI(\lambda)\} \qquad \min_{\lambda}\{GGI(\lambda),\mathrm{GFI}(\lambda)\}$$

Subject to

$$R_b \in [5\mathrm{m}, 12.5\mathrm{m}] \qquad \mathrm{R}_p \in [5\mathrm{m}, 12.5\mathrm{m}]$$

$$\phi_b \in [0.08\mathrm{rad}, 2.01\mathrm{rad}] \qquad \phi_p \in [0.08\mathrm{rad}, 2.01\mathrm{rad}]$$

$$h \in [3\mathrm{m}, 15\mathrm{m}]$$

$$\text{Workspace} \in [\pm 0.58\mathrm{m}] \times [\pm 1.24\mathrm{m}] \times [\pm 0.83\mathrm{m}] \times [\pm 2.83^\circ] \times [\pm 0.48^\circ] \times [\pm 0.23^\circ]$$

$$R_b - R_p \geq 0.25\mathrm{m}$$

$$\phi_b - \phi_p \geq 0.2\mathrm{m}$$

$$2 \arcsin\left(\frac{1}{2R_{b,p}}\right) - \phi_{b,p} \leq 0$$

$$2 \arcsin\left(\frac{1}{2R_{b,p}}\right) - (120 \cdot \frac{\pi}{180} - \phi_{b,p}) \leq 0$$

TWO OBJECTIVES

First, the multi-objective algorithm is used to compute three Pareto fronts with two indices for each front, see Figure 7.5. Figure 7.5a shows GCI is directly proportional to GPI, maximizing GCI maximizes GGI. This, while GGI must be minimized. For low GCI values, GGI increases slowly for higher GCI values. For GCI values above 0.6, the GGI increases rapidly for higher GCI values. Thus, an optimum design is for GCI values below 0.6, which makes sure GGI is not high. Figure 7.5b shows GCI is directly proportional to GFI, maximizing GCI maximizes GFI. This, while GFI must be minimized. Figure 7.5c shows the Pareto front for GFI and GGI. Here it is shown that GFI is inversely proportional to GGI, minimizing GFI maximizes GGI. This, while GGI must be minimized. For GFI values below 0.35, the GGI value increases rapidly. Concluding from the above, an optimum design is for GCI values below 0.6 and GFI values above 0.35, making sure the GGI is not high.

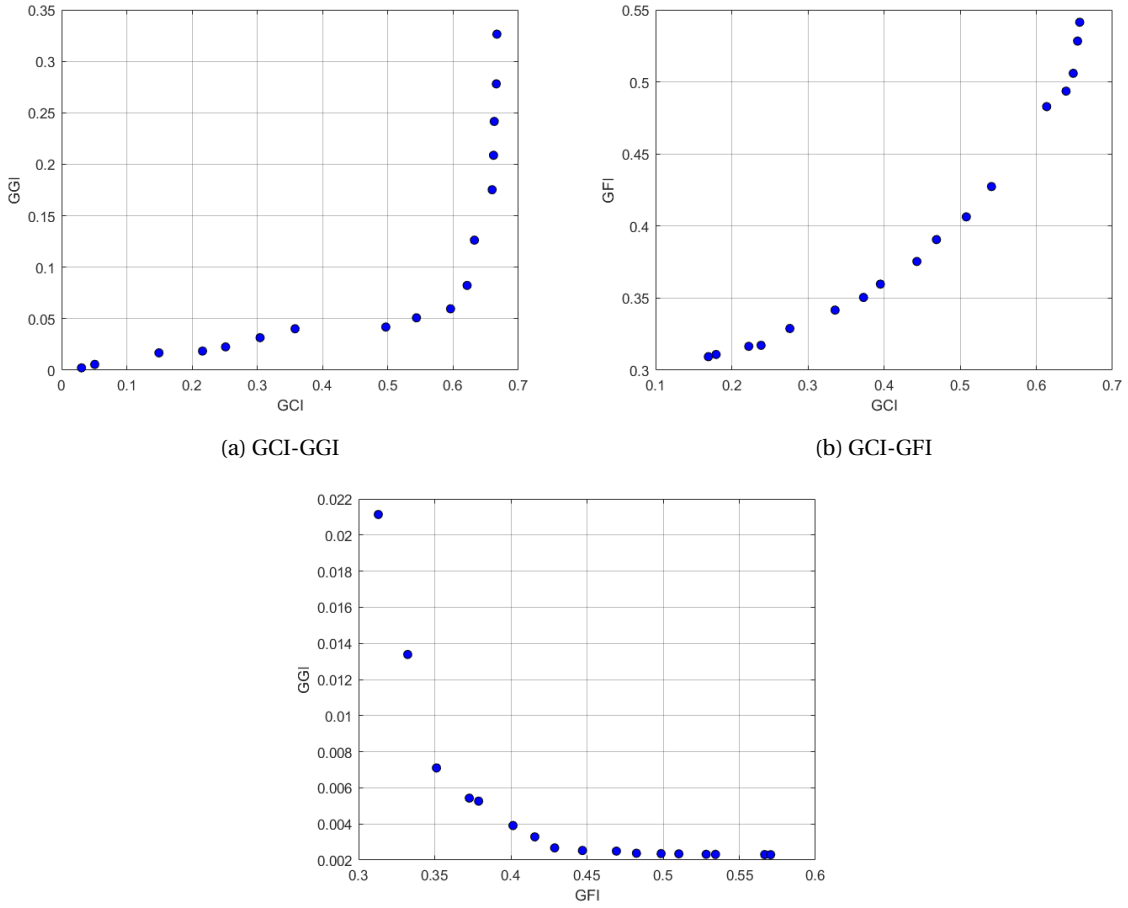

(a) GCI-GGI

(b) GCI-GFI

(c) GFI-GGI

Figure 7.5: 2D fronts for GCI, GGI & GFI combinations.

THREE OBJECTIVES

After running the multi-objective algorithm for all three indices, the 3D Pareto front is found. The plot coming directly from the algorithm lacked resolution because of the small amount of Pareto points. To increase the resolution, all the non-dominated solutions found by the algorithm are used as input for the script shown in Appendix G.3. This script filters the set of points according to Pareto dominance, which means points that are dominated are filtered. All filtered points are plotted in Figure 7.6, showing the Pareto front. The empty stroke in the surface is a result of the non-linear constraints.

Points beyond extreme values of the indices, which are not considered as optimal solution, are not shown to increase the visibility of the plot. In contrast to the 2D plots, this front is not a single line but a surface. This since when plotting all possible designs in 3D a cloud of points is formed of which the Pareto front is a surface. This Pareto front is formed by a non-smooth surface. This, because the workspace has been discretized and computing the Pareto front numerically differs from the real front. Increasing the number of points in the front and decreasing the tolerances of the algorithm will result in a smoother front. However, this increases the computational time significantly.

From the multi-objective 3D Pareto front and the single-objective 2D Pareto fronts one can find the same proportionalities between the indices. Because of the proportionalities, the optimal design will be design choice. However, following from the 3D Pareto front, the options for a final design can be narrowed down to a design space. The design space is a clustered amount of points giving the optimal designs. Narrowing done the number of points is done with the following steps. First, the bounds for the GCI and GFI are set. An optimum design is with a GCI value below 0.6 and a GFI value above 0.35, which makes sure the points are not close to the limits where GGI increases rapidly. This makes sure that for small changes in either the platform pose or design parameters, there will not suddenly be a low sensitivity to position errors. As stated before, this is concluded by assessing the 2D Pareto fronts.

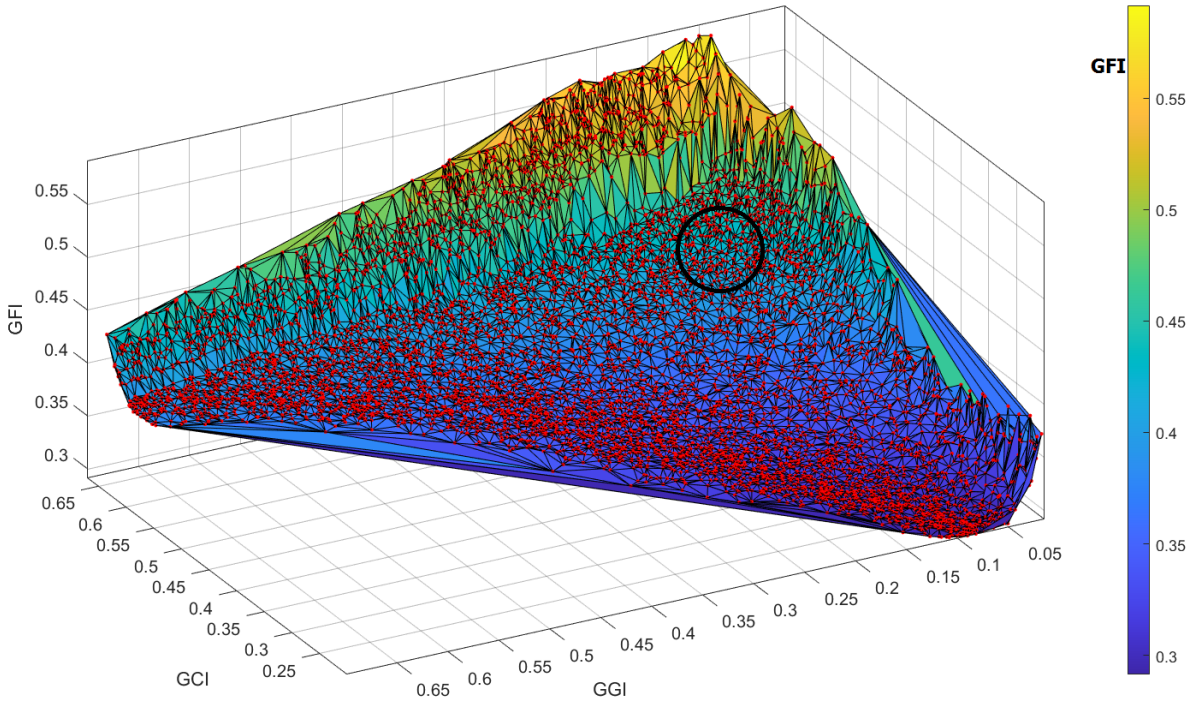

Figure 7.6: 3D Pareto front formed by Delaunay triangulation of red points indicating the pareto points. Black circle indicates selected design space. Colorbar is a function of GFI.

Second, the selection between two arbitrarily points is made based on the amount to which the indices change. For example, if one point in comparison to another point has a slightly higher GGI, which is not beneficial, but has a significant lower GFI, which is beneficial, this point is preferred above another. At last, the design space is selected more on the performance of the GCI and GGI index than the GFI index. This, since the complexity of the system will be with the control systems which must have high accuracy to install a WTG on a foundation.

By using the three steps as discussed above, the design space in Figure 7.6 is found. Points located within this space are the optimal points which comply to all boundaries and constraints. All points have the following characteristics. R_b values go to the upper limit of 12.5 m with R_b being approximately a meter smaller. Also, ϕ_b goes to the upper limit of 2 rad with ϕ_b being approximately half of that value. The height h ranges from 7 to 9 m. This all shows that a range of designs exist, with slightly different design parameters, giving the design space which consists of the optimal designs.

By again using the approach as above, only single optimal design can be found which is shown in Table 7.4 and Figure 7.2. This point has been fine-tuned by tweaking the parameters to find an even better solution after which the design parameters are rounded to give a manufacturable and clear design. For this design the R_b and ϕ_b values are at the upper limits as set in Table 7.1. One should note the selected design space and the selected point within this space are a choice and are not single optimal solutions. Other designs can be chosen based on a different interest in one of the indices. This, while keeping in mind one must comply with the linear and non-linear constraints.

Table 7.4: Optimized design and corresponding kinematic indices

Parameter	$R_b[m]$	$R_p[m]$	$\phi_b[rad]$	$\phi_p[rad]$	$h[m]$	GCI	GGI	GFI
Value	12.5	11.3	2.0	1.0	8.0	0.52	0.11	0.45

7.7. DESIGN SENSITIVITY ANALYSIS

The design sensitivity analysis is used to obtain the sensitivity of the kinematic indices with respect to changes in the design parameters. One should note that changing an individual parameter will lead to a less optimal design when considering all three indices. However, when designing this system for real-life, changing the parameters might be desirable. This analysis will give more insight into the design freedom of the Stewart platform's geometry. As stated before, changing all five parameters can give a different design which has better indices then when changing a single parameter. However, because of the complexity, this is not researched here. Each parameter will be increased and decreased while keeping in mind the lower and upper bounds of Table 7.1. For each parameter, the results are discussed below.

R_b RADIUS OF BASE CIRCLE

This assessment is based on Figure 7.7a. The value of R_b cannot be increased because of its upper bound. As stated before, increasing it beyond 12.5 m requires too much deck space and makes the system unreasonably large. Decreasing R_b but keeping in mind the linear constraint R_b - $R_p \geq 0.25$ m lowers the GFI value thus decreasing the cylinder forces. However, this will significantly decrease GCI and increase GGI, which for both is not beneficial. Thus, by lowering R_b a compromise must be made between reducing the cylinder forces and increasing the complexity of controlling the system. Decreasing R_b below R_p thus below 11.3 is not advised since all indices perform significantly worse. GCI decreases while GGI and GFI increases which is not beneficial for all.

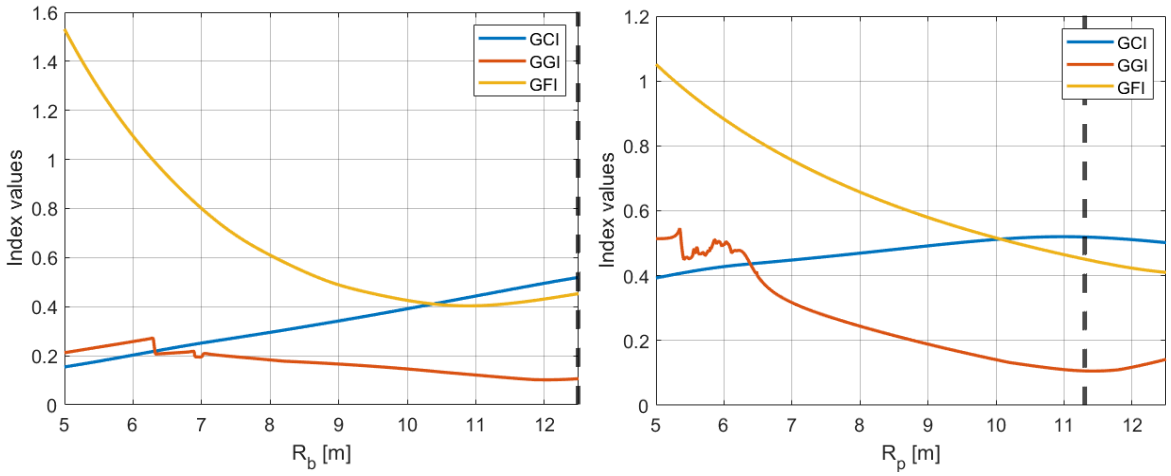

(a) Indices vs Radius of platform R_b

(b) Indices vs Radius of platform R_p

Figure 7.7: Sensitivity analysis of parameters R_b & R_p on index values. Vertical dotted lines show chosen design parameter.

R_p RADIUS OF PLATFORM CIRCLE

This assessment is based on Figure 7.7b. Increasing the R_p value above 11.3 and setting it closer to the R_b value reduces the cylinder forces. This, since the cylinder unit vectors are directed more vertically being able to more effectively apply vertical forces and overturning moments. However, increasing the R_p value is not beneficial for GCI and GGI. Again, a compromise must be made between the cylinder forces and the control system. Significantly lowering the R_b will not be beneficial for all three indices.

ϕ_b SEPARATION ANGLE BETWEEN ADJACENT ACTUATOR ATTACHMENT POINTS ON BASE

This assessment is based on Figure 7.8a. To prevent cylinder collisions, the value of ϕ_b cannot be increased because of its upper bound. Decreasing ϕ_b lowers the cylinder forces but increases GGI and extremely decreases GCI which is not beneficial. Lowering ϕ_b below approximately 1.5 rad is not advised since it has a negative influence on all three indices. Above all, lowering ϕ_b below 1 rad must be avoided. As stated in Subsection 7.6.1, having a ϕ_b/ϕ_p ratio of almost 1 makes the Jacobian matrix singular making the system uncontrollable.

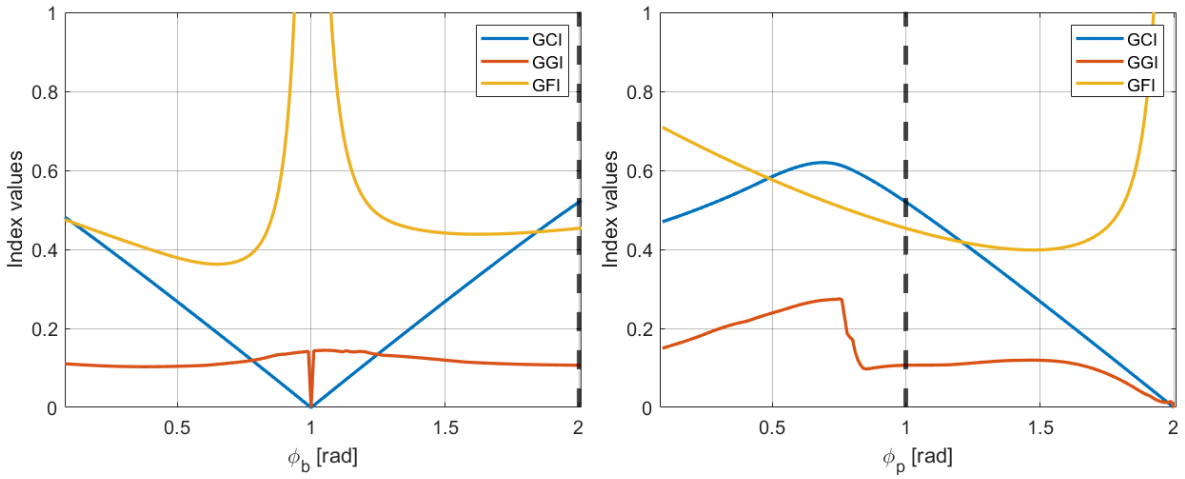

(a) Indices vs Separation angle between adjacent actuator attachment points on base ϕ_b

(b) Indices vs Separation angle between adjacent actuator attachment points on platform ϕ_p

Figure 7.8: Sensitivity analysis of parameters ϕ_b & ϕ_p on index values. Vertical dotted lines show chosen design parameter.

ϕ_p SEPARATION ANGLE BETWEEN ADJACENT ACTUATOR ATTACHMENT POINTS ON PLATFORM

This assessment is based on Figure 7.8b. To avoid a singular Jacobian matrix resulting in numerical difficulties, the value of ϕ_p must be chosen in such order that the ratio of ϕ_b/ϕ_p is far from 1. Increasing ϕ_p significantly decreases GCI while GGI is approximately kept constant. Thus, the dexterity decreases but is maintained almost constant throughout the workspace. The cylinder forces are decreased, but less significant than the GCI decreases. Thus, designing the Stewart platform with a higher ϕ_p value decreases the cylinder forces but comes with a high cost in terms of the GCI value. Increasing ϕ_p beyond approximately 1.5 rad is not advised since it has a significant negative influence on GCI and GFI. This is because of the ϕ_b/ϕ_p ratio getting closer to 1. Lowering ϕ_p increases GCI which is beneficial but increases GGI and GFI which is not beneficial. Lowering it below approximately 0.85 rad is not advised since this is not beneficial for all indices. At last, one can find a rapid change in GGI for ϕ_p at approximately 0.75. This is because at this point the platform joints of cylinder 2 and 5 are located close to the X-axis. With ϕ_p below and above 0.75 rad located at respectively the positive and negative X-axis. Thus, with a small change in platform pose the location can change from positive to negative X-axis or the other way around. This results in rapid change in dexterity or GCI thus giving a high value of GGI.

h VERTICAL DISTANCE BETWEEN O_o AND O_p

When considering pure heavy motion, the only parameter that changes is h. With an positive heave motion the height h decreases and the other way around. By knowing that the maximum heave motion is approximately 1 m, increasing or decreasing h with at least 1 m should not change the three indices significantly. As seen in Figure 7.9 the indices stay within reasonable changes with h between 7 and 9 m. Increasing h to its upper limit of 15 m decreases all indices having a positive influence on GGI and GFI while having a negative influence on GCI. Lowering GCI results in a low dexterity, thus a low ability to accurately control the system. Because the GGI also becomes smaller, the bad dexterity throughout the workspace is almost constant. Again a compromise must be made between the cylinder forces and the control system. At last, for h is 7.5 m a rapid change in GGI can be found. Since no clear explanation can be found, this behaviour should be assessed in further researched. To make sure the design is not near the rapid increase of GGI, advised is not to decrease h below its value of 8 m.

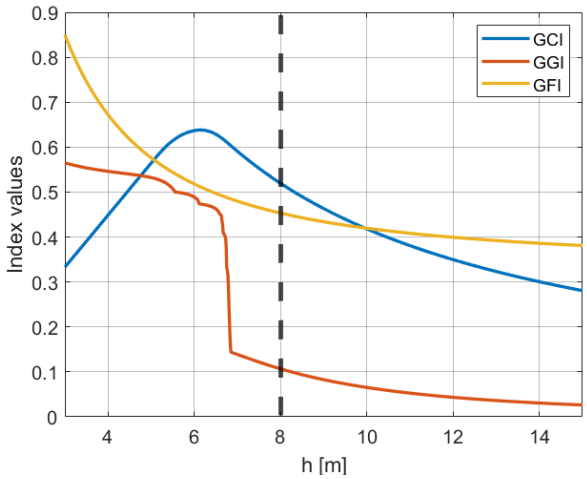

Figure 7.9: Indices vs height h which is the vertical distance between O_o and O_p. Vertical dotted line shows chosen design parameter.

7.8. CYLINDER FORCES

By using Equation 7.13, the forces g_l in the legs are calculated. This is a slightly different method which uses fewer computations than the method used in Subsection 6.2.1 and gives the same outputs. Table 7.5 shows the maximum forces in the legs for load case 1b. This load case is discussed in Subsection 6.2.1. As stated before, all inputs remain the same except for the motions since the measurement location has been adjusted. One should note these are the maximum forces in the legs for one corresponding most severe pose, giving the maximum required power. The forces in cylinder 1 and 6 are the largest. This is as expected, since these two cylinders are the two closest to the offloading direction thus counteracting the largest part of the overturning moment exerted on the platform by the WTG. Cylinders 3 and 4 provide tension since these cylinders are located at the negative X-axis. Thus, the tension in these cylinders provides a counteracting moment. The maximum required power is calculated by multiplying the sum of the maximum forces by the maximum required cylinder velocity of 0.69 m/s. This gives a maximum required power of 32 MW. The calculated forces and required power differ from those calculated in Subsection 6.2.1 since the measurement point for this calculation is located closer to amidship thus has lower motions. This especially reduces the maximum required cylinder velocity which is used to calculate the required power. These values are found more precise and less conservative and will be used in further research.

Table 7.5: Cylinder forces in 6 legs for optimal design with load case 1b [MN] and required power

1	2	3	4	5	6	Power [MW]
14.7	5.3	-4.3	-6.5	0.7	15.0	32

7.9. VERIFICATION OF ALGORITHM

The algorithm results must be verified. This is done by decoupling the indices computations from any algorithm. A MATLAB script is made in which the indices for 10^5 random designs are computed. One should note that for an infinite number of designs as input, the verification script should give the same outputs as the optimization. However, this which will result in unreasonable computation time. First, the maximum and minimum values of the indices are found approximately the same as the those belonging to the single-objective optimal designs. Second, the maximum and minimum values of the indices are also approximately the same as the maximum and minimum values in the Pareto fronts. Also, the proportionality between the different indices is found to be equal in this computation and the Pareto fronts. At last, plotting all indices in a 3D scatter-diagram with the three indices on the three axis gives a cloud of possible designs. The optimal edges of this cloud form the Pareto front of Figure 7.6. Overall, the algorithm is found to be verified.

7.10. CONCLUSION

A kinematic optimization is carried out by means of a genetic algorithm to find the optimal values of the five parameters describing the Stewart platform's geometry. The parameters consist of the base R_b and platform R_p radius, the separation angle between the adjacent joints of the base ϕ_b and platform ϕ_p and the height h between base and platform.

Three indices are used to indicate the kinematic performance of a parameter set: the global conditioning index, global gradient index and, self-made, global force index. The indices describe respectively the dexterity, the gradient of the dexterity and the sum of the cylinder forces. Optimizing for each index individually highlighted that the optimization should include all three indices, since improving the performance of one index has a negative impact on the other indices. This since GCI is directly proportional to GFI and GGI. And GGI is inversely proportional to GFI.

The single-objective optimizations in which only one index is optimized showed the following. Optimizing for GCI results in high R_b/R_p ratios. Hence, a large base radius and smaller platform radius. Besides, the base joint pairs $1/2$, $3/4$ and $5/6$ are located close to each other, so ϕ_b is large and ϕ_p is small. Optimizing for GGI results in ϕ_b/ϕ_p ratio being 1. This results in the joints of the lower and upper platform being above each other. Optimizing for GFI results in ϕ_p and h going to the upper bound. The single-objective optimizations also highlighted that the GCI and GFI perform worse for a R_b/R_p ratio below 1.

The optimal set of design parameters is selected by taking advantage of the Pareto front, which is computed with a multi-objective optimization including all indices. In the optimal design, the R_b and ϕ_b values are at their upper limits and the maximum required power is 32 MW.

A design sensitivity analysis is performed to obtain the sensitivity of the kinematic indices with respect to changes in the design parameters. The results of the sensitivity analysis showed that the optimal design of a Stewart platform is a design choice based on a trade-off between performance and required power. Besides, one should comply with the linear and non-linear constraints, the lower and upper bounds of the parameters and having a ϕ_b/ϕ_p ratio far from one.

8

SIMULATION OF THE MOTION COMPENSATION SYSTEM

In this chapter, a model is developed in MATLAB and Simulink to simulate the dynamics of the Stewart platform as optimized in Chapter 7. The model gives other insights than Chapter 6 and 7 in which conservative assumptions are made, making the system less feasible. By getting more insights from this model, which presents the real-life system more accurately, the feasibility of the system can be assessed in-depth. One of the insights gained is the feasibility of including a passive system besides the currently active system. Compared to similar applications, it is expected that including a passive system reduces the required power. This will be verified in this chapter. For more detailed information about the model, see Appendix H.

Three different models are assessed. The effect on the results of adding the hydraulic system, supposed to make a more realistic system which takes into account the hydraulic and valve dynamics, are assessed. Also, the effect of adding a passive system is assessed. All three model configurations are listed below and their abbreviations are given. For all, only the behaviour after 25 seconds, thus excluding the initial transient behaviour, is assessed.

1. Stewart platform without hydraulic system without passive system
   Ideal Motion Compensation (IMC)

2. Stewart platform with hydraulic system without passive system
   Active Motion Compensation (AMC)

3. Stewart platform with hydraulic system with passive system
   Passive-Active Motion Compensation (PAMC)

8.1. SOFTWARE

The model is developed in Simulink, a graphical extension to MATLAB for modeling and simulation of systems. Matlab is used for post-processing and calculates all required inputs for Simulink, see Appendix H. The model is developed in Simulink with the Simscape Multibody First Generation toolbox [38]. In Simulink a model is built up with different building blocks connected with lines. An ordinary Simulink model without using the toolbox only represents the system with mathematics, thus algebraic and differential equations. With the use of these equations, the model can be simulated by predicting the systems next state. With the Simscape Multibody toolbox the system is represented with physical structures, instead of only mathematics, including mass properties and geometric and kinematic relationships between rigid bodies. Rigid bodies connected with joint blocks can be added in which the lines or connections represent a physical connection. Simscape Multibody converts the physical structures to an equivalent mathematical model after which it is simulated in Simulink. Using the Simscape Multibody will save significant time and effort. Besides, another advantage of this toolbox is that the model can be visualised, see Appendix H. In Simulink the variable time step ode23t solver is used which gives accurate results with a low computational time for stiff systems.

8.2. ASSUMPTIONS & SCOPE

To reduce the complexity of the model and stay within the capabilities of the used Software, a scope including assumptions is defined. The scope and assumptions are discussed below.

The installation is divided into two phases. The first phase of the installation is where the Stewart platform is not yet connected to the TP and where the WTG is in the centre of the platform. The second phase is the phase where the system is connected to the TP, providing a vertical force counteracting the overturning moment, after which the WTG is skidded to the TP. For the first and second installation phase, two different control systems must be designed. This since after connecting the system to the TP, one DoF is lost. The second phase is out of the scope because the control system design is not the aim of the current research as the goal is understanding the basic design parameters of the hydraulics and the added benefit of a passive hydraulic system. Besides, the complexity of the second installation phase is in the TP exerting a force on the system and losing one DoF. In conclusion, only the part of the installation where no connection between the system and vessel exists with the WTG loaded at the platform centre is considered.

The dynamic coupling between the system and the vessel and its DP system is not taken into account. This since it reduces the model complexity. Although, it will have an influence on the control system. However, it is expected that this interaction will have a limited influence on the platform hydraulic system. Furthermore, the system inertia and mass are small compared to the vessel mass and inertia reducing the effect of dynamic coupling. By making this assumption, the vessel motions can be directly imposed on the base CoG. Thus, the base CoG will perfectly follow the unaffected vessel motions. In further research, the dynamic coupling between the system and the vessel should be assessed.

For simplification and because of Simulink's restricted capabilities, all rigid bodies and cylinders are assumed to have no deflections. Besides the exact mass and inertias of all components are assumed to be known. At last, the cylinders and joints are modelled without Coulomb and viscous friction, which are relatively small compared to the axial cylinder forces.

8.3. MODEL INPUTS

The Simulink model is inspired by the Simscape Multibody User's Guide case study of the Stewart platform [38]. Other models of the Stewart platform typically connect the base of the Stewart Platform to the ground and apply motions to the platform. This, while for the motion compensating system the goal is to keep the platform earth fixed with vessel motions being imposed to the base.

The computations of the model are set up as follows. First, the required leg lengths to keep the platform in a earth fixed position are calculated. The required leg extensions of all 6 legs are calculated by subtracting the nominal leg lengths $l_{n,i}$, see Equation 8.1. This equation is similar to Equation 7.1 as used in Chapter 7, now including the subtracting of the nominal leg lengths.

$$l_{ext,i} = q + R \cdot p_i - b_i - l_{n,i} \tag{8.1}$$

$l_{ext,i}$ = Required extension leg i	R_{matrix} = Rotation matrix	$l_{n,i}$ = Nominal length leg i
q = Base O_0 to platform CoG O_p	p_i = Joint coordinate i in platform plane	b_i = Joint coordinate i in base plane

The required leg extensions are compared with the actual leg extensions. This gives errors, from now on position errors, which are used as input for the controller. Besides the position error, the required leg velocity is used as input for the controller. By applying the controller gain to both inputs, a output signal is computed which controls the system. In Section 8.3.7, the controller is discussed in detail. By measuring all motions, controlling the hydraulic cylinders and supporting the platform to produce the counteractive vessel motions, the platform is kept in earth fixed steady position.

8.3.1. MATLAB POST-PROCESSING

The Matlab script used for post-processing computes the neutral pose of the optimized design of Table 7.4. This includes calculating the joint locations, leg lengths and leg vectors, primitive revolute axis of the uniform joints and primitive revolute of the cylindrical joints. The mass and inertia of the platform plate are calculated by simplifying it as a circular plate with a thickness of 10 cm. The WTG is added to the model by adding its mass and inertia to that of the platform plate. The inertia of the WTG is transferred to the platform's CoG with Steiner's theorem which is the same method as used in Section 4.4.

One should note the mass and inertia of the base do not affect the system. This, since the vessel motions are imposed on the base CoG. Thus, the base is not manipulated by the hydraulic cylinder force or the system itself but by the imposed base CoG motions induced by the vessel motions. In real-life, the mass and inertia of the base will influence the system behaviour and vessel motions to a small extent. The same applies to the cylinder, rod, platform and WTG mass and inertia which in real-life will influence the vessel motions thus the system behaviour. However, the dynamic coupling of the system and vessel is not within the scope of this thesis as stated in Section 8.2.

8.3.2. BASIC CYLINDER DESIGN

The hydraulic cylinders are designed by using the DNV-standard for hydraulic cylinder [DNVGL-CG-0194]. First, some design choices are made. The minimal operational cylinder stroke is 2.6 m, which is the sum of the maximum leg extending and maximum leg retraction of the cylinders during the 3-hour period. The error margin in cylinder length, dedicated as a software buffer on two sides, is set at 0.2 m which is assumed to suffice. Thus, the minimal required stroke length is 3 m. For structural purposes, as will be discussed below, and to allow for a larger safety margin in operational stroke, the stroke length is set as 5 m. With the optimized design, the length between the joints in neutral position is approximately 10 m which fits the stroke length. Both the cylinder tube and piston rod, which is the solid upper extending part of the hydraulic cylinder, are modelled as bodies with a mass and inertia. The diameter and wall thickness of both are determined with the buckling checks of the DNV-standard of which Figure 8.1 shows the parameters. The moment of inertias and Z factor are calculated in respectively Equation 8.2 and 8.3. With a safety factor of 4, the maximum allowable actual load P_a is calculated, see Equation 8.5. Knowing the maximum actual load to be 15 MN from Section 7.8, Table 7.5 and by using an iterative process, the cylinder inner and outer diameter are calculated. All parameters given in Table 8.1 are used as inputs for the model.

$$I_{cyl} = \frac{\pi(D_0^4 - D_i^4)}{64}\ ,\ I_{rod} = \frac{\pi d^4}{64} \tag{8.2}$$

$$Z = \frac{L1}{I_{cyl}} + \frac{L2}{I_{rod}} + \left(\frac{1}{I_{rod}} - \frac{1}{I_{cyl}}\right)\frac{L}{2\pi} sin\left(2\pi\frac{L1}{L}\right) \tag{8.3}$$

$$P_E = \frac{E \cdot \pi^2}{L \cdot Z} \tag{8.4}$$

$$\frac{P_E}{P_a} \geq 4 \tag{8.5}$$

I_{cyl} = Moment of inertia cylinder
I_{rod} = Moment of inertia rod
d = Diameter rod
D_0 = Outer diameter cylinder
D_i = Inner diameter cylinder
$L1$ = Length of cylinder tube
$L2$ = Length piston rod
$L = L1 + L2$
P_E = Buckling load
P_a = Actual max. load
E = Young's modulus = 206 GPa

Table 8.1: Parameters of the six designed hydraulic cylinders. L gives the fully extended length.

Parameter	$L1$	$L2$	L	D_o	D_i	d
Value $[m]$	7.5	5.0	12.5	1.05	1.0	0.525

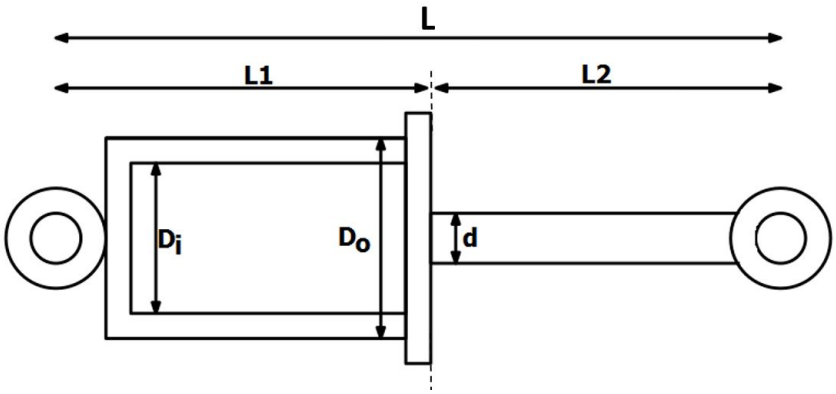

Figure 8.1: Hydraulic cylinder design in fully extended pose with parameters used in buckling checks

A hydraulic cylinder can be designed asymmetric or symmetric. Symmetric cylinders have the main advantage that the push and pull area on which the pressure acts are equal enabling simpler valve control. However, the symmetric cylinder needs to be designed larger to resist against buckling, resulting in larger fluid flows. Asymmetric hydraulic cylinders have many advantages such as small size requiring less fluid flow, convenient manufacture and low price. Therefore, asymmetric cylinders are chosen. Each of the six cylinders is implemented in Simulink as shown in Figure 8.2. This includes the three joints, cylinder and rod body with mass and inertia, a sensor measuring the position and velocity and a force actuator extending the cylinder.

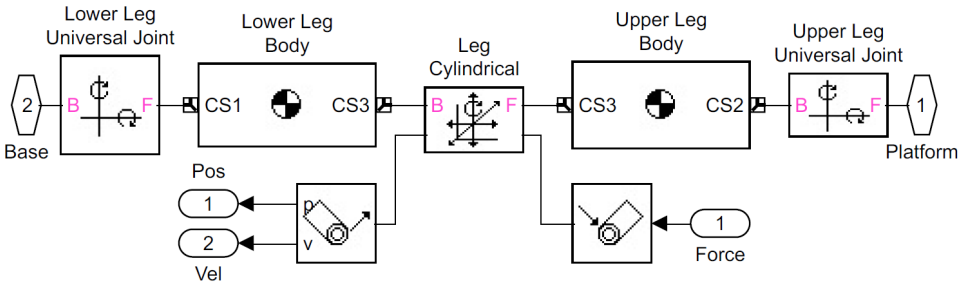

Figure 8.2: Hydraulic cylinder in Simulink.

8.3.3. HYDRAULIC SYSTEM

The hydraulic system is modelled as shown in Figure 8.3 and consists of the hydraulic cylinder including the two pressure chambers A and B and the valve. The piston and rod side indicated with respectively A and B. The valve, which is controlled by the controller, will control the fluid flow inside the chambers by varying the size of the flow passage. All parameters of the hydraulic system are calculated and discussed below. An overview is given in Table 8.1. One should note, six identical hydraulic systems are used in the model, representing one hydraulic system for each leg. To simplify the hydraulic system, the scope does not extend beyond the tank pressure p_T and supply pressure p_S which are both assumed to be constant inputs. Additional pumps, pressure tanks and pipes are thus not modelled. The assumption of a constant supply pressure is found to be justifiable by Jelali & Kroll [39]. The tank pressure can be assumed constant since it is small compared to the system pressure.

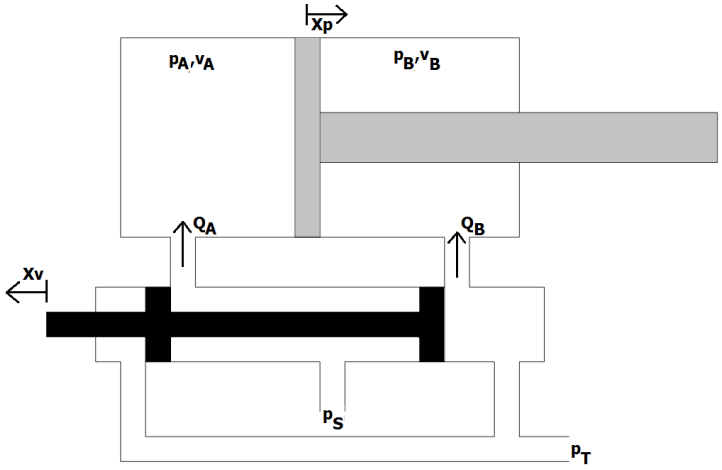

Figure 8.3: Hydraulic system including hydraulic cylinder and rod. Valve and rod indicated in black and gray respectively. Current pose gives high pressure in cylinder chamber A resulting in extending of cylinder. x_p is zero is located at half the cylinder length. All sign directions indicate the positive direction.

DIFFERENTIAL EQUATIONS

The differential equations belonging to the extending and retracting of the cylinder are given [39]. Equation 8.6 and 8.7 are for the piston A and rod B side respectively in which the volume time derivative equals surface times the piston velocity.

$$\frac{\delta p_A}{\delta t} = \frac{\beta_e}{v_A}\left(Q_A - \frac{\delta v_A}{\delta t}\right) = \frac{\beta_e}{v_A}\left(Q_A - A_p \cdot \frac{\delta x_p}{\delta t}\right) \tag{8.6}$$

$$\frac{\delta p_B}{\delta t} = \frac{\beta_e}{v_B}\left(-\frac{\delta v_B}{\delta t} + Q_B\right) = \frac{\beta_e}{v_B}\left(A_r \cdot \frac{\delta x_p}{\delta t} + Q_B\right) \tag{8.7}$$

p_A = Pressure at piston side	v_A = Volume at piston side	x_p = Piston displacement
p_B = Pressure at rod side	v_B = Volume at rod side	β_e = Effective bulk modulus
Q_A = Flow at piston side	A_p = Cylinder area at piston side	
Q_B = Flow at rod side	A_r = Cylinder area at rod side	

The flows Q_A and Q_B are calculated in Equations 8.6 and 8.7 respectively. These equations calculate the flow through the valve which is a function of both pressure differences and valve characteristics.

$$Q_A = Q_N \cdot \frac{x_v}{100} \begin{cases} \frac{\sqrt{p_S - p_A}}{\Delta p_n} \cdot sgn(p_S - p_A) & \text{for } x_v > 0 \\ \frac{\sqrt{p_A - p_T}}{\Delta p_n} \cdot sgn(p_A - p_T) & \text{for } x_v < 0 \end{cases} \tag{8.8}$$

$$Q_B = -Q_N \cdot \frac{x_v}{100} \begin{cases} \frac{\sqrt{p_B - p_T}}{\Delta p_n} \cdot sgn(p_B - p_T) & \text{for } x_v > 0 \\ \frac{\sqrt{p_S - p_B}}{\Delta p_n} \cdot sgn(p_S - p_B) & \text{for } x_v < 0 \end{cases} \tag{8.9}$$

Q_N = Nominal flow	sgn = sign of substraction = + or -	p_S = Supply pressure
x_v = Percentage valve is opened	Δp_n = Nominal pressure difference	p_T = Tank pressure

At last, the cylinder force F_{cyl} is calculated with Equation 8.10.

$$F_{cyl} = p_A \cdot A_r - p_B \cdot A_p \tag{8.10}$$

FLUID FLOW

The minimum required flow in the chambers is calculated with Equation 8.11. The required flow is the maximum of the piston flow Q_{piston} and rod flow Q_{rod}. The maximum required cylinder extending and retracting velocity equals the maximum and minimum required leg velocity respectively. This velocity is calculated as the maximum time derivative of the required leg extension as calculated in Equation 8.1. The maximum retracting and extending velocity are respectively 0.62 m/s and 0.67 m/s. The required maximum flow in one cylinder is calculated to be 29000 l/min which is the nominal flow Q_n, the flow with the valve completely open. To comply to available valves, Q_n is rounded to 30000 l/min.

$$Q_{piston} = A_p \cdot \frac{\delta x_p}{\delta t} \quad , \quad Q_{rod} = A_r \cdot \frac{\delta x_p}{\delta t} \tag{8.11}$$

Q_{piston} = Minimal piston flow A_p = Cylinder area at piston side x_p = Piston displacement
Q_{rod} = Minimal rod flow A_r = Cylinder area at rod side

MAXIMUM PRESSURE

The maximum required pressure in the piston is calculated. This maximum pressure times the piston area should equal the opposite force, consisting of the mass of all components times the gravity acceleration. Since in the ideal system the platform does not move, no acceleration force is taken into account. As stated in Section 7.8, Table 7.5, the maximum actual load is 15 MN. Dividing this load by the piston area gives the required pressure to be 190 bar. To built in a safety margin, which takes into account the neglecting of the platform acceleration, a maximum required pressure of 225 bar is set.

VALVE DESIGN

Since designing the complete hydraulic valve is out of the scope, assumptions are made regarding the design parameters of the valves. By bench-marking with an existing Boskalis hydraulic system, the parameters are estimated. First of all, the valve is assumed to be a proportional valve with zero overlap. The zero overlap means the valve can instantaneously switch between extending or retracting the cylinder. The proportionality results in both the percentage the valve is opened, x_v, and the percentage of the maximum flow through the valve, Q_n, are exactly the same. Thus, 50% open gives 50% of the maximum flow. The valve dynamics are modelled linear with a valve range and valve rate limiter. The valve range of x_v for extending is between 0 %, fully closed, and 100 %, fully open. For retracting this is between -100 % and 0 % giving opposite flow direction than in the extending case. The maximum rate of change of x_v is the maximum valve speed. The maximum speed is given in the required time to go from fully closed to fully open and the other way around. This is 1e-2 s. The nominal pressure difference Δp_n and tank pressure pT are set at respectively 25 bar and 1 bar. The required supply pressure is calculated as the sum of the maximum pressure and the nominal pressure difference Δp_n. Thus, the supply pressure pS is 225 bar plus 25 bar which is 250 bar.

INITIAL CONDITIONS

To make sure the system is stable, initial pressure conditions for the cylinder are given. The initial rod side pressure p_{B0} is set at an initial 125 bar. The initial cylinder side pressure p_{A0} is calculated to equal the sum of the force exerted by the rod side pressure and the total mass above the cylinder consisting of the platform and WTG, being 140 bar

HYDRAULIC OIL

The hydraulic fluid is mineral oil which is common in hydraulic cylinders. The effective bulk modulus β_e of this oil takes into account the compressibility of the oil and depends on the oil pressure. The effective bulk modulus is calculated with Equation 8.12 [39]. For simplification and to reduce computational time, the bulk modulus is calculated for the maximum and minimum pressure after which the average bulk modulus of both is used as input. The maximum and minimum pressure are respectively the supply pressure pS and tank pressure pT. The calculated effective bulk modulus is 12000 bar

$$\beta_e = \beta_{max}\left(1 - exp(-0.4 - 2 \cdot 10^{-7} p_{oil})\right) \quad [39] \tag{8.12}$$

β_e = Effective bulk modulus p_{oil} = Oil pressure

β_{max} = Maximum bulk modulus = $1.8 \cdot 10^9$ Pa

Table 8.2: Hydraulic cylinder and valve design parameters

Parameter	Value	Unit
Supply pressure p_S	250	bar
Tank pressure p_T	1	bar
Initial pressure p_{A0}	140	bar
Initial pressure p_{B0}	125	bar
Nominal pressure difference Δp_n	25	bar
Valve range	-100,100	%
Valve slope	100/1e-2	%/s
Nominal flow Q_N	30000	l/min
Nominal flow Q_N	0.5	m^3/s
Effective bulk modulus β_e	12000	bar

8.3.4. PASSIVE-ACTIVE MOTION COMPENSATION SYSTEM

To reduce the required cylinder forces and thereby reducing the required power, a passive system is added to the system. The main goal of this passive system is to compensate for the static weight. Several options exist to insert a passive system in the design. For simplification, only one option which is often used in offshore motion compensation applications, is considered. This is a hydraulic accumulator [40]. A hydraulic accumulator is a high pressure storage reservoir which stores and discharges energy in the form of pressurizing and depressurizing gas. Figure 8.4 shows the hydraulic system including the accumulator. This passive system is implemented in the hydraulic cylinder by adding a third chamber besides the cylinder and rod chamber. This requires the previous design to be changed as will be discussed below. The controller for this system is discussed in Section 8.3.7.

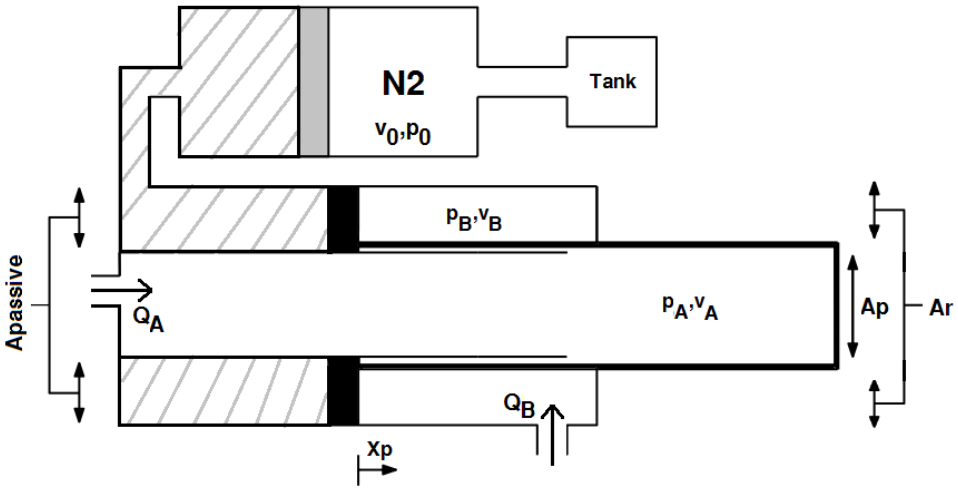

Figure 8.4: Schematic overview of the hydraulic cylinder including a hydraulic accumulator. x_p is zero is located at half the cylinder length. Black and gray respectively indicates the cylinder and accumulator piston. Striped surface indicates the passive oil. All sign directions indicate the positive direction.

The hydraulic accumulator is modelled as a spring of which the stiffness is dependent on the initial pressure p_0 and initial volume v_0 of the storage. As advised by literature, the best approach to simplify the problem is to linearize the stiffness at the average operating point [40]. The average operating point is the point where the piston is in the equilibrium position. Thus, at x_p is zero. Before linearization, the assumption is made that the change in pressure and volume of the accumulator's gas is an adiabatic process where the relation between two states is depended on the adiabatic constant of the gas n, see Equation 8.13. After making this assumption, the spring stiffness and resulting force can be calculated with Equation 8.14 and 8.15 respectively [41]. As shown in these equations, the force the hydraulic accumulator exerts on the piston is dependent on the system behaviour. The more the cylinder is retracted, the higher the force becomes.

$$p_1 \cdot V_1^n = p_2 \cdot V_2^n \qquad [41] \tag{8.13}$$

$$k_{passive} = \frac{n \cdot p_0 \cdot A_{passive}^2}{V_0} \qquad [41] \tag{8.14}$$

$$F_{passive} = p_0 \cdot A_{passive} - k_{passive} \cdot x_p \tag{8.15}$$

$k_{passive}$ = Stiffness passive system $\quad$ p_0 = Initial pressure accumulator $\quad$ x_p = Piston displacement

$A_{passive}$ = Passive area $\quad$ V_0 = Initial volume accumulator $\quad$ n = Adiabatic constant

As proposed by literature and as been used throughout industry, nitrogen is chosen as the most suitable gas for the accumulator [40]. The adiabatic constant n of nitrogen under high pressure is 1.5 [40].

CYLINDER DESIGN INCLUDING PASSIVE SYSTEM

Because the passive system is added as a third chamber in the hydraulic cylinder, the cylinder design has to be changed. First, the piston, rod and passive surface areas are designed. To fit in the passive system and to still have a structural stable design, the rod A_r and piston A_p area are designed as one-third of the old piston area. This results in the areas being equal which benefits the control system. The surface in the cylinder on which the passive spring force applies, the passive area $A_{passive}$, is half the original piston area. Identical to the calculations of the original cylinder, the required nominal flow Q_n, supply pressure p_S, initial conditions and bulk modulus β_e are calculated. An overview of all parameters used in the cylinder with a hydraulic accumulator model is shown in Table 8.3.

By changing the initial settings of the hydraulic accumulator in equilibrium position, the spring stiffness can be changed. The initial pressure p_0 is calculated to take up the static weight. Thus, the required force is divided by the passive surface area $A_{passive}$ resulting in a p_0 of 90 bar. By tuning the initial volume V_0 the stiffness of the system can be changed. This is shown in Figure 8.5. This figure shows that the larger the initial volume, the lower the stiffness and the less the passive force changes in piston displacement.

Ni et al. assessed a passive heave compensation system in the form of a hydraulic accumulator and states that the larger the initial volume the higher the system performance. However, it is also stated that for ever-increasing initial volumes, the performance only changes insignificantly [42]. It is assessed whether this behaviour is also applicable to a PAMC system. This is done by simulating the system with different initial volumes V_0 of 5 m^3, 10 m^3, 25 m^3 and 50 m^3 while keeping the initial pressure constant. The passive force, dependent on piston position, for these volumes is given in Figure 8.14. Larger volumes are not considered because of limitations in the feasibility and cost of adding large nitrogen tanks on deck. Besides, Ni et al. found that for ever-increasing volumes the system performance becomes dominated and limited by the length and diameter of the pipe attaching the accumulator to the compensation cylinder [42]. Smaller volumes are not considered since this will result in too high accumulator pressures. Besides, the initial volume should be at least 10% larger than the maximal rod displaced volume [40].

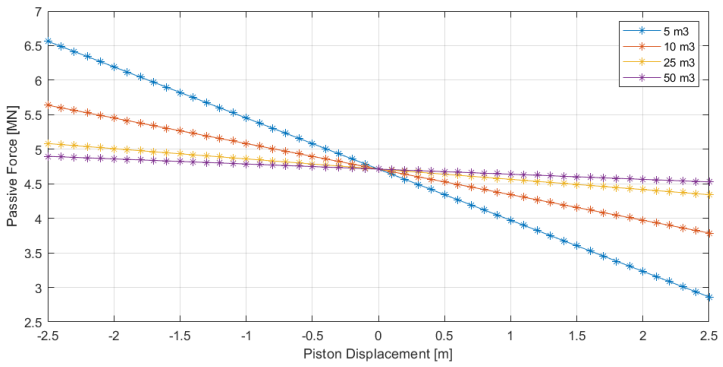

Figure 8.5: Stiffness of hydraulic accumulator dependent on the piston displacement

The simulation runs showed that the remaining motions and required power are higher for higher initial volumes. This is in contradiction to the conclusions of Ni et al. [42]. This contradiction is due to the difference in analysed system. For Ni et al. a purely passive system for heave compensation is assessed in which the piston is vertically orientated and its pose does not change. Therefore, in the passive heave compensation system no extra force is required at large piston displacements. This will only result in an unstable system with less performance.

For the PAMC system, the most severe poses of the platform come with large piston displacements. These poses require more or less force dependent on whether the rod is extended or retracted. The pose where the cylinder has a large extension and needs to be retracted again, requires less force. Thus, less passive force is beneficial for large piston extensions. While in the pose where the piston is retracted and the piston needs to be extended again, more force is required. Thus, more passive force is beneficial for large piston retractions. For both extending and retracting, this is achieved by having a large stiffness for the passive system. With a higher stiffness of the passive system, more passive force is exerted when the piston is retracted and less passive force is exerted when the piston is extended. This will reduce the required active force to be added to the passive force, reducing the required power. In conclusion, a smaller initial volume is beneficial for the PAMC system. Therefore, the lowest volume of 5 m^3 is chosen. The complete design including the hydraulic accumulator settings which are used in the model is shown in Table 8.3.

Table 8.3: Hydraulic cylinder, accumulator and valve design parameters

Parameter	Value	Unit
Supply pressure p_S	250	bar
Tank pressure p_T	1	bar
Initial pressure p_{A0}	100	bar
Initial pressure p_{B0}	100	bar
Nominal pressure difference Δp_n	25	bar
Valve range	-100,100	%
Valve slope	100/1e-2	%/s
Nominal flow Q_N	10000	l/min
Nominal flow Q_N	$\frac{1}{6}$	m^3/s
Effective bulk modulus β_e	12000	bar
Initial accumulator pressure p_0	90	bar
Initial accumulator volume V_0	5	m^3
Accumulator stiffness $k_{passive}$	740	kN/m

8.3.5. BASE TRAJECTORY

The motions of the vessel which are used before this chapter are static maximum displacements, velocities and accelerations and do not represent a continuous time-series. To have a continuous motion input, or trajectory, a time-series must be computed. Six time series, one for each DoF, are retrieved from the Boskalis R&D Department. These time-series are computed with the use of Orcaflex based on an AQWA model. The limiting sea-state maintains the same as in previous calculations thus with a H_s and T_p of respectively 2 m and 8 s and an α-factor of 0.84, see Section 3.6. Since the exact design is known now, the motion measurement point is determined more precisely. The time-series motions are measured at the location [80,-12.5,20], which is the location of the base CoG or origin of the model O_0. These time-series motions are imposed on the base CoG.

Since the retrieved time series only consist of first-order motions, the second-order motions must be added. Again, the DP system has been modelled as a mass-spring-damper system. The same proportional Kp value belonging to the spring and derivative Kd term belonging to the damper as calculated in Section 6.1 are used. These four values, two for surge and two for sway, represent the fictive mass-spring-damper DP system and are used as input for the Boskalis R&D department Orcaflex runs. These runs resulted in the variance of the second-order vessel motions. Which, as stated in Section 6.1, can be seen as the position variance or DP footprint of the vessel. The total time series are computed by adding the first and second-order time series. Part of the 3-hour or 10800 s total time-series is shown in Figure 8.6.

In real-life, such a time-series is not available thus must be measured. An option is to measure the motions with a Motion Reference Unit (MRU). In particular, the *MRU 5+ MK-II* designed by Kongsberg [43]. This MRU has maximum data output rate of 200 Hz equal to a sampling period of 0.005 s. A low sampling frequency is required, because minimizing the time delay in the system is critical to achieve a high motion compensation performance. To make the system more realistic, this sampling period is set as the sampling period of the 6 DoF time-series. Since the retrieved time-series have a time step of 0.1 s the time-series are filtered and spline interpolated to a time step of 0.005 s, for more detailed information see Appendix I.

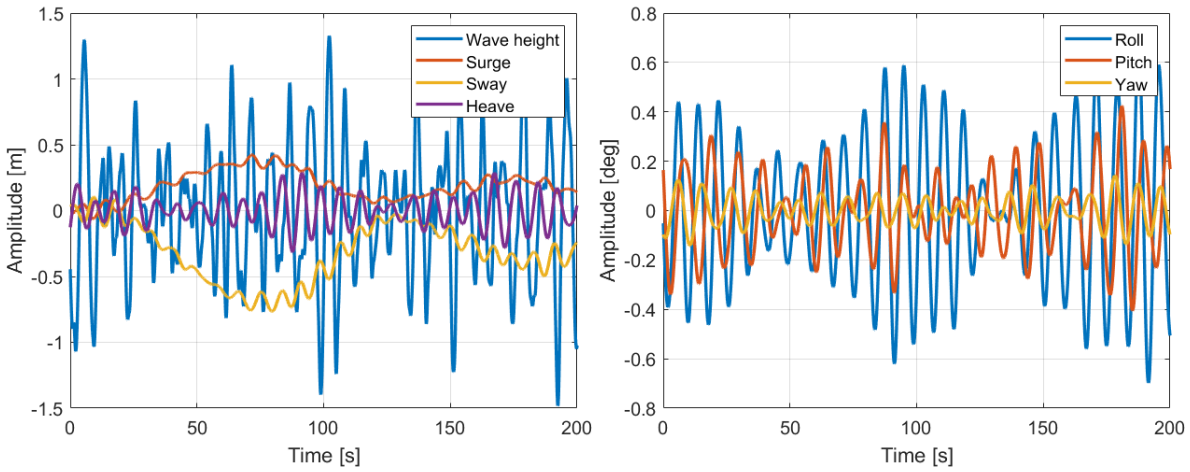

(a) Time-series of surge, sway, heave and wave elevation

(b) Time-series of roll, pitch, yaw

Figure 8.6: Part of the time-series used as input for the model's trajectory in the base CoG

8.3.6. WIND FORCES

The limiting wind conditions as set in 3.2 are used to calculate the wind forces. This is with a mean wind speed at 10 m altitude U_{10} of 15 m/s. A theoretical wind spectrum is used because there is an absence in wind data. As proposed by the DNV standard [DNV-RP-C205], a Kaimal spectrum $S_u(f)$ is used which is defined in Equation 8.16. The frequency f is ranged from 0.001 to 0.25 Hz with 10000 components. Equation 8.18 calculates L_u as 238 m with z is 10 m and z_0, the terrain roughness, is 0.005.

$$S_u(f) = \sigma_u^2 \frac{6.868 \frac{L_u}{U_{10}}}{(1 + 10.32 \frac{f \cdot L_u}{U_{10}})^{5/3}} \tag{8.16}$$

σ_u = Wind speed standard deviation

U_{10} = Mean wind speed at 10 m height

L_u = Integral length scale

f = frequency

$$\sigma_u = U_{10} \cdot A_x \cdot k_a \cdot \frac{1}{\ln \frac{z}{z_0}} \tag{8.17}$$

$A_x = \sqrt{4.5 - 0.956 \ln(z_0)}$

z = Height above mean sea level

k_a = Von Karman's constant 0.4

z_0 = Terrain roughness

$$L_u = 300 (\frac{z}{300})^{0.46 + 0.074 \ln(z_0)} \tag{8.18}$$

After calculating the wind spectrum, the spectrum is transferred to a time series with Equation 8.19 and 8.20 [44]. Identical to the 3-hour wave time series, a 3-hour time series is computed for the wind speed, see Figure 8.7. This, with a time step of 0.005 which is the sampling time of the MRU.

$$U_{10}(t) = U_{10} + \sum_{n=1}^{10000} A_i \cos(2\pi t + \xi_i) \quad [44] \tag{8.19}$$

$$A_i = \frac{2}{\pi} \sqrt{S_u(f) \cdot \Delta f} \quad [44] \tag{8.20}$$

ξ_i = Stochastic variable uniformly distributed [-π ,π]

$S_u(f)$ = Power spectral density at f

Δf = Frequency step size

t = time 0 to 10800 s with 0.005 s step size

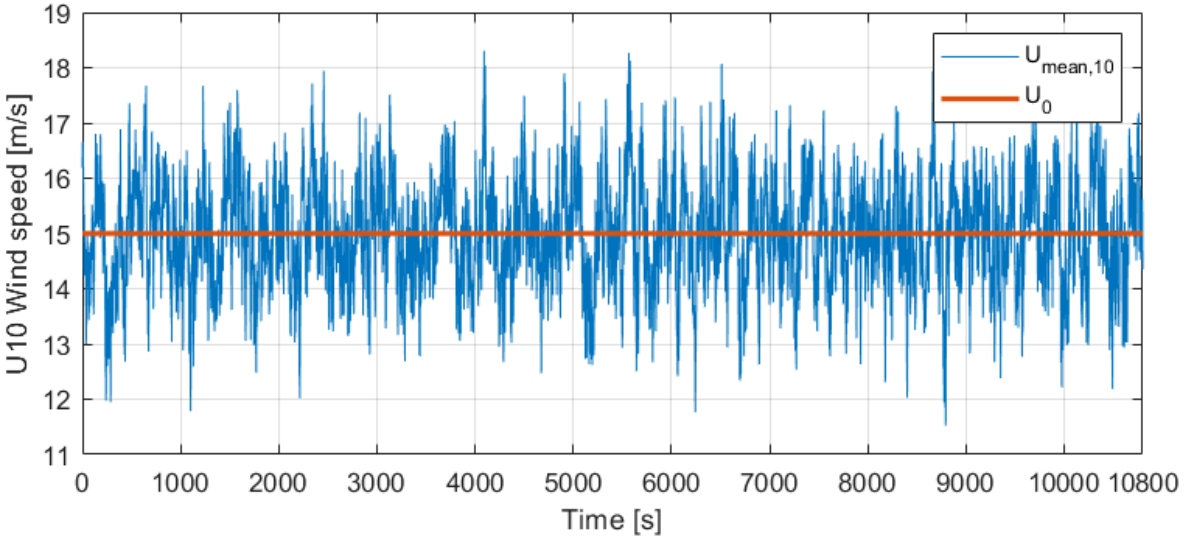

Figure 8.7: Wind speed time series $U_{10}(t)$ at 10 m height above mean sea level for 3 hour or 10800 s with mean wind speed U_{10} of 15 m/s

The time serie at 10 m height above mean sea level is calculated at heights belonging to the WTG thus ranging from 0 m to 125 m. This is done with a logarithmic profile, shown in Equation 8.21 [DNV-RP-C205]. The wind speed is discretized from 0 m/s to 25 m/s in steps of 1 m/s. By using the same approach as stated in Section 6.2.1, the wind forces belonging to the discretized wind speeds are calculated. This with taking into account the α-factor of 0.8, see Section 3.6. The wind forces are transferred to the Stewart platform's CoG. This results in two horizontal forces and three overturning moments for each discretized wind speed. It assumed the vertical force due to wind is zero. The model uses the wind time series as input to construct a lookup table transferring wind speeds to forces and moments. For each wind speed from the wind time series, this lookup table interpolates its discretized wind speeds and belonging forces and moments. This results in the forces and moments belonging to a certain wind speed. The forces and moments are applied to the platform's CoG.

$$U_z(t) = U_{10}(t) \cdot \left(1 + \frac{\ln \frac{10}{z_0}}{\ln \frac{z}{z_0}}\right) \tag{8.21}$$

$U_z(t)$ = Wind speed time series at height z z = Height above mean sea level

$U_{10}(t)$ = Wind speed time series at 10 m z_0 = Terrain roughness

8.3.7. PID CONTROLLER

As the aim of this thesis is not on control system design, only a proportionalintegralderivative (PID) controller is considered and implemented. This controller is widely used in the offshore branch [45], [46]. In this controller, a control loop is used to continuously minimize the required signal minus the actual signal, also known as the error. To have controllers which suit both the IMC and the AMC and PAMC model, two different controllers are designed. Both are discussed below. For each model, six identical controllers are implemented, one for each leg.

CONTROLLER FOR IMC SYSTEM

Figure 8.8 shows the controller as used in the IMC model, thus without hydraulics. The error is continuously measured as the difference between the required leg extension minus the real leg extension. This can also be seen as the required position $r - pos$ minus the actual position pos. This error is used as input for the proportional P and derivative D term. Besides, the actual leg velocity is used as input for the derivative D term. Hence, the P, I and D term all use feedback control which all are dependent on the system behaviour resulting in the D term to act as a damper. By multiplying the input signals by the Kp, Ki and Kd values and summing them, an output signal which is the cylinder force $Fcyl$ is computed.

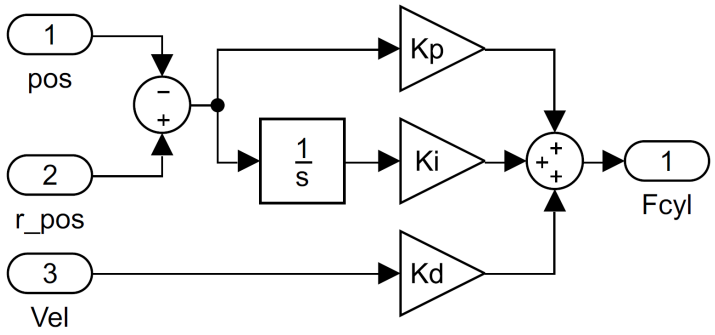

Figure 8.8: PID controller used in the basic model without hydraulics or passive system

CONTROLLER FOR AMC AND PAMC SYSTEMS

Figure 8.9 shows the controller as used in the AMC and PAMC model where the dynamics of the hydraulics and valve are added. In this model, the output of the controller is the required valve opening instead of the required leg force as in IMC controller. Also, the initial condition of the integrator I is now the initial percentage the valve is open instead of the initial force applied on the cylinder rod.

The performance of the controller is improved by using velocity feed-forward instead of the velocity feedback as used in the IMC controller. Besides, no high controller gains are required to achieve this high performance. The feed-forward input is independent of the system's behaviour and makes faster controlling possible. This velocity feed-forward is the required velocity of the leg, calculated as the time derivative of the required leg extension $r - pos$. This controller is inspired by the control system of the Barge Master motion compensation system. *"For the Barge Master application it was foreseen by Barge Master, Bosch-Rexroth and MARIN that the combination of position feedback and velocity feed-forward is the preferred way to go."* [45]

With the velocity feed-forward input, the required output value u_{req} can be calculated with Equation 8.22 which is dependent on the system behaviour. This equation calculates the required percentage the valve has to open u_{req} to keep the platform at the required position. Even though u_{req} is calculated continuously, it is calculated for the static system. Since the system is dynamic, a Kp and Kd gain is required to prevent the platform from drifting off. These values are tuned as discussed below.

$$u_{req} = \frac{\sqrt{\Delta p_n}}{\sqrt{p_S - p_A} + \sqrt{p_B - p_T}} \cdot \frac{(A_p + A_r)\frac{\delta x_p}{\delta t}}{Q_n} \cdot 100 \tag{8.22}$$

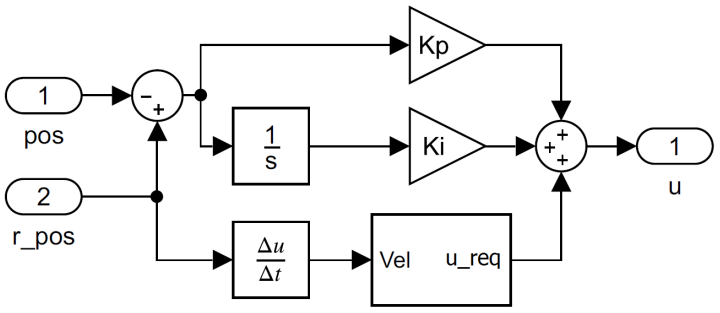

Figure 8.9: PID controller used in the model including the hydraulics and passive system

TUNING

Different methods can be used to find the ideal PID values, also known as tuning. First, the ZieglerNichols method is applied to tune [47]. This is a heuristic method of tuning a PID controller. The P gain is increased until the output of the control loop has stable and consistent oscillations after which all PID values are based on this particular P gain. Since this method did not give stable results, it is not used further more. An alternative to the Ziegler-Nichols method is manually tuning the PID controller. Since enough information about the system is known, this approach is applied. See Table 8.4 for the PID values for each configuration. The $InitCond$ is tuned to compensate for the initial transient behaviour of the system.

For the IMC model, a trade-off between a stiff and soft controller with respectively high and low gains is made. This is a trade-off between power and performance in which the stiff controller requires more power but has a higher performance. For now, a maximum stiff and soft controller are assessed. Making the stiff controller stiffer makes the simulation to fail due to uncontrollable high cylinder forces. Also, a very stiff controller works fine for numerical methods but in practice these high gains may result in an unstable system [45]. This since in practice, noise, latency and backlash may be present. Making the soft controller softer will mean that the controller cannot actuate the legs sufficiently to make them keep up with the reference trajectory signal. This results in the platform to slowly drift off its required pose and fail. For the second controller for the hydraulic configurations, no difference between a soft and stiff controller can be made since the system-dependent u_{req} controls the system almost solely.

Table 8.4: PID gains with initial conditions for the integrator for all configurations

	IMC stiff	**IMC soft**	**AMC + PAMC**
P	7e9	1e8	5
I	1e10	1e8	0.01
D	1e8	1e8	-
InitCond	-4e-5	-4e-5	0

8.4. MOTION COMPENSATION PERFORMANCE

To assess the motion compensation performance of the system, the motion compensation performance index, Compensation Efficiency (CE), is introduced [48]. The CE is defined by Equation 8.23 in which the standard deviation σ_{in} of all input motions for one DoF is divided by all output motions σ_{out} for the same DoF. Thus, 6 CE values, one for each DoF, will be calculated based on the 3-hour motion input and output data. The value gained from the division is also called the Root Mean Square (RMS) reduction factor. The RMS reduction factor is used because it provides an average measure of the effectiveness of the compensation systems over the range of vessel motions. Another option is to simply calculate the percentage of input motions which are compensated. However, this does not give a good representation of the complete range of vessels motions. Besides, for the case the output motions are small and the input motions go to zero in between wave periods this value will be zero or infinitely large. Besides the CE value, the maximum remaining motions are given for all 6 DoF.

$$\text{Compensation Efficiency} = CE = \left(1 - \frac{\sigma_{out}}{\sigma_{in}}\right) \cdot 100\% \qquad [48] \tag{8.23}$$

8.5. RESULTS

Three different models are assessed as listed below. For all, only the behaviour after 25 seconds, thus excluding the initial transient behaviour, is assessed. The results are shown in Table 8.5.

1. Stewart platform without hydraulic system without passive system
   Ideal Motion Compensation (IMC)
2. Stewart platform with hydraulic system without passive system
   Active Motion Compensation (AMC)
3. Stewart platform with hydraulic system with passive system
   Passive-Active Motion Compensation (PAMC)

Table 8.5: Results comparison between the three configurations on remaining motions, Compensation Efficiency CE and maximum power. For the IMC the results for a stiff and soft controller are given.

	IMC stiff		**IMC soft**		**AMC**		**PAMC**	
	Remain	**CE**	**Remain**	**CE**	**Remain**	**CE**	**Remain**	**CE**
Surge	1.0 mm	99.9%	7.1 mm	99.3 %	4.2 mm	99.7 %	2.3 mm	99.8 %
Sway	2.4 mm	99.9%	18.1 mm	98.8 %	7.7 mm	99.0 %	5.6 mm	99.3 %
Heave	3.2 mm	99.9%	25.2 mm	94.9 %	8.3 mm	98.6 %	2.2 mm	99.2%
Roll	9e^{-3}deg	99.4%	0.07 deg	94.9 %	0.05 deg	95.7 %	0.06 deg	94.8 %
Pitch	6e^{-3}deg	99.3%	0.03 deg	95.5 %	0.02 deg	96.6 %	0.04 deg	95.6 %
Yaw	9e^{-3}deg	97.8%	0.01 deg	95.4 %	0.01 deg	96.6 %	0.01 deg	97.7 %
Power	21.7 MW		11.6 MW		10.4 MW		4.2 MW	

IDEAL MOTION COMPENSATION (IMC)

As discussed in Section 8.3.7, a trade-off must be made between a stiff and soft controller with respectively high and low gains. This is a trade-off between power and performance. As seen in Table 8.5, the stiff controller requires more power but also performs better. The other way around for the soft controller. With the IMC soft remaining motions still being within the limitations, the preference goes to this softer controller which requires half the power.

The IMC stiff results showing almost perfect compensation are as expected. This structure is close to being a ideal system in which masses and inertia are moved directly with force. Because of this, the IMC model does not present the system behaviour as in practice accurately. Besides, as stated before, a very stiff controller works fine for numerical methods but may be unstable in practice due to noise, latency and backlash [45].

ACTIVE MOTION COMPENSATION (AMC)

The model which includes hydraulics performs better than the IMC model. This is not as expected since adding the hydraulic and valve dynamics makes the model more realistic in which hydraulic and valve losses are present. However, for the AMC model, the controller performance is improved by adding velocity feedforward and controlling on flow instead of directly on force. With this more sophisticated controller, the system performs better. Less power is required than both the soft and stiff controller. The maximum required flow in all cylinders combined is 84000 l/min, which is an extensive amount of oil. This amount of hydraulic power would likely impact the economic feasibility of the system.

PASSIVE ACTIVE MOTION COMPENSATION (PAMC)

By adding a passive system to the model, the required power is reduced to 4.2 MW. This, while also reducing the translational remaining motions significantly while keeping the rotational remaining motions small. Apart from the motions, the great advantage of adding the hydraulic accumulator is the reduction in required power. Besides, the maximum required flow in all cylinders combined is reduced to 28000 l/min. Which is a significant reduction compared to the AMC system.

8.6. VERIFICATION & VALIDATION

In a subsequent design phase, the system should be tested experimentally. This means doing extensive scale tests of the system in a test tank. Eventually, the real size system should also undergo extensive test trials in real circumstances to guarantee its workability and safety. Since doing scale or real size system tests is outside the feasibility of this thesis, validation is outside the scope.

Verification is part of the scope. Verification of the model is done by comparing both the IMC and AMC model to analytical calculations. The analytical calculations will be performed with the same method as described in Section 6.2 and Section 7.8. For both models, the maximum required power and corresponding cylinder forces are given, see Table 8.6. The wind forces and moments, platform and base pose and cylinder velocities corresponding to the maximum required power for both models are used as input for the analytical calculations. See Table 8.6 for the results. Differences between both models and the analytical calculations exist since the analytical calculations are for a static system while the numerically calculated values are for a dynamic system. This gives an underestimating of the required power. Besides, in the Simulink model, real wave and wind time series are added compared to a constant wind and wave input in the analytic calculations. Nevertheless, no significant differences exist in the maximum power and the same proportionalities between the leg forces is found in which most forces are exerted by leg 1 and 6. As a last verification step, the model is also verified by visualising the model dynamics as can be seen in Appendix H, Figure H.3.

Table 8.6: Verification of model results by comparison to analytical calculations on power and leg forces

	Leg 1	**Leg 2**	**Leg 3**	**Leg 4**	**Leg 5**	**Leg 6**	**Power**
IMC soft model	7.3	4.7	6.8	3.6	2.6	7.8	11.6
IMC analytical	6.5	3.8	5.1	2.5	2.3	7.2	9.9
AMC model	7.4	2.5	3.7	2.4	2.7	9.3	10.4
AMC analytical	6.6	3.3	5.3	2.7	1.9	7.4	9.7
Unit	MN	MN	MN	MN	MN	MN	MW

8.7. CONCLUSION

In this chapter, a model is developed in MATLAB and Simulink to simulate the dynamics of the motion compensation system. In total, three different model configurations are assessed. An ideal motion compensation (IMC) system. An active motion compensation (AMC) system in which hydraulic and valve dynamics are added. And a passive-active motion compensation system (PAMC) in which a passive system is added. All configurations are compared on the remaining motions, required power and compensation efficiency (CE).

For the IMC, a PID controller is used with position and velocity feedback. A stiff and soft controller with respectively high and low gains is assessed. This showed that the stiff controller has less remaining motions and a higher CE value but requires more power. Thus, choosing between the stiff and soft controller is found to be a trade-off between performance and required power. The results of the IMC system include small remaining motions because the masses and inertia are directly moved with force and without any other losses. Because of this, the IMC system is not found to representable to the real-life system behaviour. However, it gave some valuable insights.

For the AMC and PAMC system the controller's performance is improved by using velocity feed-forward. The feed-forward is independent of the systems behaviour and makes faster controlling possible. Besides, the performance is improved by calculating the required controller output as a function of the feed-forward velocity instead of setting it as constant. The AMC model including the hydraulic and valve dynamics performs better than the IMC model because of the performance of the controller. The simulations showed that the maximum required flow in all cylinders combined is 84000 l/min with a required net power of 10.4 MW. This required amount of hydraulic power has a great impact on the economic feasibility of the system.

By adding a passive system in the form of a hydraulic accumulator, the system's performance is drastically improved. The simulated results show that adding a passive system in the form of a hydraulic accumulator reduces the required maximum flow in all cylinders combined to 28000 l/min with a net power of 4.2 MW.

9

CONCLUSIONS & RECOMMENDATIONS

Boskalis is interested in finding an innovative way to install offshore wind turbine generators (WTGs) with a floating asset. Therefore, the research question: How can the next-generation offshore wind turbine generator be installed, enabling competitive installation by using an existing floating vessel without a crane? is answered in this thesis. The findings of this thesis which answer the research question are summarized in Section 9.1. The recommendations for further research are discussed in Section 9.2.

9.1. CONCLUSIONS

The conclusions are split up into the four focus areas of this thesis.

- Dynamic analysis of a vessel with a WTG on deck
- Concept development
- Kinematic optimization of a Stewart platform
- Simulation of a Stewart platform

DYNAMIC ANALYSIS OF A VESSEL WITH A WTG ON DECK

A vessel dynamic analysis is performed in the hydrodynamics program Seaway Octopus. The analysis showed that the Mighty Servant 1 is the most suitable Boskalis vessel to install WTGs from. Besides, offloading at starboard side has shown optimal. The same dynamic analysis also highlighted that a motion compensation system is required to mitigate wave-induced dynamics, enabling WTG installation in floating conditions.

CONCEPT DEVELOPMENT

After developing multiple concepts of motion compensation systems, a multi-criteria analysis in the form of an analytic hierarchy process is performed resulting in two most feasible concepts. The first concept is a tower on skids, grabbing and motion compensating the WTG with two XY-tables at two distant vertical locations. The second concept is a Stewart platform which motion compensates the WTG at the bottom of the tower with six hydraulic cylinders. The Stewart platform is connected to the Transition Piece (TP) after which the WTG is skidded towards it, reducing the motions the further it is skidded. This connection is required to limit the overturning moment on the Stewart platform. The connection between the Stewart platform and the WTG is made with a clamp below a flange on the tower. The Stewart platform concept is found most promising since it provides the highest motion compensation capabilities.

KINEMATIC OPTIMIZATION OF A STEWART PLATFORM

A kinematic optimization is carried out by means of a genetic algorithm to find the optimal values of the five parameters describing the Stewart platform's geometry. Three indices are used to indicate the kinematic performance of a parameter set: the global conditioning index, global gradient index and, self-made, global force index. The indices describe respectively the dexterity, the gradient of the dexterity and the sum of the cylinder forces. Optimizing for each index individually highlighted that a kinematic optimization of a Stewart platform should include all three indices, since improving the performance of one index has a negative impact on the other indices. The optimal set of design parameters is selected by taking advantage of the Pareto front, which is computed with a multi-objective optimization including all indices. A design sensitivity analysis is performed to obtain the sensitivity of the kinematic indices with respect to changes in the design parameters. The results of the sensitivity analysis showed that the optimal design of a Stewart platform is a design choice based on a trade-off between performance and required power.

SIMULATION OF A STEWART PLATFORM

A model is developed in MATLAB and Simulink to simulate the dynamics of the motion compensation system for 3-hours. Only the installation phase where the Stewart platform is not yet connected to the TP and where the WTG is in the centre of the platform is considered. The simulated results showed that a controller with velocity feed-forward and position feedback is the preferred way to go. The feedback includes a constant P and I gain. The feed-forward includes a gain which is depended on the cylinder and rod chamber pressure and the required piston velocity. It is found that the maximum required flow in all cylinders combined is 84000 l/min with a required net power of 10.4 MW. This amount of hydraulic power would likely impact the economic feasibility of the system. By adding a passive system in the form of a hydraulic accumulators, the system's performance is drastically improved. The performance of the hydraulic accumulators is improved by maximizing the stiffness of the system, achieved by minimizing the initial accumulator volume.

Based on the results of this research, it can be concluded that the next generation offshore wind turbine generator can be motion-compensated with a Stewart platform including hydraulic accumulators. This, with a compensation efficiency up to 94.8 %, a maximum net power of 4.2 MW and a maximum flow in all cylinders combined of 28000 l/min. However, the next phases of installation which are connecting the Stewart platform to the TP and skidding the WTG towards it, must be assessed in further research. This, to prove the feasibility of the system in all installation phases.

9.2. RECOMMENDATIONS

In the search to answer the research question, several choices and assumptions were made. Before starting the detailed design, several topics could be assessed in more detail for which recommendations are given. The recommendations are divided into a part with general recommendations and a part with recommendations to extend the model, making it more realistic.

- It is recommended to asses a wider range of load cases. To give an broader understanding of the system's behaviour and performance, the number of load cases to which the design is analysed could be increased. Sea-states with different significant wave heights and peak periods in combination with a wider range of wind speeds could be assessed. This while alternating the incoming direction of both environmental conditions.
- Fatigue in all critical components should be assessed. Fatigue might be a pressing issue for components on which high loads are exerted in combination with a high number of loading cycles. In the detailed design phase, it is advised to design against fatigue-failure to reduce operational expenses and down-time and to assure a safe design. For practice, it is advised to continuously monitor the fatigue life of critical components. The fatigue damage and remaining fatigue life of the components could be predicted by using cyclic stress against cycles to failure curves, also known as S-N curves, in combination with Miner's rule.
- Additional components must be designed in detail. Bumpers and guides should be designed to reduce the impact load of the system and WTG on the TP and to accurately position the WTG on the TP. The proposed connection between the system and WTG must be designed in more detail. This includes the clamping system and flange on the tower. During the design, attention must be paid to quick disconnection, enabling safe removal of the system. For this quick disconnection, the implementation of the Flange Clamp Tool by IHC is advised. This tool quickly and temporarily secures the axial connection between the flanges of the tower and TP afterwards the permanent bolting connection can be made. At last, the flange on the TP which is connected to the Stewart platform must be designed. This flange must be designed for the phase of installation where the WTG is skidded above the TP. This will result in the WTG's mass being almost completely exerted on the flange.
- Extend the kinematic optimization by adding buckling checks as non-linear constraints making longer legs less optimal. Besides, a wider range of load cases could be assessed to shift the performance from one load case or one installation phase to a more generalised design. The optimization can be improved by using discrete time-series to compute the workspace points instead of randomizing these as a square workspace. This approach will give more weight to platform poses with a higher probability of occurrence.

MODEL RECOMMENDATIONS

- The dynamic coupling between the system and the vessel and between the system and the dynamic positioning system could be added. Especially for the phase where a connection to the TP is made, the dynamic coupling will play a significant role. For the coupling between the system and vessel, the change in natural roll period is most interesting to assess. When the natural roll period is closer to the wave energy peak, this will have a negative effect on the vessel motions. This also applies to the other natural frequencies.
- Viscous and Coulomb friction could be added to the system, increasing the system's damping.
- The constant supply pressure could be replaced by a pump characteristic resulting in the supply pressure to be a function of the flow. Thereby giving insights into a more realistic hydraulic system.
- The benefit of connecting an additional reservoir of hydraulic oil to the hydraulic system could be assessed. This reservoir is pressurized by a nitrogen tank at a pressure slightly lower than the supply pressure. In case a peak flow is required and the hydraulic power is insufficient, the system pressure will drop. If the system pressure drops below the pressure of the additional reservoir, the reservoir oil will flow into the system generating enough flow to meet the temporary peak demand. After the peak demand, the reservoir is refilled due to the higher system pressure.
- At last, it is recommended to assess the second installation phase where the system is connected to the TP after which the WTG is skidded towards it. Assessing this phase will prove the feasibility of the system for all installation phases. One should take into account this phase requires a different controller. This, since the system loses one DoF after connecting to the TP.

BIBLIOGRAPHY

[1] Selot, F. et al., *Offshore Wind in Europe, key trends and statistics 2018,* Wind Europe , 30 (2019).

[2] Jan De Nul, *Offshore jack-up installation vessel, voltaire specification sheet,* https://www.jandenul.com/nl/materieel/vloot/offshore-jack-up-installatieschip, retrieved on 29-07-2019.

[3] Gusto MSC, *Ng-14000x product sheet, best-in-class solution,* https://www.gustomsc.com/design/wind-installation/ng-14000x, retrieved on 06-06-2019.

[4] Lacal-Arantegui, R.,Yusta, J. M. & Dominiguiz-Navarro, J. A., *Offshore wind installation: Analysing the evidence behind improvements in installation time,* Renewable and Sustainable Energy Reviews **92**, 134 (2018).

[5] Saipem, *Hywind project,* https://www.saipem.com/en/projects/hywind, retrieved on 29-07-2019.

[6] J. Wagner, H. J. & Mathur, *Introduction to wind energy systems: Basics, technology and operation,* Green Energy and Technology , 41 (2009).

[7] Fraile, D. & Komusanac, I., *Wind energy in Europe: Outlook to 2022,* Wind Europe , 38 (2018).

[8] Ulstein, *Ulstein wind lifter,* https://ulstein.com/equipment/ulstein-windlifter, retrieved on 06-06-2019.

[9] Huisman, *Wind turbine shuttle,* https://www.huismanequipment.com/en/products/renewables/offshore_wind/wind_turbine_shuttle, retrieved on 06-06-2019.

[10] General Electric Renewable Energy, *Haliade-x offshore wind turbine platform,* https://www.ge.com/renewableenergy/wind-energy/offshore-wind/haliade-x-offshore-turbine, retrieved on 08-06-2019.

[11] Kairuz Fonseca, S., *Estimation of the Optimum Wind Turbine Size for two Different Offshore Sites and Wind Farm Rated Powers,* Master's thesis, Delft University of Technology (2017).

[12] *Hot rolled products of structural steel,* EN 10025 Standard (2004).

[13] Tijsseling, A. S. & Anderson, A., *The Joukowsky equation for fluids and solids,* CASA-report (Technische Universiteit Eindhoven, 2006).

[14] PWC, *Unlocking Europes offshore wind potential, Moving towards a subsidy free industry,* (2018).

[15] Dieijen, F. van, *Potentie van Semi-Submersibles als Installatieschip voor een Nieuwe Generatie Offshore Windturbines,* Master's thesis, Boskalis and Hogeschool Rotterdam (2018).

[16] Journée, J. M. J. & Adegeest, L. J. M., *Theoretical Manual of SEAWAY for Windows,* TUD Report No. 1370 , 15 (2003).

[17] Faltinsen, O.M. & Svensen, T., *Incorporation of Seakeeping Theories in CAD,* International Symposium on CFD and CAD in Ship Design, MARIN (1990).

[18] Journée, J.M.J. & Massie, W.W., *Offshore Hydromechanics,* 1st ed. (Delft University of Technology, 2001).

[19] Uzunoglu, S., Ribero e Silve, S., Guedes Soares, C., *Numerical and experimental study of parametric rolling of a container ship in regular and irregular head waves,* Maritime Technology and Engineering , 1047 (2014).

[20] Molland, A. F., *Maritime engineering reference book, a guide to ship design, construction and operation,* Maritime engineering reference book , 503 (2008).

[21] Saaty, T. L. & Katz, J. M., *How to make a decision: The Analytic Hierarchy Process,* European Journal of Operational Research **48**, 9 (1990).

[22] Triantaphyllou, E. & Mann, S. H., *Using The Analytic Hierarchy Process for Decision Making in Engineering Applications: Some Challenges,* The International Journal of Industrial Engineering: Applications and Practice **2**, 35 (1995).

[23] *3D Motion Compensated Platform, BM-T700,* Barge Master (2019).

[24] Burton, T. & Sharpe, D., *Wind Energy Handbook,* John Wiley & Sons Ltd , 94 (2006).

[25] Heistermann, C., Husson, W. & M.Veljkovic, *Flange connection vs. friction connection in towers for wind turbines,* Division of structural engineering-steel structure, Lulea Unviversity of Technology , 301 (2009).

[26] J. Angeles, *Fundamentals of Robotic Mechnical Sytems: Theory, Methods, and Algorithms* (Springer, 2014).

[27] D. Faugère, J.C & Lazard, *Combinatorial classes of parallel manipulators,* Mechanism and Machine Theory **30**, 765 (1995).

[28] Xie, Z., Li, G., Liu, G. & Zhao, J., *Optimal Design of a Stewart Platform using the Global Transmission Index under Determinate Constraint of Workspace,* Advances in Mechanical Engineering **9**, 7 (2017).

[29] Lara-Molina, F.A., Rosario, J.M. & Dumur, D., *Multi-Objective Design of Parallel Manipulator Using Global Indices,* The Open Mechanical Engineering Journal **4**, 37 (2010).

[30] Kurtz, R. & Hayward, V., *Multiple-Goal Kinematic Optimization of a Parallel Spherical Mechanism with Actuator Redundancy,* IEEE Transactions on Robotics and Automation **8**, 644 (1992).

[31] Fassi, I., Legnani, G. & Tosi, D., *Geometrical Conditions for the Design of Partial or Full Isotropic Hexapods,* Journal of Robotic Systems 22 , 507 (2005).

[32] Liu, X., Wang, J. & Pritschow, G., *Preformance Atlases and Optimum Design of Planar 5R Symmetrical Parallel Mechanisms,* Mechanism and Machine Theory 41 , 1111 (2006).

[33] Mathworks, *Global optimization toolbox: User's guide (r2011b),* https://nl.mathworks.com/help/pdf_doc/gads/gads_tb.pdf (), retrieved on 20-10-2019.

[34] Lara-Molina, F.A., Korosihi, E. H. & Dumur, D., *Combined Structure-Control Optimal Design of the Stewart-Gough Robot,* IEEE , 19 (2015).

[35] Gen, M. & Cheng, R., *Genetic Algorithms and Engineering Optimization,* Wiley Series in Engineering Design and Automization (2000).

[36] Zadeh, L., *Optimality and non-scalar-valued performance criteria,* IEEE Transactions on Automatic Control **8**, 59 (1963).

[37] Awad, M. & Khanna, R., *Efficient Learning Machines, Theories, Concepts, and Applications for Engineers and Systems Designers* (Apress Open, 2015).

[38] Mathworks, *Simscape multibody: User's guide (r2019b),* https://www.mathworks.com/help/pdf_doc/physmod/sm/mech_ug.pdf (), retrieved on 20-10-2019.

[39] Jelali, M. & Kroll, A., *Hydraulic Servo-systems. Modelling, Identification and Control* (Springer, 2004) pp. 32–59.

[40] P. Albers, *Motion Control in Offshore and Dredging* (Springer, 2010) pp. 208–211.

[41] Woodacre, J.K., Bauer, R.J., Irani, R.A., *A Review of Vertical Motion Heave Compensation Systems,* Ocean Engineering **104** (2015).

[42] Ni, J., Liu, S., Wang, M., Hu, X. & Dai, Y., *The Simulation Research on Passive Heave Compensation System for Deep Sea Mining,* International Conference on Mechatronics and Automation **104**, 5111 (2009).

[43] Kongsberg, *Mru 5+ mk-ii the ultimate marine motion sensor,* https://www.kongsberg.com/globalassets/maritime/km-products/product-documents/datasheet_mru5plus-mkii.pdf, retrieved on 25-02-2019.

[44] Gavriluta, C. et al., *Complete methodology on generating realistic wind speed profiles based on measurements* (2012) pp. 1757–1762.

[45] Jaouen, F., van den Berg, J., van der Schaaf, H., May, E. & Koppenol, J., *How does Barge-Master Compensate for the Barge Motions: Experimental and Numerical Study,* Marin & Barge-Master (2012).

[46] Cerda Salzmann, D. J., *Development of the Access System for Offshore Wind Turbines*, Ph.D. thesis, Delft University of Technology (2010).

[47] Ziegler, J.G. & Nichols, N.B., *Optimum settings for automatic controllers,* Transactions of the ASME **64**, 759 (1942).

[48] Liu, T. et al., *Performance evaluation of active wireline heave compensation systems in marine well logging environments,* Geo-Marine Letters **33** (2012).

A

REFERENCE WTG

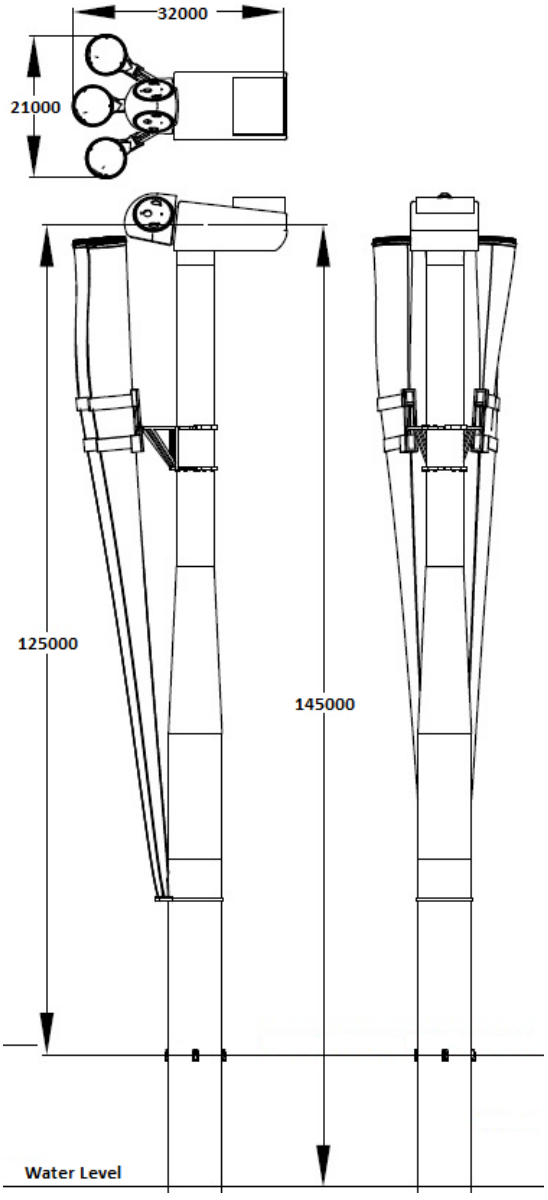

Figure A.1: Schematic drawing of reference Wind Turbine Generator in carousel configuration

Table A.1: Specifications of reference Wind Turbine Generator in carousel configuration

Description	Value	Unit
General		
Capacity	12	MW
Rotor diameter	220	m
Tower		
Bottom diameter	[redacted]	m
Bottom thickness	[redacted]	mm
Top diameter	[redacted]	m
Top thickness	[redacted]	mm
Length	120	m
Nacelle		
Length	[redacted]	m
Width	[redacted]	m
Height	[redacted]	m
X-aft tower centre	[redacted]	m
Blade		
Length	110	m
CoG from rootend	[redacted]	m
Weights		
Tower	[redacted]	t
Nacelle	[redacted]	t
Blade	[redacted]	t
Blade rack	[redacted]	t
Total WTG	[redacted]	t
VCGs from tower base		
Tower	[redacted]	m
Nacelle	[redacted]	m
Blades & frame	[redacted]	m
Total WTG	[redacted]	m
VCGs above LAT		
Tower	[redacted]	m
Nacelle	[redacted]	m
Blades & rack	[redacted]	m
Total WTG	[redacted]	m
Transition Piece		
Height of TP relative to LAT	20	m

A.1. FREE BODY DIAGRAM

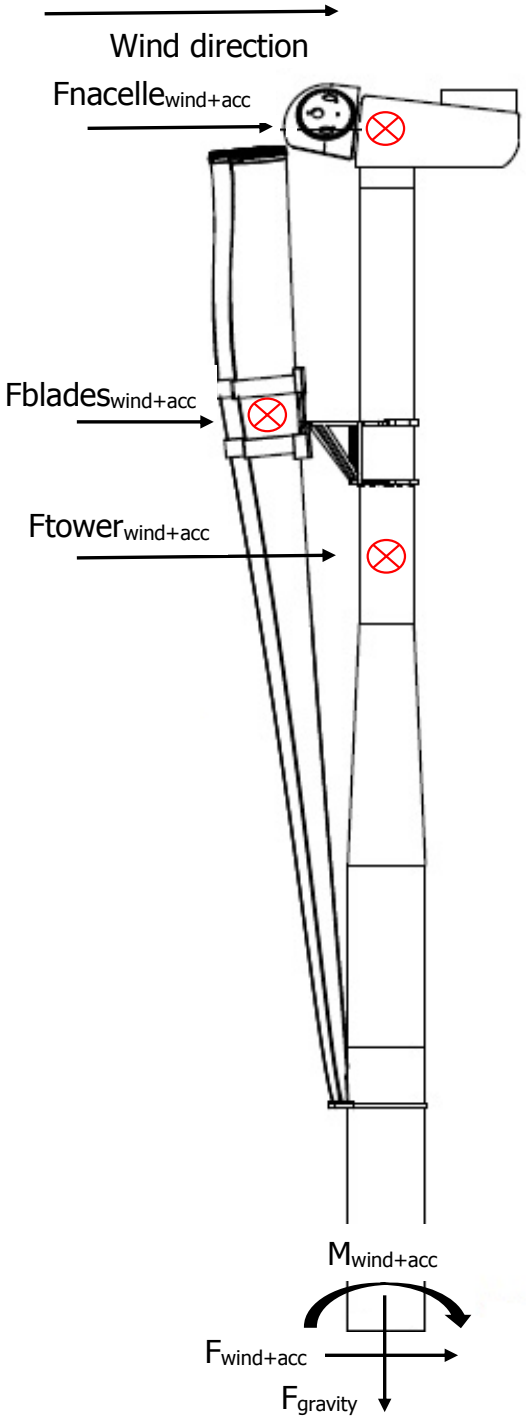

Figure A.2: 2D Free Body Diagram of reference Wind Turbine Generator in carousel configuration with wind, acceleration and gravity forces on nacelle, blades + blade rack and tower CoGs indicated with red cross giving force and overturning moment at WTG base.

B

SCATTER DIAGRAM

Table B.1: Scatter diagram of Dogger bank. Latitude: 55.5 Longitude: 2.5

H_s [m] | T_p [s]	0-1	1-2	2-3	3-4	4-5	5-6	6-7	7-8	8-9	9-10	10-11	11-12	12-13	13-14	14-15	15-16	16-17	17-18	>18	Total [%]
0-0.25	0	0	0	0.03	0.03	0.01	0.02	0.03	0.03	0.04	0.03	0	0.01	0	0	0	0	0	0.01	0.24
0.25-0.5	0	0	0.03	0.57	1.07	0.49	0.25	0.30	0.14	0.26	0.12	0.08	0.08	0.03	0.02	0	0.01	0.01	0	3.44
0.5-0.75	0	0	0.02	0.80	2.16	2.34	1.00	0.68	0.64	0.68	0.45	0.19	0.18	0.14	0.08	0.02	0.01	0.01	0.01	9.40
0.75-1	0	0	0	0.49	1.87	3.77	2.17	0.94	0.81	0.76	0.56	0.31	0.16	0.11	0.06	0.01	0.08	0	0	12.09
1-1.25	0	0	0	0.03	1.81	3.50	2.64	1.02	0.77	0.79	0.64	0.42	0.19	0.12	0.03	0	0.02	0.01	0	11.98
1.25-1.5	0	0	0	0.02	0.70	3.67	2.98	0.90	0.75	0.75	0.92	0.54	0.16	0.08	0	0	0.01	0.01	0.01	11.51
1.5-1.75	0	0	0	0	0.19	2.62	3.09	1.09	0.66	0.53	0.58	0.44	0.23	0.08	0.02	0	0	0	0	9.54
1.75-2	0	0	0	0	0.05	1.42	3.16	1.12	0.52	0.43	0.40	0.46	0.23	0.04	0.02	0	0	0	0	7.84
2-2.25	0	0	0	0	0.01	0.60	2.73	1.36	0.48	0.38	0.21	0.32	0.27	0.08	0	0	0.01	0	0	6.45
2.25-2.5	0	0	0	0	0	0.16	2.60	1.24	0.55	0.31	0.21	0.27	0.25	0.03	0.01	0	0	0	0	5.63
2.5-2.75	0	0	0	0	0	0.07	1.76	1.36	0.69	0.37	0.15	0.29	0.17	0.04	0.02	0	0.01	0	0	4.93
2.75-3	0	0	0	0	0	0.01	0.92	1.41	0.58	0.25	0.14	0.19	0.12	0.04	0.03	0	0	0.01	0	3.71
3-3.25	0	0	0	0	0	0.01	0.44	1.07	0.45	0.30	0.10	0.06	0.08	0.08	0.03	0	0	0	0	2.61
3.25-3.5	0	0	0	0	0	0.01	0.21	0.83	0.68	0.24	0.13	0.11	0.08	0.05	0.03	0	0.01	0	0	2.36
3.5-3.75	0	0	0	0	0	0	0.06	0.57	0.58	0.26	0.10	0.07	0.07	0.05	0.02	0	0	0	0	1.79
3.75-4	0	0	0	0	0	0	0.03	0.34	0.70	0.27	0.12	0.08	0.04	0.05	0	0	0	0	0	1.64
4-4.25	0	0	0	0	0	0	0	0.17	0.47	0.30	0.10	0.06	0.03	0.02	0.02	0	0	0	0	1.18
4.25-4.5	0	0	0	0	0	0	0	0.04	0.31	0.27	0.09	0.08	0.01	0.01	0	0	0	0	0	0.81
4.5-4.75	0	0	0	0	0	0	0	0.02	0.24	0.23	0.13	0.05	0.02	0.02	0.01	0	0	0	0	0.72
4.75-5	0	0	0	0	0	0	0	0.01	0.17	0.22	0.10	0.05	0.03	0	0.01	0	0	0	0	0.60
>5	0	0	0	0	0	0	0	0.01	0.11	0.49	0.34	0.25	0.17	0.07	0.05	0	0	0	0	1.50
Total [%]	0	0	0.05	1.94	7.91	18.66	24.07	14.50	10.33	8.15	5.61	4.32	2.59	1.16	0.47	0.03	0.14	0.04	0.02	**100**

The theoretical energy spectra to represent these ocean waves is the JONSWAP spectrum which has variables H_s and T_p. Equation 3.4 with inputs of Equations 3.5 represents this spectrum. For this entire research, all the waves are assumed to be unidirectional. Also known as a long-crested sea, all waves are coming from the same direction.

C

Vessel Cost Comparison

Table C.1 shows the cost build up for the two different vessels with varying number of WTGs per sail out. One should note all numbers are estimations based on Boskalis experience and based on utilisation for 3 projects consisting of 80 WTGs per park.

Table C.1: Installation cost build up of Mighty Servant 1 and White Marlin for Number of WTGs per sail out

WTGs per park	80	-					
Day rate shore, grillages	30000	€/*day*					
Cost per shore foundation	1500000	€					
Number of projects	3	-					
Vessel	Mighty Servant 1	Mighty Servant 1	White Marlin	White Marlin	White Marlin	White Marlin	
Number of units	1	1	1	1	1	1	-
Sailing distance	78	78	78	78	78	78	*nm*
Average sailing speed	13	13	14,5	14,5	14,5	14,5	*kn*
WTGs per sailout	1	2	1	2	4	6	-
Day rate							
Extra investment on vessel	30000	30000	30000	30000	30000	30000	€/*day*
Main vessel	70000	70000	120000	120000	120000	120000	€/*day*
Crew	20000	20000	20000	20000	20000	20000	€/*day*
Onshore + grillages	36250	42500	36250	42500	55000	67500	€/*day*
Total	156250	162500	206250	212500	225000	237500	€/*day*
Cycle time							
Loading time per WTG	6	6	6	6	6	6	*hr*
Total loading time in port	6	12	6	12	24	36	*hr*
Sailing to site	6,0	6,0	5,4	5,4	5,4	5,4	*hr*
Positioning vessel	1	1	1	1	1	1	*hr*
WTG installing time	4	4	4	4	4	4	*hr*
Sailing to next WTG	1	1	1	1	1	1	*hr*
Sailing back from site	6,0	6,0	5,4	5,4	5,4	5,4	*hr*
Workability	70	70	65	65	65	65	%
Total time per sail out	29	41	28	41	67	93	*hr*
Time per WTG	1,2	0,9	1,2	0,9	0,7	0,6	*day*
Cost per WTG	186.012	140.253	241.400	182.250	157.783	154.169	€
Utilisation	0,26	0,19	0,26	0,19	0,15	0,14	*year*/*year*

D

Equipment Sheets Vessels

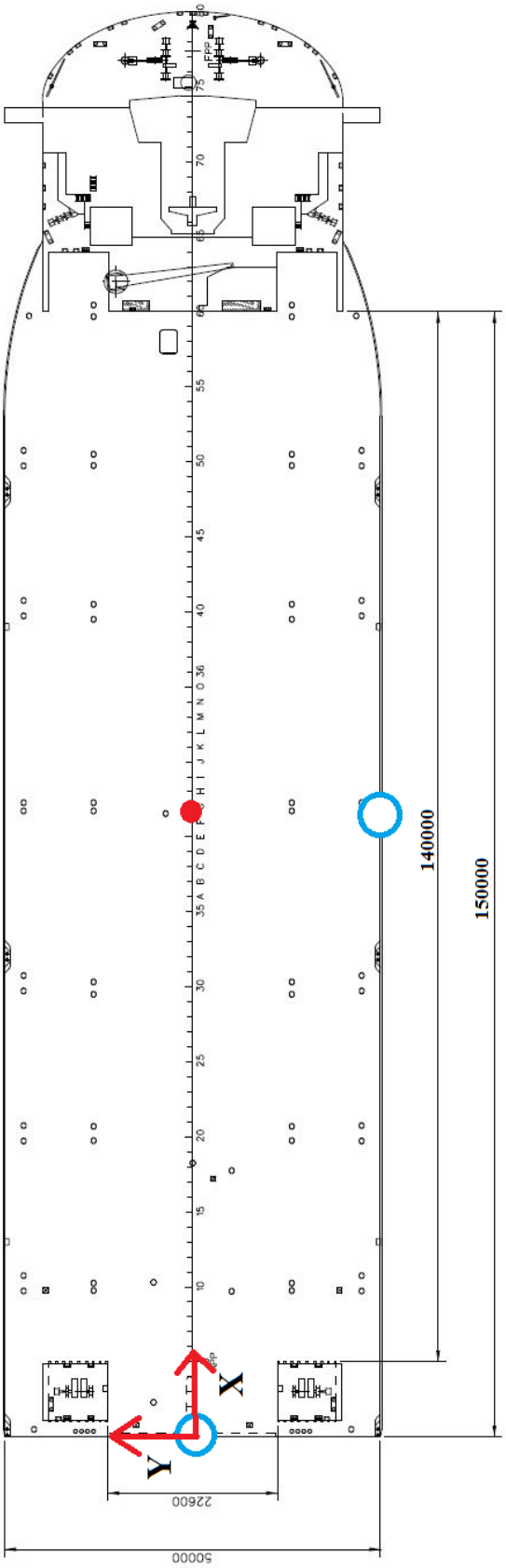

Figure D.1: Mighty Servant 1 top view with blue indicating the offloading locations starboard and stern. Red point indicates CoG of combined vessel and WTG.

Boskalis

EQUIPMENT SHEET

MIGHTY SERVANT 1
SEMI-SUBMERSIBLE HEAVY TRANSPORT VESSEL

CONSTRUCTION/CLASSIFICATION

Built by	Oshima yard-Nagasaki/Japan
Year of construction	1983
Classification	Bureau Veritas I ✠ HULL, ✠ MACH, Special service, Semi submersible heavy lift vessel, unrestricted navigation, AUT-UMS (SS), MON-SHAFT
IMO number	8130875
Flag	Curaçao
Port of registry	Willemstad

MAIN DATA

Length overall	190.03 m
Breadth moulded/max	50.00 m
Depth	12.00 m
Draft submerged at FPP/APP	21.38 / 26.00 m
Summer draft	8,77 m
Deck space [l x w]	150.00 x 50.00 m
Deadweight	40,910 t
Trial speed	13.00 kn
Total installed power	14,220 kW
Main engines	2 x 6,500 kW
Main propulsion	2 x 4-bladed c.p. propellers driven by four E-motors of 3,100 kW each
Bow thruster	2 x 500 kW

NAVIGATION EQUIPMENT

- Two radar, one ARPA coupled
- Two GPS navigator
- Echo sounders fore and aft
- Magnetic log
- Two gyro compasses
- SPOS - Ship Performance Optimisation System
- OCTOPUS - Octopus onboard system (ship motion monitoring and decision support system by Amarcon)

COMMUNICATIONS EQUIPMENT

- Inmarsat Mini M and C (telex/telephone/fax)
- SSB radio telephony
- Telex over radio
- VHF radio telephony
- Weather facsimile
- Irridium mobile phone
- NAVTEX receiver
- GMDSS
- Global wireless communication system
- SafetyMax

BALLASTING

- Four main ballast pumps 2,000 m^3/hr@ 30 m head
- One fire gen. service pump 90 m^3/hr@ 60 m head or 170 m^3/hr@ 30 m head
- One fire bilge pump 90 m^3/hr@ 60 m head or 170 m^3/hr@ 30 m head
- One emergency fire pump 45 m^3/hr@ 60 m head
- Four deballast compressors 3,000 m^3/hr@ 1 atg
- Two ejector pumps 150 m^3/hr@ 30 m head

Figure D.2: Equipment sheet Mighty Servant 1

Boskalis

EQUIPMENT SHEET

DOCKWISE WHITE MARLIN
SEMI-SUBMERSIBLE HEAVY TRANSPORT VESSEL

CONSTRUCTION/CLASSIFICATION

Built by	Guangzhou Shipyard International Co. Ltd.
Year of construction	2015
Classication	Bureau Veritas | ✠ HULL, ✠ MACH, ✠ AVM-IPS, ✠ AUT-UMS, Special service, Semi submersible heavy lift vessel, unrestricted navigation, CPS (WBT), MON-SHAFT, BWT, CLEANSHIP, ICE CLASS ID, ERS-S, INWATERSURVEY
IMO number	9670224
Flag	Malta
Port of registry	Valletta

MAIN DATA

Length overall	216.70 m
Breadth moulded/max	63.00 m
Depth	13.00 m
Draft submerged at FPP/APP	26.00/26.00 m
Summer draft	10.00 m
Deck space [l x w]	177.60 x 63.00 m
Deadweight	72,146 t
Trial speed	14.5 kn
Total installed power	16,728 kW
Main engines	4 x 3,840 kW
Main propulsion	2 x 5,250 kW
Azimuth thrusters	1 x 8,700 kW
Bow thruster	2 x 1,200 kW

NAVIGATION EQUIPMENT

- Two radar
- 2 GPS navigators
- ECHO sounder
- Two gyro compasses
- Two ECDIS
- Magnetic compass
- Doppler speed log
- Navigational echo sounder
- Automatic identification system
- Voyage data recorder
- Bridge navigational watch alarm system
- Bridge monitor
- Autopilot

COMMUNICATIONS EQUIPMENT

- Inmarsat C
- Inmarsat Fleet broad band
- VHF radio telephony
- MF/ HF radio telephony
- Weather facsimile
- NAVTEX receiver
- GMDSS alarm
- EPIRB
- Two SART

BALLASTING

- Two ballast pumps in fore 1,500 m^3/hr@ 3.0 bar
- Two ballast pumps in aft 250 m^3/hr@ 3.0 bar
- Two topping up ballast pumps in fore 160 m^3/hr@ 3.0 bar

Figure D.3: Equipment sheet White Marlin

E

SEAWAY OUTPUT

This Appendix is divided into two sections. One for each location of the WTG. Section 1 is for the vessels with a WTG at starboard while section 2 is for a WTG at the stern. In each section the RAOs for all DoF are given. The significant displacements (amplitudes) and accelerations are given at deck and nacelle height. All outputs are given for a significant wave height of 1 meter. These motions originate from the second-order wave forces. The given displacements are amplitudes thus should be multiplied by two to get the total displacements.

E.1. WTG AT STARBOARD

E.1.1. RAOS MIGHTY SERVANT 1

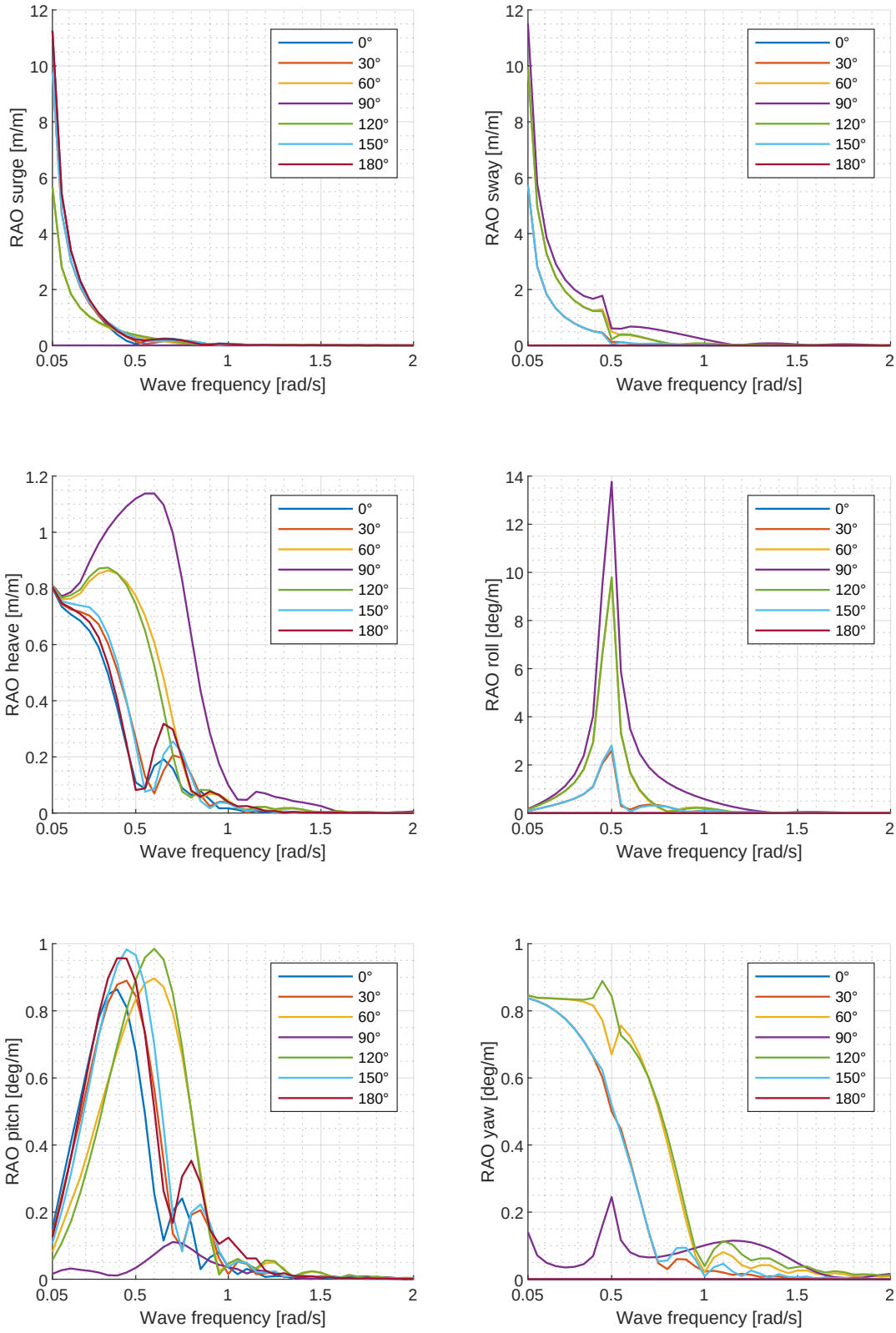

Figure E.1: Mighty Servant 1, RAOs with one turbine at Starboard

E.1.2. RAOS WHITE MARLIN

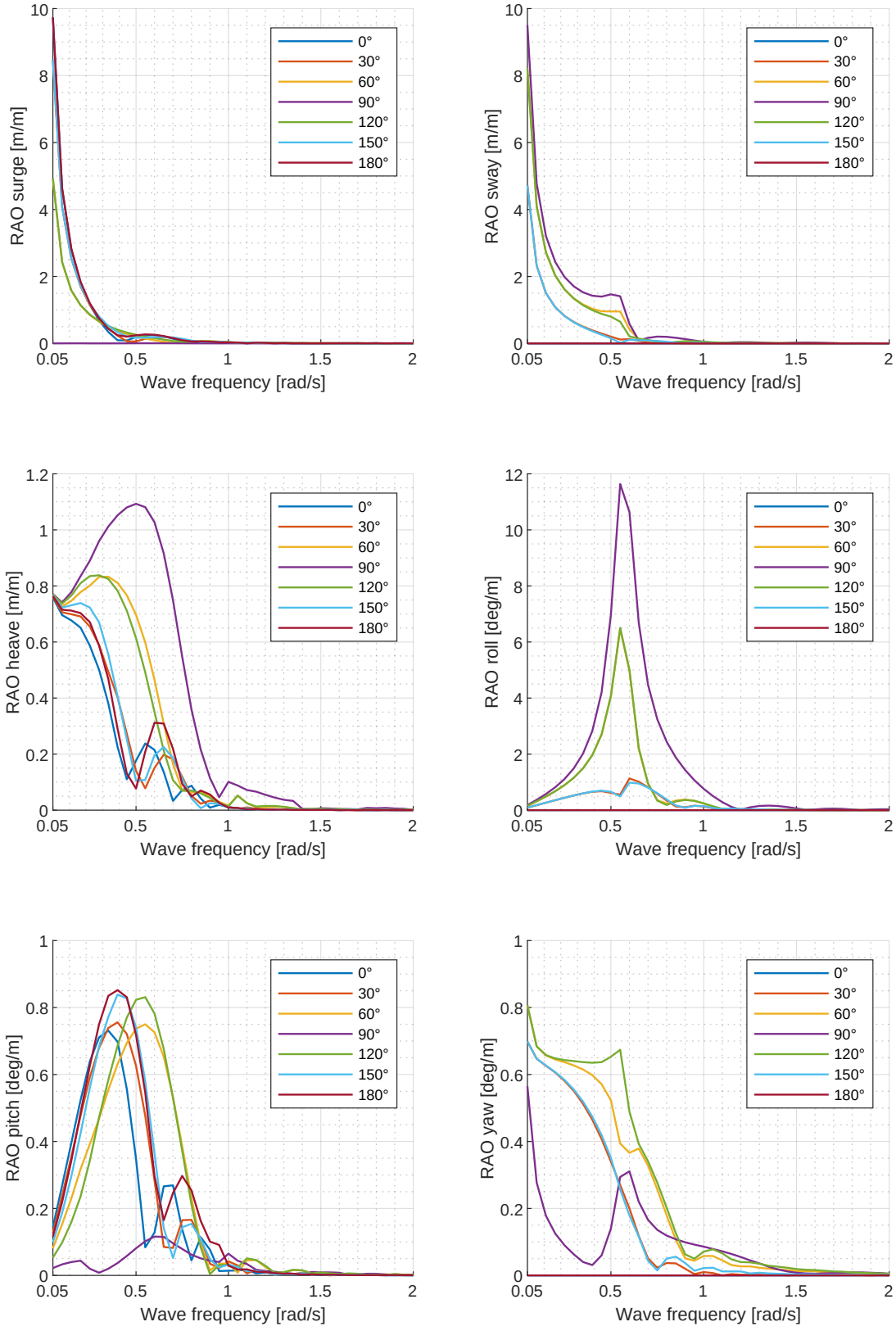

Figure E.2: White Marlin, RAOs with one turbine at Starboard

E.1.3. AMPLITUDE SIGNIFICANT DISPLACEMENTS MIGHTY SERVANT 1 & WHITE MARLIN

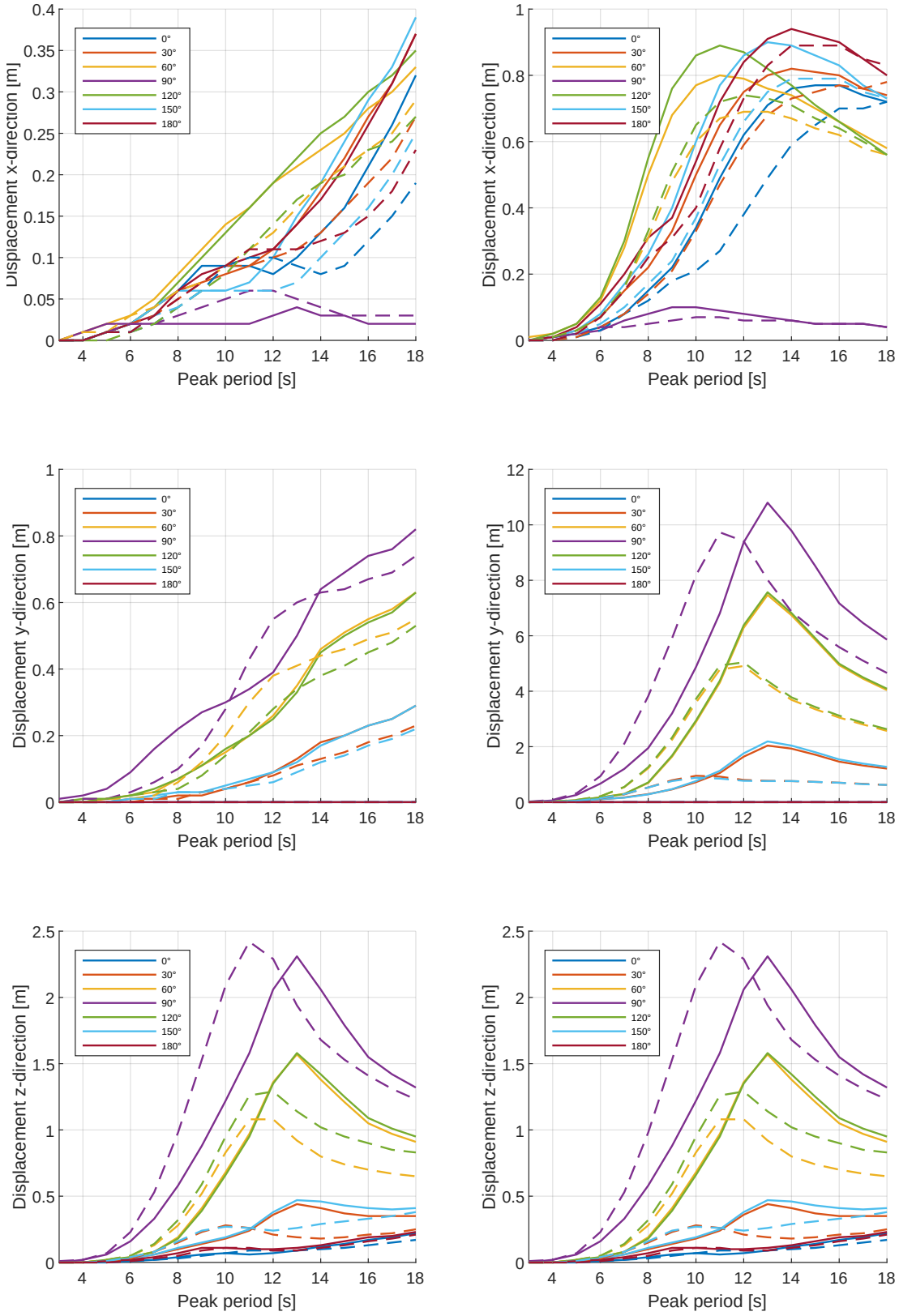

Figure E.3: Amplitude significant displacements Mighty Servant 1 (continuous line) and White Marlin (dotted line) with WTG at Starboard. Left and right side are respectively tower bottom and nacelle CoG measurement points

E.1.4. SIGNIFICANT ACCELERATIONS MIGHTY SERVANT 1 & WHITE MARLIN

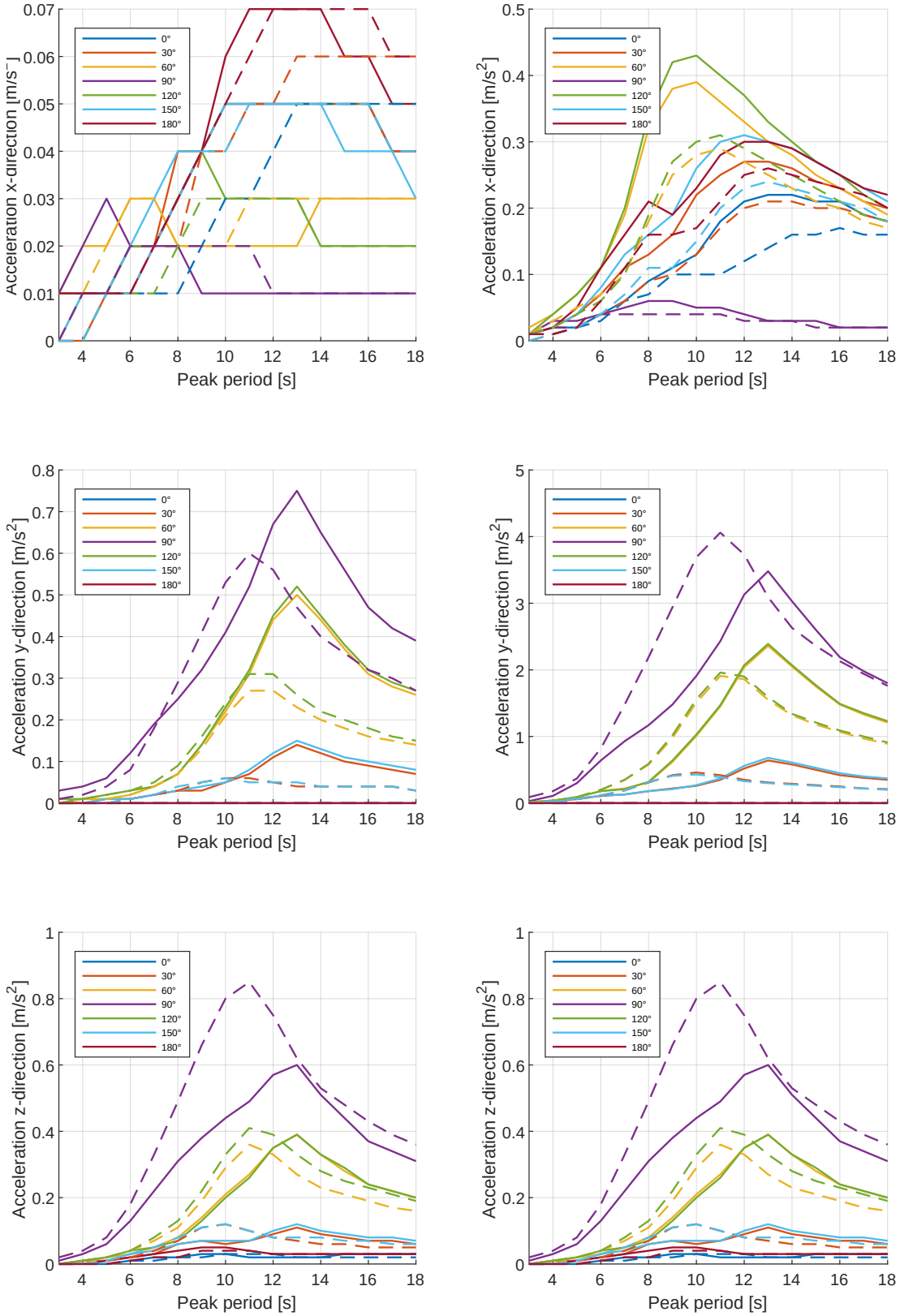

Figure E.4: Accelerations Mighty Servant 1 (continuous line) and White Marlin (dotted line) with WTG at Starboard. Left and right side are respectively tower bottom and nacelle CoG measurement points

E.2. WTG AT STERN

E.2.1. RAOS MIGHTY SERVANT 1

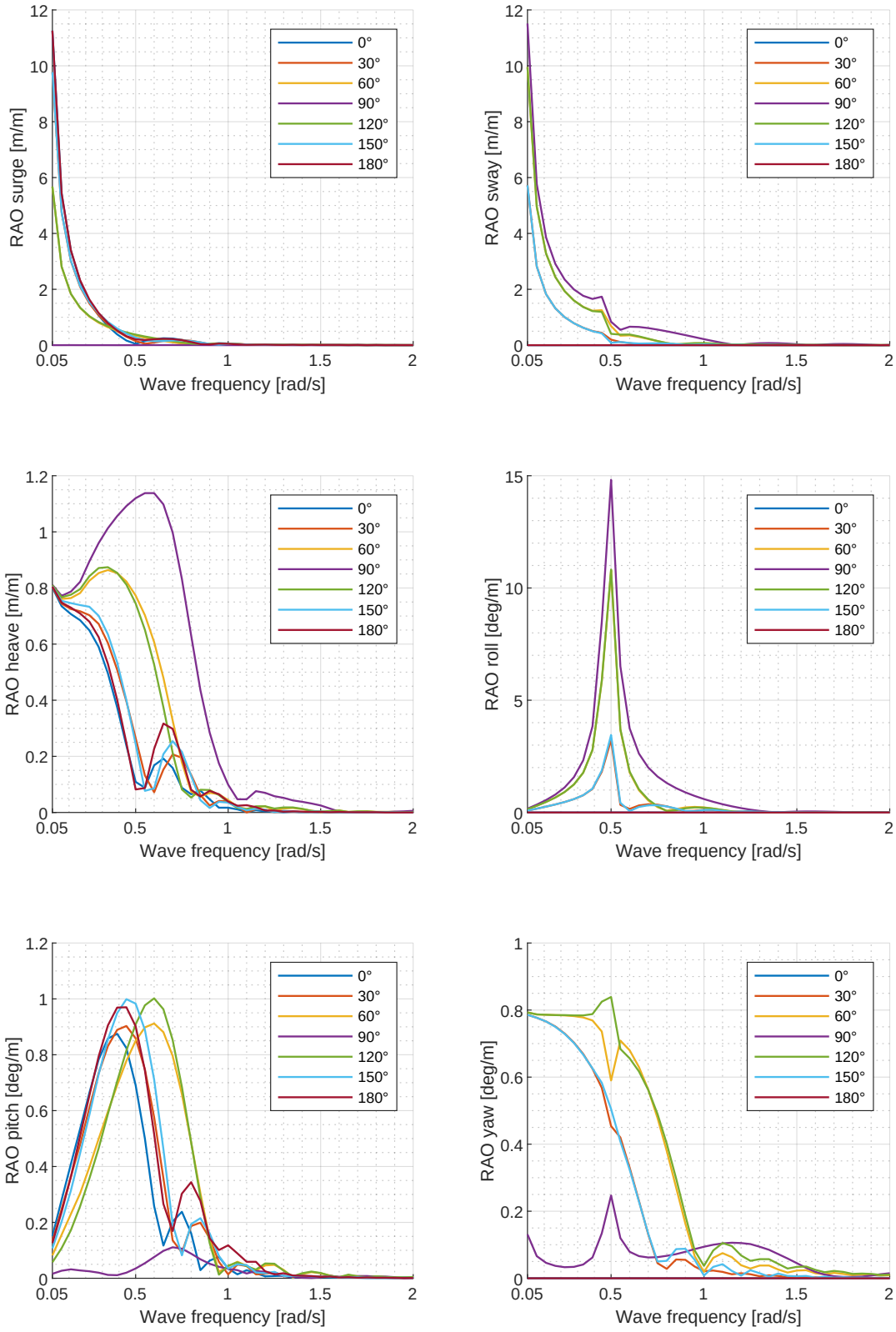

Figure E.5: Mighty Servant 1, RAOs with one turbine at Stern

E.2.2. RAOS WHITE MARLIN

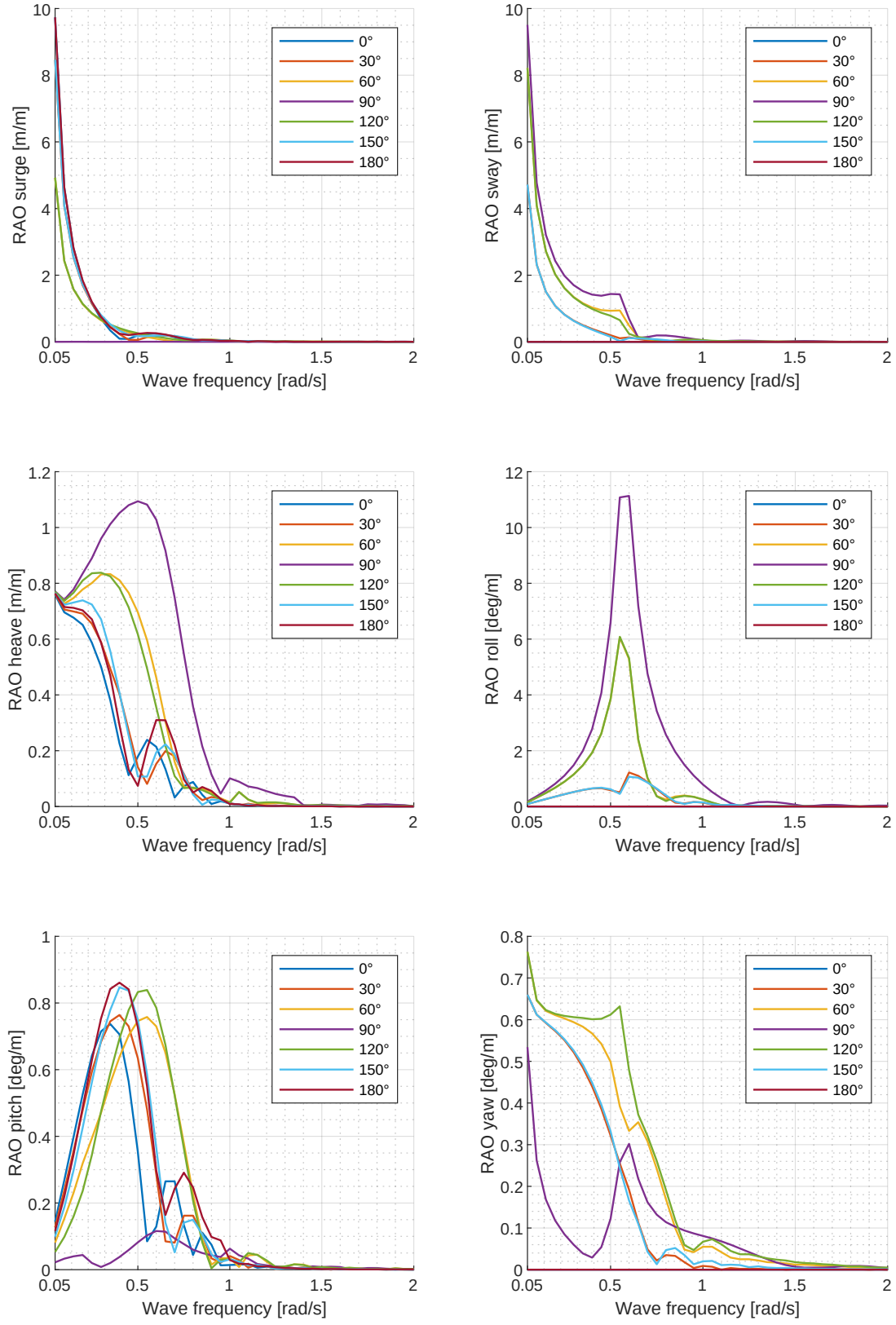

Figure E.6: White Marlin, RAOs with one turbine at Stern

E.2.3. AMPLITUDE SIGNIFICANT DISPLACEMENTS MIGHTY SERVANT 1 & WHITE MARLIN

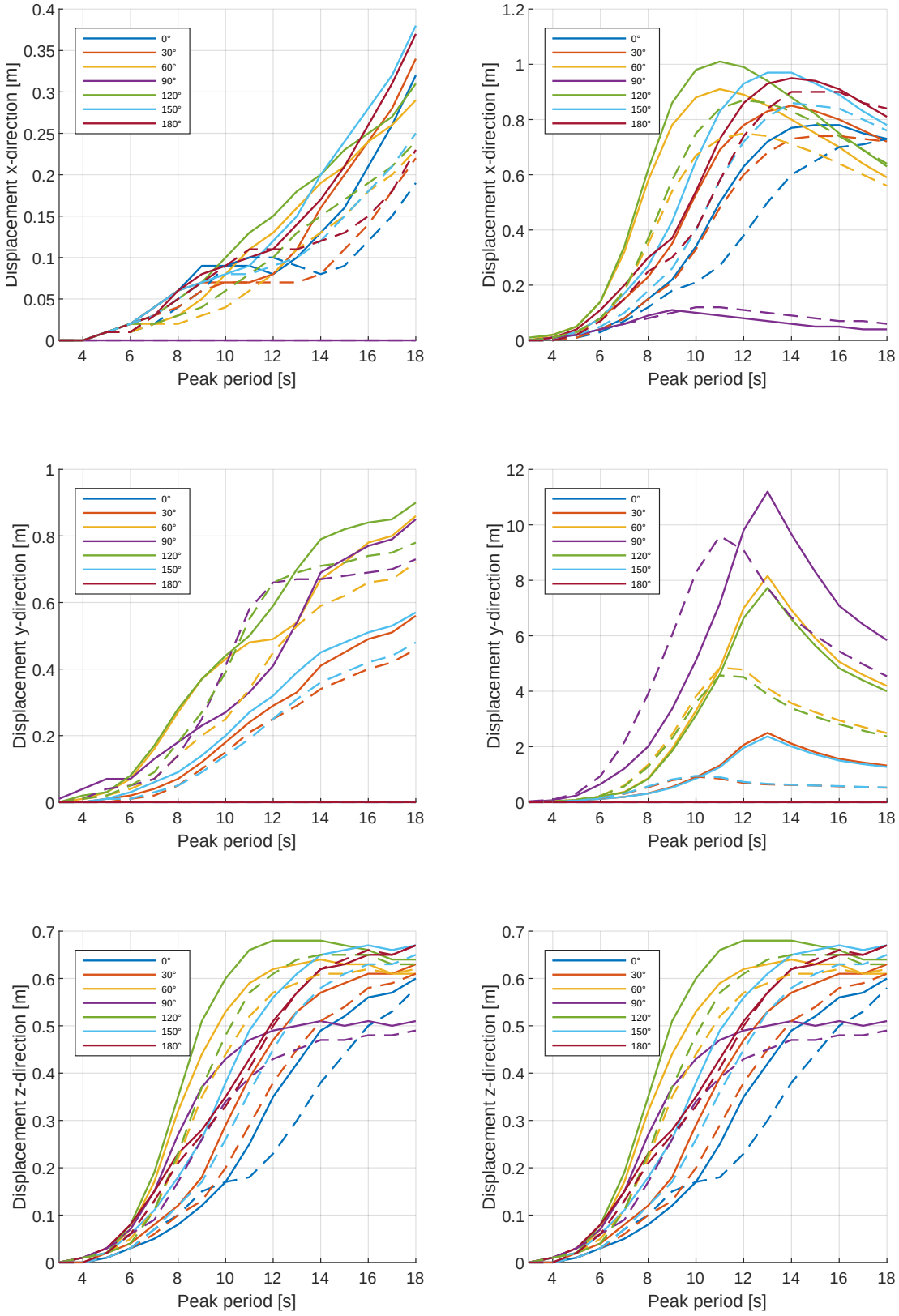

Figure E.7: Amplitude significant displacements Mighty Servant 1 (continuous line) and White Marlin (dotted line) with WTG at Stern. Left and right side are respectively tower bottom and nacelle CoG measurement points

E.2.4. SIGNIFICANT ACCELERATIONS MIGHTY SERVANT 1 & WHITE MARLIN

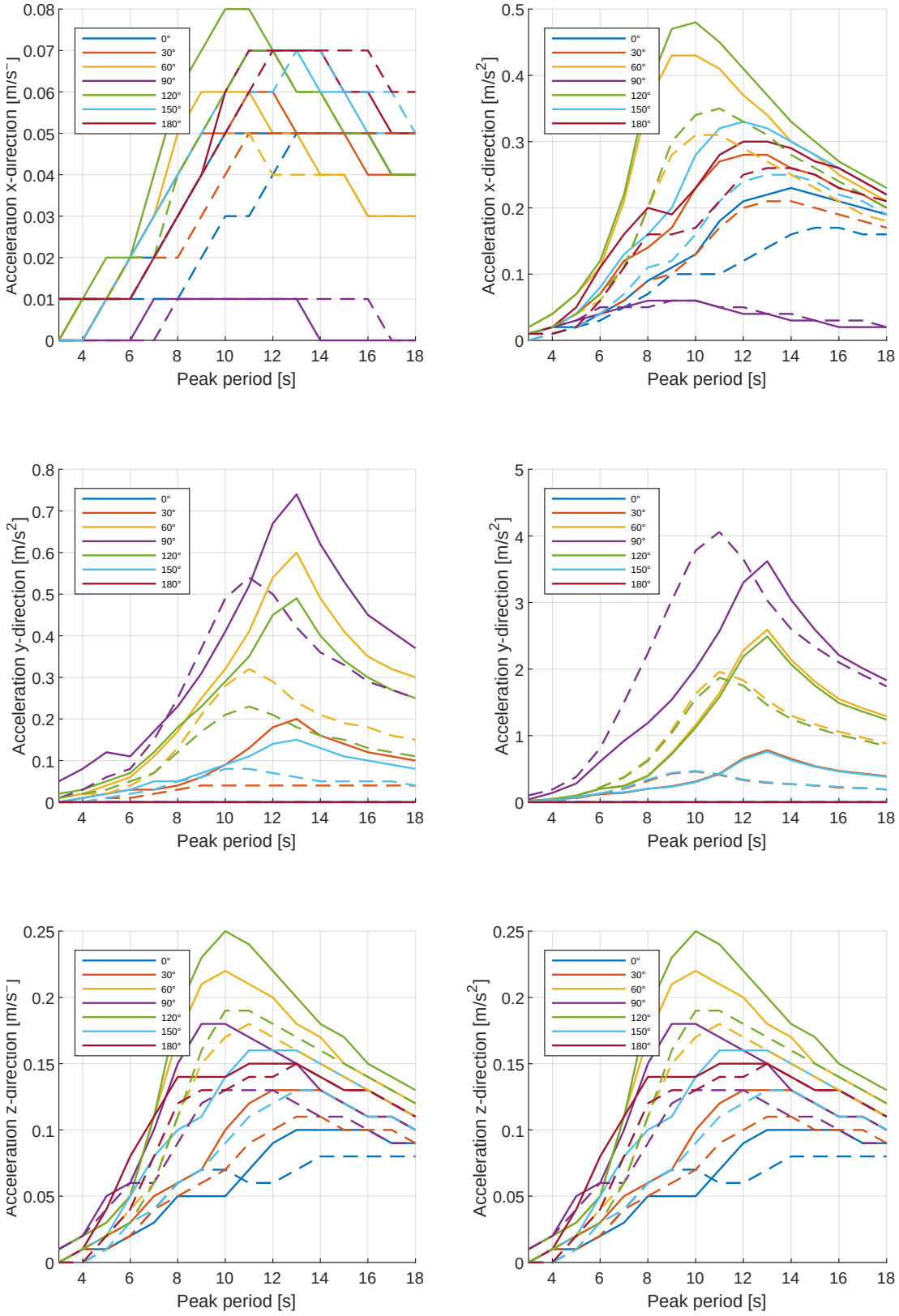

Figure E.8: Accelerations Mighty Servant 1 (continuous line) and White Marlin (dotted line) with WTG at Stern. Left and right side are respectively tower bottom and nacelle CoG measurement points

F

Analytic Hierarchy Process

In this Appendix the input values of the Analytic Hierarchy Process are given based on the proposed rankings by Saaty [21]. Also, a MATLAB script is provided which shows the calculations done with the inputs.

F.1. Input Values

Below, the inputs for the MATLAB script are shown. In the first table, the comparisons between the criteria are made. All other tables show the comparison of the concepts based on a criteria. The tables can be read as follows. An item in the first column is a certain amount better than an item in the first row. One should not that a number below 1 indicates that the item in the first column is worse than the item in the first row. Looking at Table F.1, Technical feasibility is 3 times as important as applicable for future WTGs. The diagonal only has ones since comparing the same criteria results in no difference.

Table F.1: Input values for AHC, criteria-criteria comparison

Criteria-criteria	Technical Feasibility	Applicable for future WTGs	Installation time	Attachable on existing vessel	HSE
Technical feasibility	1	3	2	3	3
Applicable for future WTGs	1/3	1	1/4	1/3	2
Installation time	1/2	4	1	2	3
Attachable on existing vessel	1/3	3	1/2	1	2
HSE	1/3	1/2	1/3	1/2	1

Table F.2: Input values for AHC, concepts compared on Technical feasibility

Technical feasibility	Concept 1	Concept 2	Concept 3	Concept 4	Concept 5	Concept 6	Concept 7	Concept 8
Concept 1	1	2	2	7	8	6	4	4
Concept 2	1/2	1	1/3	3	4	4	3	3
Concept 3	1/2	3	1	7	7	5	4	4
Concept 4	1/7	1/3	1/7	1	2	1/3	1/3	1/3
Concept 5	1/8	1/4	1/7	1/2	1	2	1/2	1/2
Concept 6	1/6	1/4	1/5	3	1/2	1	1/2	1/3
Concept 7	1/4	1/3	1/4	3	2	2	1	1
Concept 8	1/4	1/3	1/4	3	2	3	1	1

Table F.3: Input values for AHC, concepts compared on Applicable for future WTGs

Applicable for future WTGs	Concept 1	Concept 2	Concept 3	Concept 4	Concept 5	Concept 6	Concept 7	Concept 8
Concept 1	1	2	1	1/3	1/4	3	3	3
Concept 2	1/2	1	1/3	1/3	1/4	2	1	2
Concept 3	1	3	1	1/2	1/2	4	3	4
Concept 4	3	3	2	1	1	4	4	5
Concept 5	4	4	2	1	1	3	3	4
Concept 6	1/3	1/2	1/4	1/4	1/3	1	1	1
Concept 7	1/3	1	1/3	1/4	1/3	1	1	2
Concept 8	1/3	1/2	1/4	1/5	1/4	1	1/2	1

Table F.4: Input values for AHC, concepts compared on Installation time per WTG

Installation time per WTG	Concept 1	Concept 2	Concept 3	Concept 4	Concept 5	Concept 6	Concept 7	Concept 8
Concept 1	1	1/3	1/2	4	3	3	2	4
Concept 2	3	1	3	5	4	4	3	6
Concept 3	2	1/2	1	3	2	3	2	4
Concept 4	1/4	1/5	1/3	1	1/3	1/4	1/3	2
Concept 5	1/3	1/4	1/2	3	1	2	1	3
Concept 6	1/3	1/4	1/3	2	1/2	1	1	3
Concept 7	1/2	1/3	1/2	3	1	1	1	4
Concept 8	1/4	1/6	1/4	1/2	1/3	1/3	1/4	1

Table F.5: Input values for AHC, concepts compared on Attachable to existing vessel

Attachable to existing vessel	Concept 1	Concept 2	Concept 3	Concept 4	Concept 5	Concept 6	Concept 7	Concept 8
Concept 1	1	4	3	3	4	6	4	5
Concept 2	1/4	1	1	1/2	1/2	4	1/2	1/2
Concept 3	1/3	1	1	1/2	1/3	3	1/3	1
Concept 4	1/3	2	2	1	2	3	1/2	1
Concept 5	1/4	2	3	1/2	1	3	3	2
Concept 6	1/6	1/4	1/3	1/3	1/3	1	1/3	1/3
Concept 7	1/4	2	3	2	1/3	3	1	3
Concept 8	1/5	2	1	1	1/2	3	1/3	1

Table F.6: Input values for AHC, concepts compared on HSE

HSE	Concept 1	Concept 2	Concept 3	Concept 4	Concept 5	Concept 6	Concept 7	Concept 8
Concept 1	1	2	2	3	1/3	2	1/3	3
Concept 2	1/2	1	1	5	1/3	2	1/2	5
Concept 3	1/2	1	1	1/2	1/3	1	1/3	1
Concept 4	1/3	1/5	2	1	1/2	2	1/2	1
Concept 5	3	3	3	2	1	3	1	2
Concept 6	1/2	1/2	1	1/2	1/3	1	1/3	1/2
Concept 7	3	2	3	2	1	3	1	4
Concept 8	1/3	1/5	1	1	1/2	2	1/4	1

F.2. MATLAB SCRIPT

```
clear all; close all; clc;
%% Input values
k = 5; %Number of criteria
global RIvalues
RIvalues = [0,0,0.58,0.90,1.12,1.24,1.32,1.41,1.45,1.49,1.51];
%Random Consistency Index (RI) @Saaty

%% Calculations
k = k+1;

for i = 1:k
    if i==1
        [ranking,lambdamax,CI,RI,CR,n] = priorityvector(i); %i=1 is the criteria-
            criteria comparison
    else
     p = i-1;
    [vector(:,p),lambdamax(i),CI(i),RI(i),CR(i),n(i)] = priorityvector(i);
    end
end

finalpriority = vector*ranking; %Final priority vector
```

```
function [priorityvector, lambdamax, CI, RI, CR, n] = priorityvector(x)
A = xlsread('AHC.xlsx',x); % Read values from excel input sheets
n = length(A); %Number of criteria
RI = RIvalues(n); %RI belonging to number of criteria

[V,D] = eig(A);
sumV = sum(V(:,1));
priorityvector = V(:,1)/sumV;   %Normalized principal eigenvector

lambdamax = max(max(D)); %Maximal Eigenvalue
CI = (lambdamax - n)/(n-1); %Consistency Index
CR = CI/RI; %smaller or equal to 10% is acceptable

%% Tests to check for correct analysis and consistent input values
test1 = round(sum(priorityvector));
test2 = isreal(V(:,1));
test3 = CR;

    if test1 ~= 1
        note1 = 'Sum of priority vector is not 1, incorrect analysis';
        disp(note1)
    end

    if test2 == 0
        note2 = 'Eigenvector in lambdamax column not real, incorrect analysis';
        disp(note2)
    end

    if test3 > 0.1
        note3 = 'CR value not below 10%, incorrect analysis';
        disp(note3)
    end
end
```

G

Stewart Platform Optimization

G.1. Input Script

```
clear all; close all; clc;
rng default % Same seed for random generator
Q.n = 500; % Number of points in workspace
random = -1 + (1--1).*rand(6,Q.n); % Generate random numbers between -1 and 1
Q.deg2rad = pi/180;
Q.Lb = [5 5 4.59*Q.deg2rad 4.59*Q.deg2rad 3]; % Lower bounds
Q.Ub = [12.5 12.5 115.41*Q.deg2rad 115.41*Q.deg2rad 15]; % Upper bounds
Q.A = [0 0 -1 1 0; -1 1 0 0 0];
Q.B = [-0.2;-0.25]; % Rb>Rt & Gb>Gt constraints
Q.nvars = 5; % Number of design parameters

%% Maximum vessel motions at centre of hexapod for 150 degrees, Hs =2, Tp =8.
Surge_max = 0.58; % [m] + or - (Amplitudes)
Sway_max = 1.24; % [m]
Heave_max = 0.83; % [m]
Roll_max = 2.83*Q.deg2rad; % [rad]
Pitch_max = 0.48*Q.deg2rad; % [rad]
Yaw_max = 0.23*Q.deg2rad; % [rad]
Motions_max = [Surge_max Sway_max Heave_max Yaw_max Pitch_max Roll_max]';
Q.q = Motions_max.*random; % q vector

%% Call function
[x,fval,exitflag,output,population,scores,vals2,Indexes] = Multi_Objective_Script(Q)

%% Plotting 3D Pareto front
A = [1; -1; -1]; % Minimizing is maximizing negative GGI and GPI
Indexes = A.*Indexes;
[p, idxs] = DominatedSolution2ParetoFront(Indexes');
p(abs(p(:,1)) < 0.2 | abs(p(:,1)) > 0.67,:) = [];
p(abs(p(:,2)) > 0.7,:) = []; % Only show feasible designs
p(abs(p(:,3)) < 0.275 | abs(p(:,3)) > 0.6,:) = [];

figure; grid on; box on; hold on;
ax = gca; ax.GridAlpha = 0.3; set(gca,'FontSize',12)
scatter3(abs(p(:,1)),abs(p(:,2)),abs(p(:,3)),20,abs(p(:,1)));
tri = delaunay(abs(p(:,1),abs(p(:,2)); h = trisurf(tri,abs(p(:,1)),abs(p(:,2)),abs(p
    (:,3)));
xlabel('GCI'); ylabel('GGI'); zlabel('GFI'); axis equal;
```

G.2. INDEX COMPUTATION SCRIPT

```
function [x, fval,exitflag, output,population,scores, vals2,Indexes] =
    Multi_Objective_Script(Q)
    n = Q.n;
    Lb = Q.Lb; Ub = Q.Ub;
    nvars = Q.nvars;
    q = Q.q; q3 = Q.q;
    iter = 1;
    vals2 = []; Indexes = [];

    options = optimoptions('gamultiobj','PlotFcn',{@gaplotpareto,
        @gaplotscorediversity},'TolFun',0.0001,'TolCon',0.001,'PopulationSize',150);

    [x,fval,exitflag,output,population,scores] = gamultiobj(@(x)
        KinematicOptimization(x),nvars,Q.A,Q.B,[],[],Lb,Ub,@nonlcon,options);

    function [c,ceq]=nonlcon(x) % No cylinder collision
        c = [2*asin(1/(2*x(1)))-x(3);
             2*asin(1/(2*x(1)))-abs(120*Q.deg2rad-x(3));
             2*asin(1/(2*x(2)))-x(4);
             2*asin(1/(2*x(2)))-abs(120*Q.deg2rad-x(4))];
        ceq = [];
    end

    function Objectives = KinematicOptimization(x)
        %% Design parameters
        R_b = x(1); % [m]
        R_t = x(2); % [m]
        G_b = x(3); % [rad]
        G_t = x(4); % [rad]
        h = x(5); % [m]

        vals2(iter,:) = [x(1) x(2) x(3) x(4) x(5)];
        q(3,:) = q3(3,:) + h; %Workspace adjustment

        % Base description
        Phi_b = zeros(1,6);
        for i = 1:2:5
            Phi_b(i) = i*pi/3 - G_b/2;
        end

        for i = 2:2:6
            Phi_b(i) = Phi_b(i-1) + G_b;
        end

        X_b = R_b.*cos(Phi_b);
        Y_b = R_b.*sin(Phi_b);
        Z_b = zeros(1,6);
        Base = [X_b ; Y_b; Z_b];

        % Platform description
        Phi_t = zeros(1,6);
        for i = 1:2:5
            Phi_t(i) = i*pi/3 - G_t/2;
        end
```

```
52          for i = 2:2:6
53              Phi_t(i) = Phi_t(i-1) + G_t;
54          end
55
56          X_t = R_t.*cos(Phi_t);
57          Y_t = R_t.*sin(Phi_t);
58          Z_t = zeros(1,6);
59          Top = [X_t ; Y_t; Z_t];
60
61          %% Mapping Platform Coordinate system to Global CS
62          alpha = q(6,:); %[yaw]
63          beta  = q(5,:); %[pitch]
64          gamma = q(4,:); %[roll]
65
66          R = zeros(3,3,n); %Transformation matrix
67
68          for i = 1:n
69             R(:,:,i) = [cos(alpha(i)).*cos(beta(i))
70             -sin(alpha(i)).*cos(gamma(i))+cos(alpha(i)).*sin(beta(i)).*sin(gamma(i))
71              sin(alpha(i)).*sin(gamma(i))+cos(alpha(i)).*sin(beta(i)).*cos(gamma(i));
72              sin(alpha(i)).*cos(beta(i))
73              cos(alpha(i)).*cos(gamma(i))+sin(alpha(i)).*sin(beta(i)).*sin(gamma(i))
74             -cos(alpha(i)).*sin(gamma(i))+sin(alpha(i)).*sin(beta(i)).*cos(gamma(i));
75             -sin(beta(i)) cos(beta(i)).*sin(gamma(i)) cos(beta(i)).*cos(gamma(i))];
76          end
77          t = [q(1,:) ;q(2,:); q(3,:)]; %Bottom to platform origin
78
79          %% Jacobian
80          l = zeros(3,6,n); %xyz for all 6 cylinders
81          e = zeros(3,6,n); %xyz unit vector for all cylinder
82          J = zeros(6,6,n); %6x6 Jacobians
83          L = zeros(n,1); %Normalization value
84          k = zeros(n,1); % Local Dexterity matrix
85
86           for j = 1:1:n
87                      for i = 1:6 %for all 6 directions
88                       l(:,i,j) = t(:,j) + R(:,:,j)*Top(:,i)-Base(:,i);
89                       e(:,i,j) = l(:,i,j)/(sqrt(l(1,i,j)^2+l(2,i,j)^2+l(3,i,j)^2));
90                       J(i,:,j) = [e(:,i,j).'    cross(R(:,:,j)*Top(:,i),e(:,i,j)).'];
91                      end
92                  Jt = J(:,4:6,j)'*J(:,4:6,j);
93                  Jf = J(:,1:3,j)'*J(:,1:3,j);
94                  L(j,:) = sqrt(trace(Jt)/trace(Jf));
95           end
96
97          J_nonadjusted = J;
98
99          for j = 1:1:n
100             J(:,4:6,j) = J(:,4:6,j)/L(j); %Right side Jacobian also dimensionless
101             k(j,1) = cond(J(:,:,j));
102         end
103
104         %% Global Conditioning Index GCI
105         LCI = 1./k; % local Conditioning Index
106         GCI = sum(LCI)/n; % Global Conditioning Index
107
```

```
108         %% Global Gradient Index GGI
109         Delta = (1E-5).*[0.1 ; 0.1 ; 0.1 ; 0.1 ; 0.1; 0.1].*ones(6,n); %0.1 m and
                0.1 deg as delta
110         LCI2 = GGIfunction(Top,Base,q,n,Delta);
111         GGI = (LCI2-ones(n,6).*LCI)./Delta';
112
113         for i = 1:1:n
114             GGInorm(i,1) = norm(GGI(i,:));
115         end
116         GGI = max(GGInorm); % Global Gradient Index
117
118        %% Forces calculated for load case 1b
119        AMC = 0.05; %Amount of motion compensation = 0.95
120       Mx = 53.58 + AMC*(608.50+((225.5*0.48*(5.20*AMC+R_t)/1000)+(990*0.48*(2.06*AMC
              +R_t)/1000)+(720*0.48*(6.87*AMC+R_t)/1000)))+(AMC*6.87+R_t)*720*9.81/1000+(
              AMC*3.06+R_t)*990*9.81/1000+(AMC*5.20+R_t)*225.5*9.81/1000;
121       My = AMC*(101.22+0.75+12.60)+20.38;
122       Mz = 3.35+AMC*(-5.84+((225.5*0.62*(0.73*AMC+R_t)/1000)+(990*0.44*(0.42*AMC+R_t
              )/1000)+(720*0.76*(0.97*AMC+R_t)/1000)));
123        tau = [0.32 ; 1.04; 19.05; Mx; My; Mz];
124        tau2 = -[tau(2); tau(1); -tau(3); -tau(5); tau(4); tau(6)];
125        Force = zeros(6,n);
126        gsum = zeros(1,n);
127
128         for j = 1:1:n
129             Force(:,j) = (J_nonadjusted(:,:,j)')\tau2;
130             gsum(:,j) = sum(abs(Force(:,j)));
131         end
132         GPI = sum(gsum)/n/100;  % Global Payload Index
133
134         %% Gathering Indexes
135         Indexes(:,iter) = [GCI; GGI; GFI];
136         Objectives = [-GCI; GGI; GFI]; %minimize negative GCI
137         iter = iter+1;
138     end
139
140     function LCI2 = GGIfunction(Top,Base,q,n,Delta)
141         q2 = q;
142         l2 = zeros(3,6,n); %xyz for all 6 cylinders
143         e2 = zeros(3,6,n); %xyz unit vector for all cylinder
144         J2 = zeros(6,6,n); %6x6 Jacobians
145         L2 = zeros(n,1); %Normalization value
146         k2 = zeros(n,1); % Local Dexterity matrix
147         R2 = zeros(3,3,n); %Transformation matrix
148         LCI2 = zeros(n,6); %Local Dexterity Index
149
150         for b = 1:1:6
151             q2(b,:) = q(b,:)+Delta(b,:);
152
153         %% Mapping Platform Coordinate system to Global CS
154         alpha2 = q2(6,:); %[yaw]
155         beta2  = q2(5,:); %[pitch]
156         gamma2 = q2(4,:); %[roll]
157
158
159
```

```
        for i = 1:n
        R2(:,:,i) = [cos(alpha2(i)).*cos(beta2(i))
        -sin(alpha2(i)).*cos(gamma2(i))+cos(alpha2(i)).*sin(beta2(i)).*sin(gamma2(i))
        sin(alpha2(i)).*sin(gamma2(i))+cos(alpha2(i)).*sin(beta2(i)).*cos(gamma2(i));
        sin(alpha2(i)).*cos(beta2(i))
        cos(alpha2(i)).*cos(gamma2(i))+sin(alpha2(i)).*sin(beta2(i)).*sin(gamma2(i))
        -cos(alpha2(i)).*sin(gamma2(i))+sin(alpha2(i)).*sin(beta2(i)).*cos(gamma2(i));
        -sin(beta2(i)) cos(beta2(i)).*sin(gamma2(i)) cos(beta2(i)).*cos(gamma2(i))];
        end
              t2 = [q2(1,:) ;q2(2,:); q2(3,:)]; %Bottom to platform origin
              q2(b,:) = q(b,:);

              %% Jacobian
              for j = 1:1:n
                  for i = 1:6 %for all 6 directions
                    l2(:,i,j) = t2(:,j) + R2(:,:,j)*Top(:,i)-Base(:,i);
                    e2(:,i,j) = l2(:,i,j)/(sqrt(l2(1,i,j)^2+l2(2,i,j)^2+l2(3,i,j)^2));
                    J2(i,:,j) = [e2(:,i,j).'    cross(R2(:,:,j)*Top(:,i),e2(:,i,j))'];
                  end
                      Jt2 = J2(:,4:6,j)'*J2(:,4:6,j);
                      Jf2 = J2(:,1:3,j)'*J2(:,1:3,j);
                      L2(j,:) = sqrt(trace(Jt2)/trace(Jf2));
              end

              for j = 1:1:n
                  J2(:,4:6,j) = J2(:,4:6,j)/L2(j); %Right side of Jacobian
                      dimensionless
                  k2(j,1) = cond(J2(:,:,j));
              end

            LCI2(:,b) = 1./k2; % local Conditioning Index
          end
    end
end
```

G.3. DOMINATED SOLUTIONS TO PARETO FRONT

```
function [ p, idxs] = ParetoPointsDeleting( p )
% Filters a set of points p according to Pareto dominance, i.e., points
% that are dominated are filtered.
%% Inputs:
% - p    : N-by-D matrix, where N is the number of points and D is the
%          number of objectives of each point (3).
%% Outputs:
% - p    : Pareto-filtered p
% - idxs : indices of the non-dominated solutions

  [i, dim] = size(p);
  idxs = [1 : i]';
    while i >= 1
       old_size = size(p,1);
       indices = sum(bsxfun(@ge,p(i,:),p),2) == dim;
       indices(i) = false;
       p(indices,:) = []; idxs(indices) = [];
       i = i - 1 - (old_size - size(p,1)) + sum(indices(i:end));
    end
end
```

H

MODEL AND PRE-PROCESSING SCRIPT

In this Appendix the main Simulink model boxes are shown and explained in more detail. Only the model including the hydraulics is shown. The model in which the hydraulics are neglected is identical when removing the hydraulics box. Besides, a visualisation of the model is given, see Figure H.3 and H.4. At last, the pre-processing MATLAB script used in the Simulink model is given.

H.1. SIMULINK MODEL

Figure H.1 shows the complete Simulink model. This model consist of six main boxes which are all discussed below. In the green box, the required leg trajectories are calculated by using the motion time-series and the Stewart platform as input. These required leg trajectories are used as input for the PID controller. This controller gives an output based on the error between the required and actual leg trajectory. This controller output is the required valve opening. The hydraulic cylinder force is calculated in the orange box by the differential equations using the valve opening and piston position and velocity as input, see Section 8.3.3. Besides, in this box the passive system's force is added to the cylinder force. In the grey box this force is multiplied by the piston velocity giving the required power per cylinder. Summing them all gives the total required power. The red box is the plant and is shown in more detail in Figure H.2. The plant consists of the base, the hydraulic cylinders and platform. The base is displaced with the motion time series while on the platform a wind force is exerted. The WTG and vessel bodies do not influence the system and are only used for visualisation purposes. At last, the pink box computes the performance of the platform consisting of the Compensation Efficiency (CE) and the remaining platform motions. The complete model is visualised as shown in Figure H.3 and H.4.

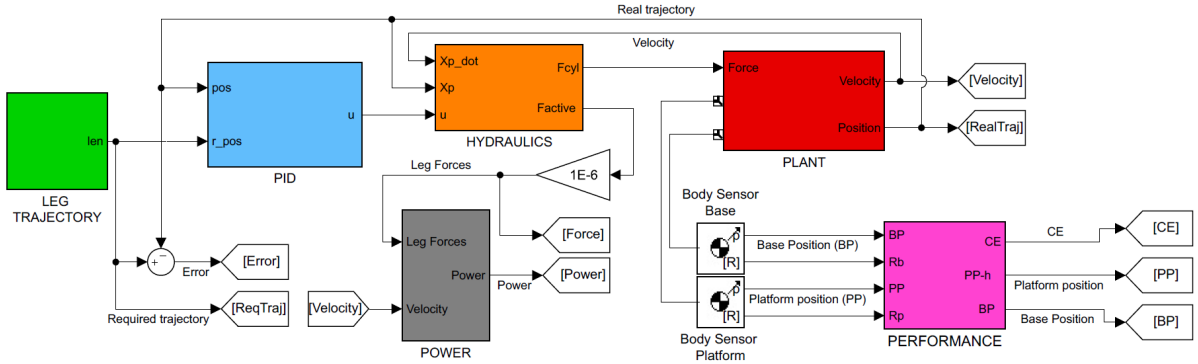

Figure H.1: Main Simulink model

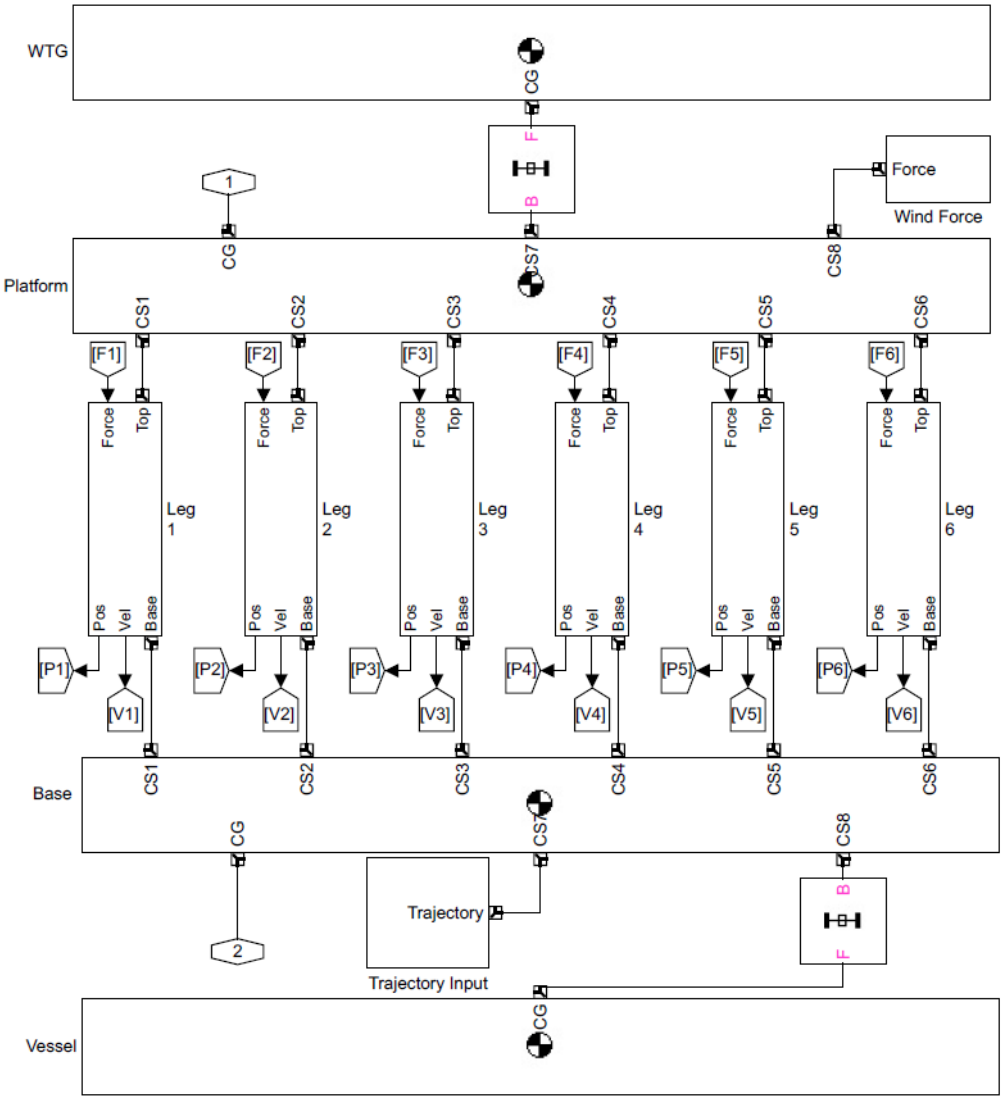

Figure H.2: Plant consisting of base, cylinders and platform. The WTG and vessel bodies are solely used for visualisation purposes.

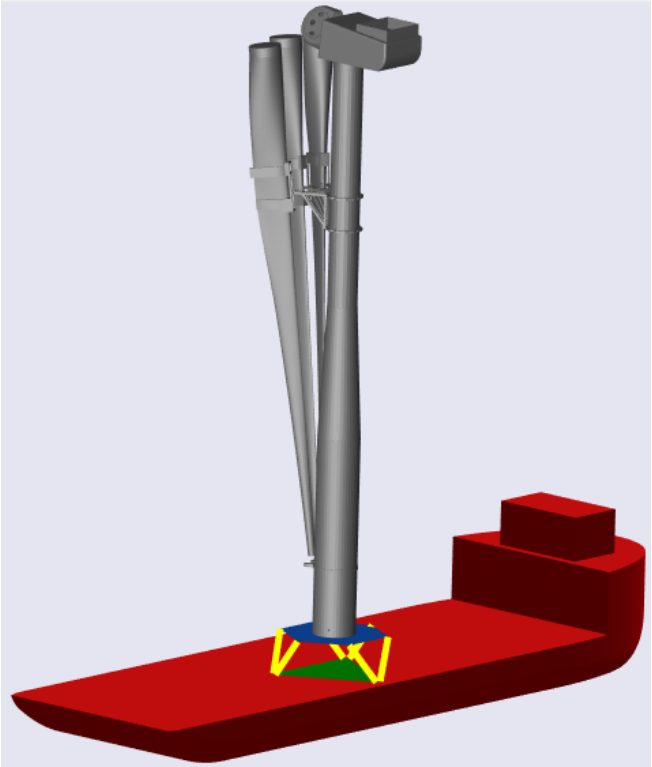

Figure H.3: Visualisation of the Simulink model including the vessel and WTG

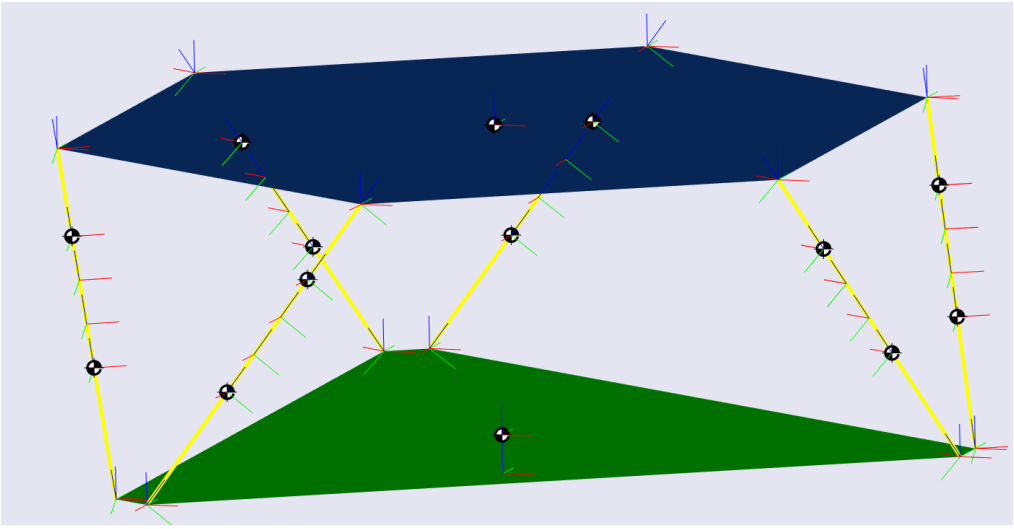

Figure H.4: Visualisation of the Stewart platform showing all body CoGs and axis systems and the axis systems of the joints. Red, green and blue are respectively the X, Y and Z-axis.

H.2. PRE-PROCESSING SCRIPT

The pre-processing MATLAB script is shown below. This script is for the model including hydraulics and excluding passive system. To change to the basic model and the model with passive system, the input parameters should be adjusted.

```
clear all; clc;
%% Inputs
R_b = 12.5; % [m]
R_t = 11.25; % [m]
Phi_b = 2; % Radians
Phi_t = 1; % Radians
h = 8; % [m]

deg2rad = pi/180;
x_axis = [1 0 0];
y_axis = [0 1 0];
z_axis = [0 0 1];

%% Design parameters
radius_b = R_b; % base radius [m]
radius_t = R_t; % top radius [m]
alpha_b = Phi_b; % base seperation angle [rad]
alpha_t = Phi_t; % top seperation angle [rad]
height = h; % height in home configuration [m]

%% Connection points on base and top plate w.r.t. world frame at the centre of the
    base plate
pos_base = [];
pos_top = [];

for i = 1:3
  % Base
   angle_m_b =  (i-1)*2*pi/3 + pi/3 - alpha_b/2;  %Cylinder 1,3,5
   angle_p_b =  (i-1)*2*pi/3 + pi/3 + alpha_b/2;  %Cylinder 2,4,6
   pos_base(2*i-1,:) = [radius_b*cos(angle_m_b), radius_b*sin(angle_m_b), 0.0];
   pos_base(2*i,:) =   [radius_b*cos(angle_p_b), radius_b*sin(angle_p_b), 0.0];

  % Top
   angle_m_t = (i-1)*2*pi/3 + pi/3 - alpha_t/2; %Cylinder 1,3,5
   angle_p_t = (i-1)*2*pi/3 + pi/3 + alpha_t/2; %Cylinder 2,4,6
   pos_top(2*i-1,:) = [radius_t*cos(angle_m_t), radius_t*sin(angle_m_t), height];
   pos_top(2*i,:) = [radius_t*cos(angle_p_t), radius_t*sin(angle_p_t), height];
end

% Compute points w.r.t. platform frame in a 3x6 matrix
body_pts = pos_top' - height*[zeros(2,6);ones(1,6)];

%% Leg vectors
legs = pos_top - pos_base;
leg_length = [ ];
leg_vectors = [ ];
for i = 1:6
  leg_length(i) = norm(legs(i,:)); %Length of leg
  leg_vectors(i,:)  = legs(i,:) / leg_length(i); %Unit vectors
end

```

```
%% Calculate revolute and cylindrical axes. 1,2 at bottom. 3,4 at top
for i = 1:6
  rev1(i,:) = cross(leg_vectors(i,:), z_axis);
  rev1(i,:) = rev1(i,:) / norm(rev1(i,:)); % To unit vector
  rev2(i,:) = - cross(rev1(i,:), leg_vectors(i,:));
  rev2(i,:) = rev2(i,:) / norm(rev2(i,:)); % To unit vector
  cyl1(i,:) = leg_vectors(i,:);
  rev3(i,:) = rev1(i,:);
  rev4(i,:) = rev2(i,:);
end

%% Coordinate systems (preallocate)
lower_leg = struct('origin', [0 0 0], 'rotation', eye(3), 'end_point', [0 0 0]);
upper_leg = struct('origin', [0 0 0], 'rotation', eye(3), 'end_point', [0 0 0]);

%% Define neutral position of upper and lower cylinder
Lower_origin = 15/40; % ratio origin/total Length of lower cylinder
Upper_origin = 1-Lower_origin; % ratio origin/total Length of lower cylinder

for i = 1:6
  lower_leg(i).origin = pos_base(i,:) + Lower_origin*legs(i,:);
  lower_leg(i).end_point = pos_base(i,:) +  2*Lower_origin*legs(i,:);
  lower_leg(i).rotation = [rev1(i,:)', rev2(i,:)', cyl1(i,:)'];
  upper_leg(i).origin = lower_leg(i).end_point;
  upper_leg(i).end_point = upper_leg(i).origin - (2*Upper_origin-1)*legs(i,:);
  upper_leg(i).rotation = [rev1(i,:)', rev2(i,:)', cyl1(i,:)'];
end

%% Inertia and mass calculation
top_thickness = 0.10; % [m]
base_thickness = 0.10; % [m]
outer_radius = 1.05/2; % [m] Cylinder outer radius
inner_radius = 1/2; % [m] Cylinder inner radius
rod_radius = 0.525/2; % [m] Rod radius
density = 7850; %Steel density [kg/m^3]

% Leg inertia and mass
[lower_leg_mass, lower_leg_inertia] = CylinderInertia(density, (2*Lower_origin)*
    leg_length(1), outer_radius, inner_radius);
[upper_leg_mass, upper_leg_inertia] = CylinderInertia(density, 2*(1-Upper_origin)*
    leg_length(1), rod_radius, 0);

% Top and base plate mass and inertia
[top_mass, top_inertia] = CylinderInertia(density, top_thickness, radius_t, 0);
[base_mass, base_inertia] = CylinderInertia(density, base_thickness, radius_b, 0);

% Add WTG mass and inertia
Ix_wtg = 3.98E9; Iy_wtg = Ix_wtg; Iz_wtg = 2.92E7;
WTG_inertia = [Ix_wtg 0 0; 0 Iy_wtg 0; 0 0 Iz_wtg]; % Inertia tensor
top_mass = top_mass + 1935.5*1000;
top_inertia = top_inertia + WTG_inertia;

%% Hydraulic cylinder and valve model. A = cylinder, B = rod
%Hydraulic cylinder
Ar = pi*(inner_radius^2-rod_radius^2); % Rod side surface [m^2]
Ap = pi*(inner_radius^2); % Piston side surface [m^2]
```

```
105 S = 5; %Stroke length (L2) [m]
106 V0p = 0.5*S*Ap; % volume piston side [m3]
107 V0r = 0.5*S*Ar; % volume rod side [m3]
108
109 %Valve characteristics
110 pS = 250e5; %Supply pressure [Pa]
111 pT = 1e5; %Tank pressure [Pa]
112 dpn = 25e5; %Nominal pressure difference [Pa]
113 valveslope = 100/(1e-2); %Maximum spool speed [%/s] %100% open or closed in 1e-2 s
114 valverange = 100; %Valve range [%] 0 = closed, 100 = fully opened
115 overlap = 0; % Overlap in valve + and -
116
117 % Initial settings
118 pB0 = 125e5; % Initial pressure B
119 Fload0 = 9.81*(top_mass/6+(upper_leg_mass+lower_leg_mass)); % Initial load
120 pA0 = (Fload0 + Ar*pB0)/Ap; % Initial pressure A
121
122 % Nominal flow
123 Vmax  = 0.67; %[m/s]
124 Vmin = -0.62; %[m/s]
125 Qrod = Ar*Vmax; %[m^3/s]
126 Qcyl = Ap*abs(Vmin); %[m^3/s]
127 Qn = max(Qrod,Qcyl); % nominal flow [m3/s]
128 Qn_LperMin = Qn*60*1000; % nominal flow [L/min]
129 Qn_LperMin = roundn(Qn_LperMin, 4);
130 Qn = Qn_LperMin/(60000);
131
132 %% Bulk modulus
133 beta_low = (1.8*10^9)*(1-exp(-0.4-(2*10^-7)*pT));
134 beta_high = (1.8*10^9)*(1-exp(-0.4-(2*10^-7)*pS));
135 beta = (beta_low + beta_high)/2; % Bulk modulus [Pa]
136
137 %% MRU input
138 Sample_time = 0.005; %200 Hz (kongsberg MRU)
139
140 %% Trajectory Input
141 [MRUOutput, MRUsensor] = TrajectoryInput(Sample_time);
142 MRUsensor = MRUsensor';
143 MRUsurge = [MRUsensor MRUOutput(:,1)]; MRUsurgedot = [MRUsensor MRUOutput(:,7)];
      MRUsurgedotdot = [MRUsensor MRUOutput(:,13)];
144 MRUsway =  [MRUsensor MRUOutput(:,2)]; MRUswaydot =  [MRUsensor MRUOutput(:,8)];
      MRUswaydotdot =  [MRUsensor MRUOutput(:,14)];
145 MRUheave = [MRUsensor MRUOutput(:,3)]; MRUheavedot = [MRUsensor MRUOutput(:,9)];
      MRUheavedotdot = [MRUsensor MRUOutput(:,15)];
146 MRUroll =  [MRUsensor MRUOutput(:,4)]; MRUrolldot =  [MRUsensor MRUOutput(:,10)];
      MRUrolldotdot =  [MRUsensor MRUOutput(:,16)];
147 MRUpitch = [MRUsensor MRUOutput(:,5)]; MRUpitchdot = [MRUsensor MRUOutput(:,11)];
      MRUpitchdotdot = [MRUsensor MRUOutput(:,17)];
148 MRUyaw =  [MRUsensor MRUOutput(:,6)]; MRUyawdot =  [MRUsensor MRUOutput(:,12)];
      MRUyawdotdot =  [MRUsensor MRUOutput(:,18)];
149
150 %% PI Values
151 Kp = 5;
152 Ki = 0.01;
153
154
```

```
%% Passive system
p0_estimate = 9.81*(top_mass/6+upper_leg_mass)/mean(leg_vectors(:,3))/Apassive; %
    Static
p0 = roundn(p0_estimate,6); % Initial pressure N2
V0a = 50; % [m^3] Initial volume accumulator (>Xp_max*Ap)
n = 3/2; %Adiabatic constant
Kpassive = n*p0*Apassive^2/V0a;

%% Wind Time-series
load('Wind_time series'); %Computed in wind-time series script
load('WindSpeedToForce+Moment'); %Excel sheet
Wind2Force(:,2:6) = Wind2Force(:,2:6)*1000; %[kN and kNm (excel) to N and Nm]

%% Inertia and Mass of cylinder and rod
function [mass, inertia] = CylinderInertia(dens, length, rout, rin)
    mass = pi*(rout^2-rin^2)*length*dens; % Compute mass
    % Compute principal inertias
    Ix = mass*(3*(rout^2 + rin^2) + length^2)/12;
    Iy = Ix;
    Iz = mass*(rout^2 + rin^2)/2;
    inertia = [Ix 0 0; 0 Iy 0; 0 0 Iz]; % Inertia tensor
end
```

TRAJECTORY INPUT

```
function [MRUOutput_Resolution, Sensortime] = TrajectoryInput(Sample_time)
    %% Load Input Orcaflex
    load(MRUOutput'); % First-order motions
    load(MRUtime'); % Time vector
    load(MRUOutput_DP'); % Second-order motions

    %% Alpha factor
    Alpha_factor = 0.84; %First-order is 0.84, Second-order is 0.84^2
    MRUOutput = MRUOutput/Alpha_factor;
    MRUOutput_DP = MRUOutput_DP/(Alpha_factor^2);
    MRUOutput_DP(:,1) = MRUOutput_DP(:,1)*Alpha_factor;

    %% Add second-order to first-order motions
    % No I term in DP so set average at zero
    SurgeAverage = sum(MRUOutput_DP(:,2))/length(MRUOutput_DP(:,2));
    SwayAverage = sum(MRUOutput_DP(:,3))/length(MRUOutput_DP(:,3));
    MRUOutput_DP(:,2) = MRUOutput_DP(:,2)-SurgeAverage;
    MRUOutput_DP(:,3) = MRUOutput_DP(:,3)-SwayAverage;

    MRUsimulation = MRUOutput(:,2:19);
    Sensortime = (0:Sample_time:max(MRUtime));

    for i = 1:18
    MRUsimulation2(:,i) = smoothdata(MRUsimulation(:,i),'rloess',15);
    MRUOutput_Resolution(:,i) = interp1(MRUtime,MRUsimulation2(:,i),Sensortime','
        spline');
    end
end
```

WIND TIME-SERIES

```
%% Wind Time-series
clc; clear all;

%% Inputs
t = (0:0.005:10800); %time vector
V_10 = 15; %[m/s]
Z0 = 0.005;
%Alpha factor 0.8 & 0.005 log profile included
N = 10000; % Number of frequency components
h = 10; % Height of V10

%% Kaimal spectrum
SigmaU = V_10*sqrt(4.5-0.856*log(Z0))*0.4*1/(log(h/Z0)); % IEC 61400-1
Lu = 300*((h/300)^(0.46+0.074*log(Z0)));
Su = (SigmaU^2)*((6.868*Lu/V_10)./((1+(10.32*f*Lu./V_10)).^(5/3)));

Speed = zeros(1,length(t));
for i = 1:length(t)
    Speed(i) = WindGeneration(Su,f,df,t(i),V_10);
end

Wind = [t' Speed']; %% Used in Simulink
function Speed = WindGeneration(Su,f,df,t,V_mean)
     persistent Ph  % random phase angles defined only once
     if isempty(Ph)
         n=length(f);
         Ph = (-1 + (1+1)*rand(1,n))*pi; % Wind paper -pi to pi
     end
     A = (2/pi)*sqrt(Su*df);  %Calculate amplitude spectrum from energy spectrum
     Speed = V_mean+sum(A.*cos(2*pi*f*t+Ph));  %Create Wind time series from
         amplitude spectrum
end
```

I

FILTER AND INTERPOLATION

In Figure I.1 a small part of the Orcaflex surge time-series with a 0.1 *s* time series can be found. It can be seen that the Orcaflex signal does not have sufficient accuracy. Using such a signal will introduce all kinds of spurious wave frequencies in the fourier transform that have no physical background. Using this signal as input for Simulink gives a high frequency response. As can be seen in Figure I.1, by spline interpolating the Orcaflex time-series the data is smoothens but the perturbations are maintained. Therefore, all six time-series require filtering before they are spline interpolated. This is done by using the *smooth* function in MATLAB with the *rloess* or Robust Local Regression smoothing method with a window size of 15 data points. This method applies a local regression using weighted linear least squares. For each data point, a 2nd-degree polynomial is found which has the lowest squared distance from the 15 data points in the window. For each data point, the 15 closest points are part of its window. This method applies lower weight to outliers in the regression and zero weight to data outside six mean absolute deviations. For each window, the mean absolute deviation is the average distance between each data point and the mean. Thus, it filters the small perturbations and smoothens the time-series to present the real-life motions more accurately.

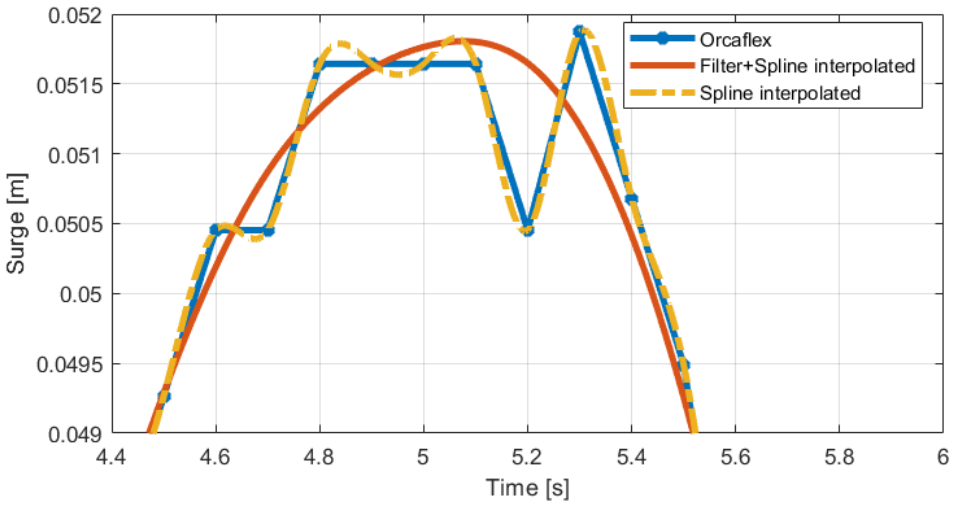

Figure I.1: Data directly from Orcaflex, only interpolated data and filtered and interpolated data.